RESULTS TOWARDS A SCALABLE MULTIPHASE NAVIER-STOKES SOLVER FOR HIGH REYNOLDS NUMBER FLOWS

A Dissertation

by

TRAVIS BRANDON THOMPSON

Submitted to the Office of Graduate Studies of
Texas A&M University
in partial fulfillment of the requirements for the degree of

DOCTOR OF PHILOSOPHY

Chair of Committee,	Jean-Luc Guermond
Committee Members,	Wolfgang Bangerth
	Joseph Pasciak
	Jean Ragusa
	Emil Straube
Head of Department,	Emil Straube

August 2013

Major Subject: Mathematics

ABSTRACT

The incompressible Navier-Stokes equations have proven formidable for nearly a century. The present difficulties are mathematical and computational in nature; the computational requirements, in particular, are exponentially exacerbated in the presence of high Reynolds number. The issues are further compounded with the introduction of markers or an immiscible fluid intended to be tracked in an ambient high Reynolds number flow; despite the overwhelming pragmatism of problems in this regime, and increasing computational efficacy, even modest problems remain outside the realm of direct approaches.

Herein three approaches are presented which embody direct application to problems of this nature. An LES model based on an entropy-viscosity serves to abet the computational resolution requirements imposed by high Reynolds numbers and a one-stage compressive flux, also utilizing an entropy-viscosity, aids in accurate, efficient, conservative transport, free of low order dispersive error, of an immiscible fluid or tracer. Finally, an integral commutator and the theory of anti-dispersive spaces is introduced as a novel theoretical tool for consistency error analysis; in addition the material engenders the construction of error-correction techniques for mass lumping schemes.

DEDICATION

For Everly,

May your curiosity remain forever unsated.

ACKNOWLEDGEMENTS

First and foremost an acknowledgement of Dr. Jean-Luc Guermond is appropriate. Possessing a clear and prescient insight, coupled with patient guidance, I count myself fortunate to have had the distinct pleasure to be your student. Secondly, a thank you to Dr. Larios is extended for many discussions on the nature of turbulence and the collaboration with the computational aspects of the entropy-viscosity based LES. In addition the assistance regarding thorough modifications and corrections to the material from my committee is also appreciated; in particular, the suggestions of Dr. W. Bangerth went far in ensuring the overall quality of the work.

On a more personal note Dr. M. Dabkowski, at the University of Texas at Dallas, Dr. I. Darcy, at the University of Iowa, Dr. G. Brook, at the Oak Ridge National Laboratory, and Dr. R. Murphy have all, at one time or another, impacted the development of my professional and intellectual development at fulcral junctures. I am indebted to and appreciative of the altruistic interest that each of these individuals has extended on my behalf.

Any dissertation acknowledgement section would be incomplete without mention of familial persuasion; towards this end I would like to thank my mother and father for never allowing me the lulling reprieve of contentment and, in addition, for decades of steadfast support. Finally, a sincere avowal of appreciation is owed to my wife, Georgia, for possessing the fortitude required for sustained sacrifice and to my daughter, Everly, for the extension to my understanding of happiness.

-T

July 5, 2013

TABLE OF CONTENTS

LIST OF FIGURES

FIGURE Page

LIST OF TABLES

TABLE Page

1. INTRODUCTION

1.1 Regarding the Navier-Stokes equations

The Navier-Stokes equations describe the motion of fluid substances. The equations are widely utilized to model many physical phenomena such as weather patterns, ocean currents, turbulent fluid flow and magneto hydrodynamics; despite their wide utilization a comprehensive theoretical understanding remains an open question. The incompressible Navier-Stokes equations are given by

$$\begin{aligned} \partial_t \mathbf{u} + (\mathbf{u} \cdot \nabla)\, \mathbf{u} - \mu \Delta \mathbf{u} + \nabla p &= \mathbf{f} \\ \nabla \cdot \mathbf{u} &= 0 \end{aligned} \tag{1.1}$$

In a bounded domain, Ω, (1.1) is typically augmented with periodic boundary conditions or the boundary condition $\mathbf{u}_{|\partial\Omega} = 0$ for all $t \in [0, T]$; in addition the initial condition $\mathbf{u}(x, 0) = u_0(x)$ for all $x \in \Omega$ is employed. The Navier-Stokes equations are a mathematically challenging set of equations. The Navier-Stokes equations present pertinent challenges at the forefront of both theoretical and computational knowledge. The problem of existence and uniqueness of solutions to the Navier-Stokes equations is multiply faceted and embodies a rather recent history. It is not within the scope of this document to fully present such an account; I will, however, briefly mention an excerpt of the historical development detailed at length in [55]. In [32] the existence and uniqueness of regular solutions for all time, in space dimension two, for the whole space is established; in [34] existence and uniqueness is shown for some interval $(0, T)$, where T depends on the data, for bounded domains. In three dimensions [33] established, for flow in the whole space, existence and uniqueness of

a regular solution on some interval $(0, T)$, where T depends on the data, and the existence for all time of a weak solution and discussed the possibility of singularities therein. Following the work of Leray, [21] proved the global time existence, in three dimensions, for a weak solution in a bounded domain with homogeneous Dirichlet boundary conditions on the velocity. A sequence of papers in the late fifties essentially concluded the two-dimensional case; [36] proved uniqueness of weak solutions in two spatial dimensions while [29, 30] improved Leray's existence results for strong solutions in two-dimensional bounded domains. For further historical context see [55]. More recently some headway has been forged in the three-dimensional case; for example, [49] show that weak solutions of the three-dimensional Navier-Stokes equations are smooth provided the negative part of the pressure, or the quantity $|\mathbf{u}|^2 + 2p$, are controlled. Despite these advances, however, the question of existence and uniqueness for the three dimensional case remains an open problem.

Computationally, the Navier-Stokes equations embody a unique set of issues; lacking any clear analytic solution in general, the praxis of utilizing Navier-Stokes is numeric in nature and the last half century has enveloped significant advancement and adaptation in numerical techniques to evince such a solution. Such approaches may, more or less, be dichotomized as either utilizing a model for turbulent effects or not doing so. Turbulent effects induce a coupling of small scale interactions with large scale behaviour; the coupling, in turn, requires these small scales be resolved or, to some degree, the fluid effects at these scales be modelled. Ultimately, the smallest scale on which turbulent effects should be resolved, if not otherwise modelled, in order to effectively present the coupling-induced behaviour, whereby small scale interactions affect large scale structure, is termed the *Kolmogorov micro-scale* and can be related to the Reynolds number of the flow. Resolving the Kolmogorov micro-scales for a direct numerical simulation is, essentially, computationally intractable;

therefore some degree of turbulence modeling is necessary for flows with appreciable Reynolds numbers. Outside of the resolution requirements, more modern numerical approaches for solving the (incompressible) Navier-Stokes equations are not *scalable*; i.e. the resulting algorithms incur large communication costs on modern highly-parallel systems.

The overall goal of the research I have undertaken is to isolate and treat the various aspects underlying multiphase incompressible flows at high Reynolds numbers and to do so in a paradigm amenable to high degrees of computational efficienty and scalability; in this way a more readily-applicable set of techniques and results is founded en-route to a general solution.

1.2 Entropy-Viscosity: localized viscous regularization

The solution of (systems of) hyperbolic conservation laws poses unique challenges; specifically high-order numerical solutions of such systems tend to introduce artificial oscillations at the location of shock fronts. In order to subdue such phenomena one approach is to track or locate discontinuities (shocks, contact, etc) in the numerical solution. Such 'shock detecting' approaches offer a venue for the redress of spurious numerical error; one particularly efficacious method of shock capture is the employment of an entropy variable. [45] studies the phenomena of entropy production in higher order methods as an indicator for the presence of shocks and contact discontinuities wherein it is shown, via computational investigation, that spurious entropy production in smooth regions, or in smooth solutions, tends to zero on the same order as the local truncation error of the discrete scheme; entropy production, on the other hand, in regions of discontinuities (shocks, contact, etc) becomes more pronounced with successive mesh refinement. Various applications of this 'shock recognition' trait embodied in the calculation of the entropy have been deployed: [1] utilize spu-

rious entropy production to produce *a posteriori* error estimations and applies these estimates to adapt local mesh refinements while [45] utilizes this quantity to track shocks and to provide local scheme adaptations (e.g. linear versus nonlinear terms).

The uses of entropy have not been restricted solely to shock capturing; [18] notes that (systems of) hyperbolic conservation laws admitting an entropy could be symmetrized if and only if an entropy for the system could be defined; the author proceeded to show that such systems could be linearized in a certain sense and proceeded to symmetrize the Euler equations of gas dynamics and the incompressible Navier-Stokes equations. Then, as in [18], the method of utilizing entropy variables to symmetrize conservation laws was applied in [22] to include heat conduction in the compressible Navier-Stokes formulation; this paved the way for an application of finite elements which preserved relevant physical quantities (Clausius-Duhem inequality, etc).

[23] begins a series of papers generalizing a streamline upwind Petrov-Galerkin method for advection-diffusion; a parameter-based shock-capturing term is added which seeks to control gradients in the numerical solution. [26] re-interpret the shock-capturing term as an artificial viscosity constructed from the residual of the PDE; a strong convergence result is proven in [53]. The relevant facet of these papers is the introduction of a local viscosity based on a residual; granted the residual utilized to construct the viscous coefficient utilized is that of the PDE.

The natural 'shock capturing' behavior entropy production suggest good candidacy for the foundation of the construction of a local viscosity for use in numerical schemes. This novel, but evolutionary, concept was put forth in [14]; at each step a (variable) viscosity is computed by evaluating a residual based on the entropy and this viscosity is utilized in the (stabilized form of the) Galerkin formulation to evince the solution method. The entropy production is expected, as in [45], to tend to

zero in regions where the solution in smooth, on the order of the local truncation error, and become pronounced at shocks. [14] perform copious tests of the method on known problems and the entropy-viscosity performs quite well. The entropy-viscosity technique shows unique promise, in both its applicability and its computational efficiency, and possible applications abound; my particular research proposal for work with the entropy-viscosity method is computational in nature and is outlined in the proceeding sections.

1.3 The overarching goal of the present work

Let Ω be a domain which, for the sake of a simple discussion, is either the whole of $\mathbb{R}^3$, 'large enough' so that boundary effects in the interior can be neglected or considered with periodic boundary conditions. Consider a sample problem in this regime whereby the incompressible Navier-Stokes equations, (1.1), are taken in conjunction with the diffusionless advection equation (1.1)

$$\partial_t \phi + \mathbf{u} \cdot \nabla \phi = 0 \tag{1.1}$$

In equation (1.1) the function $\phi(x,t)$ represents some immiscible quantity advected by the velocity field $u(x,t)$ in the absence of diffusion. Concrete examples of the conjoined paradigm of equations (1.1) and (1.1) include the far-shore behavior of deepwater oil spills or the advection of a massless tracer immersed in an ambient fluid of constant density. Each problem, considered in its own stead, embodies its difficulties; the incompressible Navier-Stokes equations and the advection of the immiscible quantity pose unique challenges in the domain of scientific computing and it is the work herein to treat some of the aspects that arise as difficulties when considering these two problems in conjunction.

The inherent difficulties of the incompressible Navier-Stokes equations are signif-

icant; as mentioned in section 1.1 even the incompressible regime is the object of ongoing theoretical intrigue. Despite the open questions of existence and uniqueness it remains that equations (1.1) are utilized, numerically, by the engineering and empirical physics community to solve problems of practical importance. The need to procure tangible results for (1.1) has drawn the attention of the numerical analysis, engineering and scientific computing communities since, at least, the numerical proposals and simulations of [16]. A primary barrier to any serious computational efforts towards a solution to (1.1) for high Reynolds numbers paradigms is the resulting resolution requirements. Essentially, due to the nonlinear term in equation (1.1), high Reynolds number flows require a direct numerical simulation (DNS) approach to resolve all dynamically significant scales in order to abet dramatic errors from accumulating in time; this imposes a significant resolution requirement on the simulation. More poignantly, if N is the total number of evenly-spaced mesh points the resolution requirements scale as $N > Re^{9/4}$; even relatively modest Reynolds numbers, such as $Re \approx 500$ then require in excess of a million grid points. In the context of ocean flow, where the characteristic length is quite large, the Reynolds number can be on the order of $Re \approx 10^{11}$. A direct numerical simulation at such a scale would require in excess of 10^{24} grid points; assuming the entire data associated to a grid point could be stored in a single byte then the mesh for the computation alone would require in excess of 8.8×10^8 petabytes of storage space. A more detailed discussion regarding such resolution requirements is presented in section 2.1; it is clear however that some mechanism for reducing the associated resolution requirements associated to solving (1.1) in the context of high Reynolds numbers would be advantageous. This is precisely the impetus underlying the discourse in chapter 2.

If the function $\phi(x,t)$, advected by the ambient velocity vector field $\mathbf{u}$, represents a homogeneous quantity, such as a density of some immiscible fluid, then, in the

absence of diffusion, $\phi(x,t)$ is referred to as a *phase function* and (1.1) can be considered an *interface tracking problem*. Such problems have a rich history; [46] give a comprehensive introduction to many methods utilized in recent literature. Among the family of front tracking methods is the so-called *level set methods* for tracking interface propagation; seminal approaches typically utilized a *distance function* for $\phi(x,t)$. This approach was taken, for example, in [41]; a caveat to such a choice of phase function is that the property of being a distance function is lost and a re-distancing procedure must be computed after each time step. Initially this procedure was incredibly costly, on the order of $\mathcal{O}(N^3)$ where N is the total number of grid points, and therefore prohibitive for DNS simulations of high Reynolds number flows where N is exorbitant. More recently [17] introduced the notion of artificial compressors and [40] adapted this two-stage approach succesfully in the context of level set methods. [57] has a fairly new one-stage methodology where the re-distancing is accomplished as part of the advection step via a modified advection equation; this work is then applied to fluid buckling problems. In the context of fluid buckling computations only the interface level set needs to be tracked and, indeed, this one-stage redistancing method does not account for the complete domain level-set function; the built-in redistancing procedure only ensures the interface level set is preserved. Nevertheless the work of [57] is a harbinger of the existence of efficient one-stage methods; Chapter 3 details an approach extending the work of [40] by introducing a one-stage level set technique which performs well for the full-domain level set function. This reduces the computational complexity of computing (1.1) dramatically in settings where more than simply an interface is needed to compute requisite details or interactions. Such a one-stage approach is vital in the context of high Reynolds number flow; the impact is intensified when utilized in conjunction with an approach to reduce the initial resolution requirements of solving (1.1).

When implementing the one-stage level set scheme presented in chapter 3 the existence of low-order dispersive error in the numerical discretization causes error waves which generate entropy; this entropy production poses issue with the particular method proposed for the one-stage level set technique. Therefore, a dispersion correction scheme based on the work of [13] was utilized; this work requires that one know a-priori when a finite element space yields a set of discrete equations for the transport problem which is free of low-order dispersive error. The canonical approach to such *consistency error analysis*, via Taylor expansion methods, is cumbersome and intractable for problems in dimension higher than one. Towards this end, in chapter 4, a new method for consistency error analysis is proposed which squarely answers this difficulty; the new method is not only efficient but, in order to verify a paradigm free of low-order dispersive error, requires only a relatively small set of quantities to be computed which, for any significantly complex problem, could even be carried out programatically.

2. AN ENTROPY-VISCOSITY FOR LES

2.1 Overview

Computationally, the Navier-Stokes equations, (1.1), embody a unique set of issues; lacking any clear analytic solution in general, the praxis of utilizing Navier-Stokes is numeric in nature and the last half century has enveloped significant advancement and adaptation in numerical techniques to evince such a solution. Such approaches may, more or less, be dichotomized as either utilizing a model for turbulent effects or not doing so. Turbulent effects induce a coupling of small scale interactions with large scale behaviour; the coupling, in turn, requires these small scales be resolved or, to some degree, the fluid effects at these scales be modelled. Ultimately, the smallest scale on which turbulent effects should be resolved, if not otherwise modelled, in order to effectively present the coupling-induced behaviour, whereby small scale interactions affect large scale structure, is termed the *Kolmogorov micro-scale* and can be related to the Reynolds number of the flow [44]. Resolving the Kolmogorov micro-scales for a direct numerical simulation is, essentially, computationally intractable; therefore some degree of turbulence modeling is necessary for flows with appreciable Reynolds numbers. Outside of the resolution requirements, more modern numerical approaches for solving the (incompressible) Navier-Stokes equations are not *scalable*; i.e. the resulting algorithms incur large communication costs on modern highly-parallel systems.

Simulating the Navier-Stokes equations at high Reynolds number is a computationally formidable challenge. Suppose a direct numerical simulation (DNS), a simulation lacking a turbulence model, of the incompressible Navier-Stokes equations were undertaken; the numerical simulation, in order to be physically meaningful,

would need to resolve scales at the Kolmogorov micro scale as well as the integral (large) scale of the fluid motion. The Kolmogorov length scale [44] is given by the expression $\eta = \left(\frac{\nu^3}{\epsilon}\right)^{\frac{1}{4}}$ where ν is the kinematic viscosity and ϵ the rate of kinetic energy dissipation. Letting L denote the integral length scale the kinetic energy dissipation can be approximated by $\epsilon \approx \frac{\bar{u}^3}{L}$ where $\bar{u}$ is the root mean square of the velocity; the Reynolds number of the flow is $R_e = \frac{\bar{u}L}{\nu}$.

Using these quantities we can express the complications inherent in DNS models explicitly. Suppose that N is the number of unknowns, evenly spaced, in one spatial direction on a computational grid of step-size h; to resolve the integral scale we must have $Nh > L$ while, to resolve the Kolmogorov length scales, we must also have $h < \eta$. Substituting the approximation for ϵ into the expression for η yields

$$\eta \approx \left(L\left(\frac{\nu}{\bar{u}}\right)^3\right)^{\frac{1}{4}} = \left(L^4\left(\frac{\nu}{L\bar{u}}\right)^3\right)^{\frac{1}{4}} = LR_e^{-\frac{3}{4}}$$

The inequalities mentioned then yield

$$h \leq \eta,\ L < Nh \rightarrow L < N\eta \approx LR_e^{-\frac{3}{4}}$$

From which the inequality $R_e^{\frac{3}{4}} < N$ follows. In three spatial dimensions, assuming a uniform mesh, the total number of grid points is $T = N^3$ so that the above implies that a lower bound on the number of grid points needed in three dimensions to fully resolve the necessary length scales is determined by the Reynolds number and is given by $R_e^{\frac{9}{4}}$. Turbulent flow occurs at different Reynolds numbers for different types of flow. Consider a very simple case of laminar flow in pipe of diameter d; [20] notes that the transition to turbulence in this regime typically occurs in the range $2000 < R_e < 4000$. In general such a transition is dependent on the fluid,

pipe roughness, etc; supposing that $R_e > 4000$, for a simple turbulent pipe flow, would yield a DNS scheme requiring $127,243,317$ grid points. [20] mentions that laminar flow has been observed, under controlled laboratory conditions, up to $R_e \approx 25,000$; such a flow would require in excess of 7.9 billion grid points to resolve after it eventually transitioned to turbulence. It is evident that, even in the context of simplistic problems, direct numerical simulation of high Reynolds number flow becomes computationally intractable.

2.2 Large Eddy Simulations

2.2.1 Overview

As put forth in section 2.1, resolving the smallest scales of the flow at which meaningful dynamics exist, the Kolmogorov length scale, is the primary computational difficulty; resolving this scale for turbulent flows can require an enormous amount of unknowns. Kolmogorov put forth the hypothesis that, for fully developed turbulence, the mean flow in the small scales was, statistically, isotropic (i.e. the same in every direction) whereas the large scales are highly anisotropic. The idea was then that one could *model* these smaller scales and eliminate the necessity to resolve them directly; this idea was, in fact, inferred in historical work. [48] puts forth a a historical account which shows that Boussinesq introduced the concept of local averaging; the Boussinesq hypothesis, in modern terms, outlines a relationship between the Reynolds stress and mean strain tensors. [48] goes on to show that, though Boussinesq had the right idea for making turbulence more approachable, his predicated relationship was incorrect; this is done by utilizing flow calculations where the stress tensors are known and comparing the results to the hypothesis. Nevertheless, we may point to this hypothesis as being a harbinger, if not a cornerstone, of LES models. The notion behind an LES model is to consider an 'average' flow; [4] includes

a treatment of LES encompassing several models. Reynolds proposed a velocity be written in terms of its mean and variation parts; e.g. $u = \bar{u} + u'$ where $u' := u - \bar{u}$. Reynolds initially proposed a time-averaging be utilized for the mean velocity; other averaging techniques, such as ensemble averaging, are employed today. Substitution of these quantities back into the Navier-Stokes equations yields an equation which is not closed. In particular [4] shows that the time-averaged Navier-Stokes equations, for an incompressible fluid, can be expressed as:

$$\begin{aligned} \bar{u}_t - \nu\Delta\bar{u} + \bar{u}\cdot\nabla\bar{u} + \nabla\bar{p} + \nabla\cdot(u'\otimes u') &= \bar{f} \\ \nabla\cdot\bar{u} &= 0 \end{aligned}$$

The diverence of the variational term $\nabla\cdot(u'\otimes u')$ causes a closure issue for the system; modeling this term, typically in terms of $\bar{u}$ alone, is referred to as *addressing the closure problem*. As stated in [4], LES can be succinctly stated as a four step approach:

- Select a useful filter, $g(\mathbf{x})$, and define $\bar{u}(\mathbf{x},t) = (g\star u)(\mathbf{x},t)$
- Derive the equations for $\bar{u}$ by
  - Set $u' = u - \bar{u}$
  - Substitute $u = u' + \bar{u}$ into the Navier-Stokes equations
- Select a closure model $\nabla\cdot(u'\otimes u') \approx f\left(\bar{u}, \nabla\bar{u}\right)$
- Impose appropriate boundary conditions

An excellent overview discussion of filtering and the subsequent derivation of a set of equations for the filtered variable, $\bar{u}$, can be found in the second section of [10]. Having addressed closure for an LES model, solving the resulting system of

equations is then tantamount to solving for the filtered flow field $\bar{u}$. Historically, one of the more utilized closure models for LES was put forth in [50] for studying the circulation of atmospheric currents; the closure is known as the *Smagorinsky-Lilly* model and follows from setting

$$\nabla \cdot (u' \otimes u') \approx -\nabla \cdot (\nu_T \nabla^s \bar{u}) \tag{2.1}$$

The quantity $(\nabla^s \bar{u})_i := \frac{1}{2}\left(\frac{\partial \bar{u}_i}{\partial x_j} + \frac{\partial \bar{u}_j}{\partial x_i}\right)$ is the symmetric gradient,commonly denoted $\mathbf{S}\bar{u}$, and $\nu_T := (C\Delta g)^2 |\mathbf{S}\bar{u}|$ is the *eddy viscosity*; Δg denotes the grid size and C is a constant. The Smagorinsky-Lilly model is a constituent of the family of *eddy viscosity closure models* in LES [4]; other choices of the eddy viscosity give rise to differing models and the author provides three other natural, unique choices for ν_T. According to [10] most subgrid LES models arise, in like manner, from an eddy-viscosity assumption; Smagorinsky-Lilly, for example, assumes that small scales are in equilibrium so that energy production and energy dissipation are in balance. Hence, the prescient relation between the eddy viscosity, ν_T, and the large-scale strain tensor $\mathbf{S}$. More recently [10] has devised a method by which the constant C, appearing in the Smagorinsky-Lilly model can be determined as a function of one spatial dimension, where the ambient space is $\mathbb{R}^3 = (x, y, z)$, and time; e.g. $C = C(y, t)$. More specifically $C(y, t)$ is determined by way of various averages involving the resolved turbulent stress tensor, $\mathcal{L}_{ij}$, and the large scale strain tensor $\mathbf{S}_{ij}$ using two different filters; a grid filter and a test filter. Results are reported in [10]; the main point being that the modeling of subgrid-scale stresses via an eddy-viscosity is an area of recent activity.

2.2.2 An entropy-viscosity based LES model

As already mentioned the primary difficulty predicating the need for subgrid-scale models is one of the lack of resolution; were infinite resolution computationally tractable there would be no issue. In turn, this implies that high Reynolds number numerical simulations are, in general, always under-resolved. That is, non-negligible gradients and eddy-phenomena, exist at the sub-grid level and cannot be correctly represented by the mesh; therefore, at the mesh scale, these solutions can be considered as behaving in a singular manner. As time progresses, these unresolved facets of the flow are likely to produce still larger gradients through the coupling of wave modes via the action of the nonlinear term; e.g. energy accumulates at the grid scale or, equivalently, in the high wave-number modes of the flow.

In order to control these sub-grid scale 'singularities' an approach motivated by work in the realm of hyperbolic conservation laws, where location and control of singularities has been well studied, is sought out. The utilization of entropy production as a technique for front capturing and shock detection was explored, numerically and for hyperbolic conservation laws, in [45]. The construction and usage of a viscosity based upon an entropy residual in the context of hyperbolic conservation laws was explored in [14]; the entropy residual itself is derived from an entropy inequality. The authors reported results from a slew of test cases including, among others, rotating transport, inviscid Burgers' equation and a KPP rotating wave problem. In the context of nonlinear conservation laws the choice of entropy inequality to utilize in the construction of an entropy-viscosity is straightforward [14] as it is the mechanism which yields the physically relevant solution. However, the selection of an "entropy inequality" for the Navier-Stokes equations is not as straightforward. [15] propose an inequality based on local balance of momentum

given by

$$\partial_t \left(\frac{1}{2}\mathbf{u}^2\right) + \nabla \cdot \left(\left(\frac{1}{2}\mathbf{u}^2 + p\right)\mathbf{u}\right) - Re^{-1}\Delta\left(\frac{1}{2}\mathbf{u}^2\right) + Re^{-1}\left(\nabla \mathbf{u}\right)^2 - f \cdot \mathbf{u} \leq 0 \quad (2.2)$$

The impetus for this choice of inequality is grounded in the seminal work of [47] who shows that equation 2.2 is a regularity condition on the Navier-Stokes equations; e.g. solutions of Navier-Stokes satisfying (2.2) posses a set of singularities which must have a particular Hausdorff measure. Weak solutions of Navier-Stokes satisfying (2.2) are called *suitable weak solutions*; it is not a new result, as mentioned by [15], that suitable weak solutions always exist but their uniqueness is still an open question. If $M(\mathbf{u}, p)$ signifies the momentum equation, the first equation of (1.1), applied to $(\mathbf{u}, p)$ then equation (2.2) arises from manipulating $M(\mathbf{u}, p) \cdot \mathbf{u}$, formally (e.g. assuming suitable smoothness), into the form of the left-hand side of (2.2) and then considering the inequality (2.2). If no singularities occur in the solution then the manipulations are justified and $M(\mathbf{u}, p) \cdot u = 0$ will hold, identically; however, if singularities do occur then the inequality $M(\mathbf{u}, p) \cdot \mathbf{u} \leq 0$ says that they must *dissipate* energy [15].

A mechanism ensuring the dissipation of energy is precisely what is necessary in simulations which are under-resolved; as mentioned at the onset of the section under-resolution fuels sub-grid scale gradients which behave singularly and induce energy accumulation at the grid scale. Hence, enforcing (2.2) at the discrete level, for under-resolved flows, would imply that these sub-grid phenomena, behaving in a numerically singular way, would be required to dissipate energy and eventually be lost; much as they would eventually be lost in a resolved flow to the action of viscosity. The operative question then is *how* to enforce 2.2 in practice; enforcing it directly could over-determine the system (1.1). One method, espoused in [15] and

used with much success in the case of hyperbolic conservation laws in [14], is via the construction of a viscosity based on the inequality; this link to the hyperbolic conservation law case spurs the use of the term 'entropy inequality' in relation (2.2). Thus, the inequality (2.2) provides a segue into an entropy-viscosity formulation for Navier-Stokes. Indeed, inspection of (2.2) shows that, in analogy to hyperbolic conservation laws, it strongly resembles an entropy inequality where the kinetic energy, $\frac{1}{2}\mathbf{u}^2$, plays the role of an entropy.

2.2.2.1 An eddy viscosity built from an entropy-viscosity

The pairing of an entropy function and an entropy inequality give rise to a *residual*; this residual can be measured against numerical solutions to determine an amount of violation : the violation quantity is referred to as *entropy production*. In the present case the kinetic energy $E(u) = \frac{1}{2}u^2$ will play the role of an entropy and equation (2.2) will serve as an entropy-inequality. Letting (u_h, p_h) be an approximate velocity and pressure where h denotes the grid scale a discrete numerical residual, $D_h(x,t)$, corresponding to the left-hand side of (2.2) is then given by

$$D_h(x,t) := \partial_t\left(\frac{1}{2}u_h^2\right) + \nabla\cdot\left(\left(\frac{1}{2}u_h^2 + p_h\right)u_h\right) - Re^{-1}\Delta\left(\frac{1}{2}u_h^2\right) + Re^{-1}\left(\nabla u_h\right)^2 - f\cdot u_h. \tag{2.3}$$

The corresponding (discreet) *entropy inequality* is, in analogy with (2.2), given by

$$D_h(x,t) := \partial_t\left(\frac{1}{2}u_h^2\right) + \nabla\cdot\left(\left(\frac{1}{2}u_h^2 + p_h\right)u_h\right) - Re^{-1}\Delta\left(\frac{1}{2}u_h^2\right) + Re^{-1}\left(\nabla u_h\right)^2 - f\cdot u_h \leq 0. \tag{2.4}$$

For resolved flows equation (2.3) is expected to be on the order of the consistency error of the method utilized to evaluate it; e.g. in the continuous case, where (2.3) is evaluated with a smooth solution, (u, p), to (1.1), $D_h(x,t) = 0$ would follow. In the case of under resolved flow (2.3) is expected to differ significantly, in magnitude, from the consistency error of the method in regions of under-resolution; e.g. at points (x_0, t_0) where large gradients in the flow cannot be resolved and are, therefore, effectively behaving in a singular manner with respect to the grid scale. If, as noted in [15], an under-resolution occurs in a neighborhood of (x_0, t_0) and (2.4) holds there then energy is being dissipated by the numerical 'singularity' and is eventually lost in the sub-grid scales; this is no grounds for alarm since such a cascade of energy to lower scales is a physically expected phenomena (see [44] §6.1) and the energy is eventually dissipated at the Kolmogorov scale into heat by viscous action anyhow. Therefore, unresolved gradients dissipating energy may not be desirable but are, at least, not in violation of the physicality of the energy cascade; conversely $D_h(x_0, t_0) > 0$, and substantially larger than the consistency error at (x_0, t_0), presents an non-physical *injection* of energy into the system due to under-resolution effects. [15] go so far as to make the following definition codifying exactly the previous sentiment:

Definition 2.1 *An LES solution is a discrete solution* (u_h, p_h) *to the Navier-Stokes equations satisfying* $D_h(x,t) \leq 0$ *for every* (x,t) *in* $Q_T = \Omega \times [0,T]$.

To construct an LES solution in the sense of [15] (2.4) must be enforced at a discrete level; as mentioned in 2.2.2 enforcing such a condition directly is not a wise approach. Instead the inequality is enforced through the construction of an entropy-viscosity; a viscosity formed from the magnitude of violation of $D_h(x,t) = 0$. The predicating notion is that such a viscosity will introduce localized regularization and thereby damp unresolved gradients; enforcing sufficient resolution and thus the

condition (2.4) in turn. As detailed in [14] the general framework for constructing an entropy-viscosity involves a choice of entropy, an entropy inequality and a positive real-valued functional which need not be linear. Having already mentioned the choice of entropy and entropy-inequality the most obvious positive functional, the absolute value, $R(\phi) = |\phi|$ is selected. The entropy-viscosity can then be defined from these elements by

$$\nu_E(x,t) := \min\left\{ c_{max} h(x) |u_h(x,t)|,\ c_E h^2(x) \frac{|D_h(x,t)|}{||u^2||_{L^\infty(\Omega)}} \right\}. \tag{2.5}$$

The minimum value in equatino (2.5) is taken pointwise between an entropy-viscosity and the first order viscosity $c_{max} h(x)|u_h(x,t)|$; the terms c_{max} and c_E are tunable constants which are expected to depend only on the domain and the particular problem being solved. This definition for the entropy-viscosity, $\nu_E(x,t)$, guarantees that it does not exceed the first-order upwind viscosity as such would be unnecessary. In analogy with (2.1) an LES closure term is then produced from ν_E. This closure model is henceforth termed EV-LES and is given by

$$\nabla \cdot (u' \otimes u') \approx -\nabla \cdot (\nu_E(x,t) \nabla \mathbf{u}_h) \tag{2.6}$$

The discrete version of the system of equations (2.2) is then augmented by the dissipative EV-LES term (2.6); this addition yields the discreet system:

$$\begin{aligned} \partial_t \mathbf{u}_h + (\mathbf{u}_h \cdot \nabla)\, \mathbf{u}_h - \mu \Delta \mathbf{u}_h + \nabla p_h - \nabla \cdot (\nu_E(x,t) \nabla \mathbf{u}_h) &= \mathbf{f}_h \\ \nabla \cdot \mathbf{u}_h &= 0 \\ \mathbf{u}_h(x,0) = \mathbf{u_0}_h(x),\ \mathbf{u}_{h|\partial\Omega} = 0 \ \text{ for all } (x,t) \in \Omega \times [0,T] & \end{aligned} \tag{2.7}$$

Comparing the Smagorinsky-Lilly eddy viscosity closure model term, (2.1), to the

term $-\nabla \cdot (\nu_E(x,t)\nabla \mathbf{u}_h)$ shows that the entropy-viscosity, ν_E, is playing the role of an eddy-viscosity in the LES sense. Naturally, the question still arises as to whether or not the entropy-viscosity provides an effective LES closure model. In the next few sections results from solving the discrete system (1.1) are reported; in order for the entropy-viscosity based LES model to be assumed valid there must be, of course, an emergency of particular well-established physical and statistical phenomena. In particular the Kolmogorov $-5/3$ law must make an appearance. Furthermore the enstrophy, the magnitude of the vorticity of the flow, must behave as expected; the point, overall, is that the efficacy of the proposed entropy-viscosity LES (henceforth EV-LES) closure model can be investigated, at least at the preliminary stages, numerically as a wealth of pre-existing data exists which can be utilized for comparison. The remainder of the discourse for this topic seeks to do precisely that; in the upcoming sections the methodology and results of the implementation of equations (2.7) are reported.

2.3 Implementation and results

This section details the methods by via which the entropy-viscosity LES (EV-LES) model has been implemented thus far and the subsequent tests within the described regime hitherto completed.

2.3.1 Implementation

Our investigations into the efficacy of the entropy-viscosity for regularizing the Navier-Stokes equation are carried out via a well-verified, periodic, spectral code with pseudo-random smoothed initial data and iso-12 forcing. The codebase was written by several contributors at Los Alamos National Lab (LANL) and is discussed in the context of [54] and [28]. Entropy-viscosity in the setting of bounded domains, utilizing an ADI approach found in [12], is currently being investigated by the authors;

results will appear in a forthcoming paper.

The spectral code mentioned above has been well validated; for instance see [5, 54, 28]. Standard 2/3's de-aliasing was utilized in a periodic box of length $L = 1$. The time-stepping scheme implemented is a fully explicit four-stage Runge-Kutta method with dynamic time-stepping respecting the CFL condition. The entropy-viscosity is formed via the canonical pseudo-spectral technique whereby derivatives are computed in spectral space and products in physical space. For this situation, $c_{max} = 0.1$ and $c_E = 0.25$ were used in (2.5). The entropy-viscosity, computed explicitly following (2.5), is formulated using the current time step in conjunction with the two time-steps prior; BDF2 is employed to compute the time derivative. The result is applied, as a regularization, for the next time-step. The action of the entropy-viscosity is not present for the first three time-steps of the simulation; in practice this has caused no stability issues, even in the case of high Reynolds numbers. Finally, the divergence free condition is enforced via the standard Chorin-Temam approach. All the simulations presented here are done with a low-wave number forcing designed to keep the total kinetic energy approximately constant, as described in [42].

2.3.1.1 Tuning the entropy-viscosity coefficients

As evidenced in equation (2.5) the entropy-viscosity, and hence the resulting LES model, is a parametric model; namely the parameters c_E and c_{max} must be determined. These parameters, based on experience with the entropy-viscosity in various paradigms, should depend on the particular problem and the domain only. The process of calibrating the c_E and c_{max} for the spectral code of [54, 28] proceeded under the mantra of 'utilize as little viscosity as possible'. The process was carried out by, effectively, setting one component of (2.5) to infinity and tuning the remaining

component in accordance with its individual perceived role.

The role of c_{max} is to condition the first-order viscosity; the first-order viscosity is utilized when the local entropy production is so large that it exceeds the level of necessity. Towards that end the first-order viscosity should still constitute a sufficient amount as to ensure the flow is sufficiently resolved; e.g. supposing that the first order viscosity is always the minimal choice in (2.5) the flow is expected to emerge resolved. The value of $c_{max} = 0.1$ was found to resolve the energy spectrum of the discretizations $N = 32^3$ and $N = 64^3$. The selected coefficient, in the case $N = 32^3$, provided a distribution of wave modes with transition in, roughly, increments of $1/3$; that is the lower $1/3$ of the wave modes were in the large scale range, the middle $1/3$ comprised the inertial range and the upper $1/3$ were in the range of pronounced viscous effects. Naturally, the case of $N = 64^3$ consisted of slightly more than $1/3$ of the wave modes in the viscous range; this is expected.

The role of c_E is to temper the entropy residual term in (2.5); the fundamental notion underlying the entropy residual term is the injection of as little localized viscosity as possible into the system in order to ensure that the central inequality of definition (2.1) is satisfied. If numerical singularities are too large, in practice, resulting in a large residual then the first-order viscosity term will be selected in (2.5) when the minimum is taken. Such phenomena notwithstanding, the entropy residual term should, effectively, provide local regularization but not be permitted to become so large as to act as a significant source of viscous dissipation. Recalling the discussion in section 2.2.2 the inequality $D_h(x,t) \leq 0$ being enforced ensures that numerical singularities arising from under-resolution are *dissipative* in nature; hence, the expected action of the entropy residual term should be, ideally, to resolve the inertial range of the energy spectrum until the limit of the grid scale is reached. That is, it is expected that the entropy residual term manifest an inertial range until

the highest wave modes of the flow are obtained; these wave modes should then be attenuated by the effective 'viscous action' of the enforcement of the 'dissipative singularities' inequality $D_h(x,t) \leq 0$. This is precisely how the value $c_E = 0.25$ was obtained; c_{max} was set to infinity, to prevent its selection in (2.5), and various values of c_E were tested on grids of resolution $N = 32^3$ and $N = 64^3$. Values larger than $c_E \approx 0.25$ seemed unnecessarily damping while values less than $c_E \approx 0.25$ did not damp enough and permitted energy accumulation in the high wave modes.

2.3.2 Consistency of the EV-LES closure model

In this section a fundamental characteristic of the EV-LES closure model and entropy-viscosity implementation, consistency, is tested numerically. As detailed in section 2.2.2 the residual $D_h(x,t)$ should be on the order of the local consistency error of the method used to evaluate it. This expectation arose, as discussed in 2.2.2, from considering the dot product

$$(\partial_t \mathbf{u} + (\mathbf{u} \cdot \nabla)\,\mathbf{u} - \mu \Delta \mathbf{u} \nabla p - f) \cdot \mathbf{u}$$

of the momentum equation with $\mathbf{u}$ and manipulating the result, formally, into the left hand side of (2.2). The discrete analogue of this process gave rise to the definition of the numerical residual (2.3). Therefore if u_h is a 'good' approximation to a solution of (1.1) and u_h is suitably smooth in a neighborhood of (x_0, t_0) then the expected relation is given, up to the order of the consistency error of $D_h(x_0, t_0)$, by

$$D_h(x_0,t_0) \approx ((\partial_t u_h + (u_h \cdot \nabla)\,u_h - \mu \Delta u_h + \nabla p - f) \cdot u_h) \approx 0 \cdot u_h = 0$$

A direct conclusion of this expectation is that in the case of smooth, laminar flow the entropy residual, and hence the entropy viscosity, should be near zero and therefore

have no noticeable impact on the dynamics of the system; framed in the context of LES this means that the EV-LES closure model is expected to be consistent. The consistency is empirically tested via a comparison of the energy spectra $E(K)$, where K is a wave number, for a laminar flow with and without the EV-LES term; a viscosity of $\mu = 0.02$ was utilized to induce a laminar regime; the plotted energy spectra results are presented in subsequent figures. In each figure, the simulation of laminar flow ($\mu = 0.02$) without EV-LES is indicated with a solid line whereas the laminar regime with EV-LES is indicated by a dashed line.

Figure 2.1: The $N = 32^3$ resolution energy spectrum of a laminar flow is shown without (solid line) EV-LES modeling and with (dashed line) EV-LES modeling.

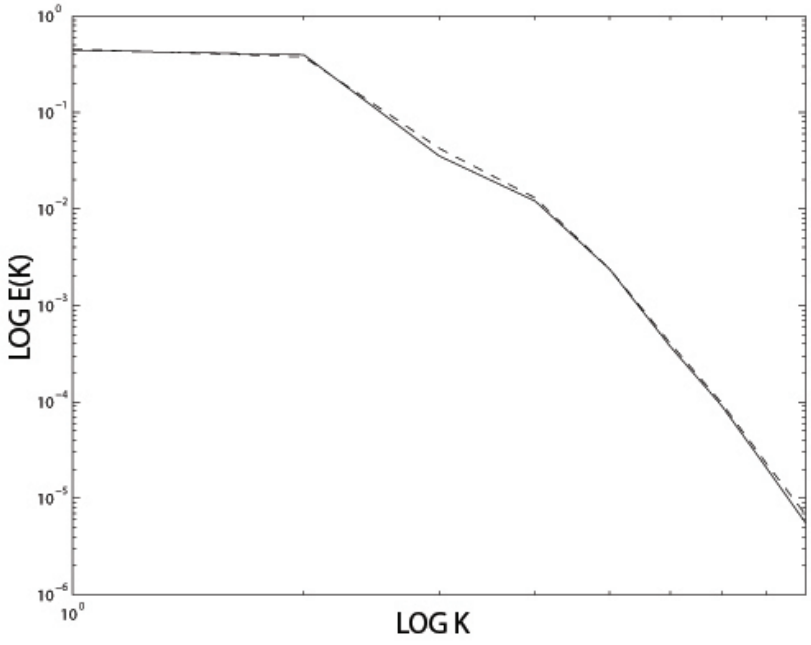

In figure 2.1 the two flows are nearly identical; commentary regarding the fact

that some deviation is not completely unexpected is warranted. As an artifact of the code-base the initial data generated for different runs can vary slightly and thus provide slightly different results; the important facet of figure 2.1 is that not only do the two curves adhere to one another quite tightly but their general topography is nearly identical. The same type of results, as expected, are seen upon refinement to

Figure 2.2: The $N = 64^3$ resolution energy spectrum of a laminar flow is shown without (solid line) EV-LES modeling and with (dashed line) EV-LES modeling. Deviation occurs on the order of 1×10^{-8}

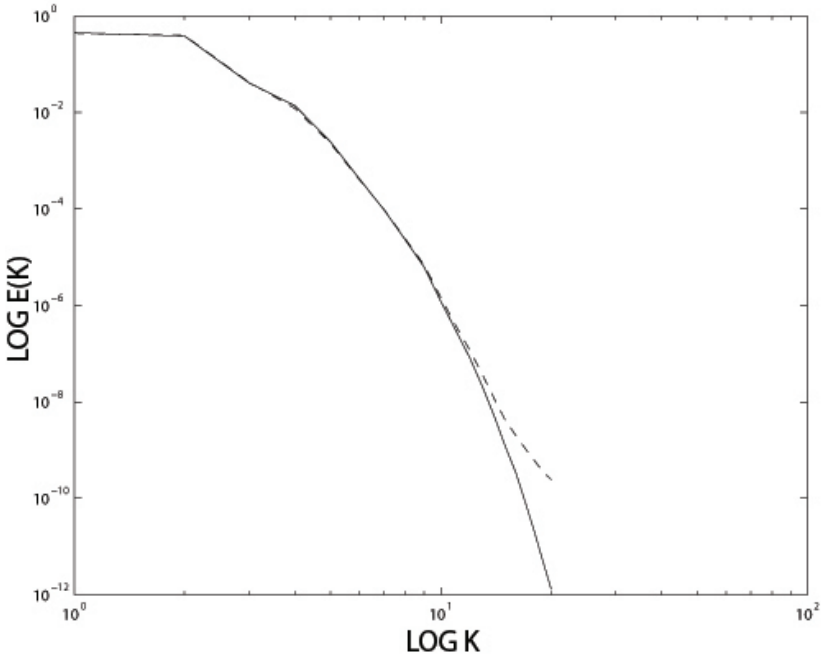

both the 64^3 case, in figure 2.2, and the case of $N = 128^3$ in figure 2.3. In each figure the laminar flow lacking the EV-LES model (solid line) and that with the EV-LES model included (dashed line) closely track one another down to negligible scales on the order of 1×10^{-8} and 1×10^{-10} in the $N = 64^3$ and $N = 128^3$ cases respectively.

In conclusion, the EV-LES term (2.6) was tested numerically for consistency with the

Figure 2.3: The $N = 128^3$ resolution energy spectrum of a laminar flow is shown without (solid line) EV-LES modeling and with (dashed line) EV-LES modeling. Deviation occurs on the order of 1×10^{-10}

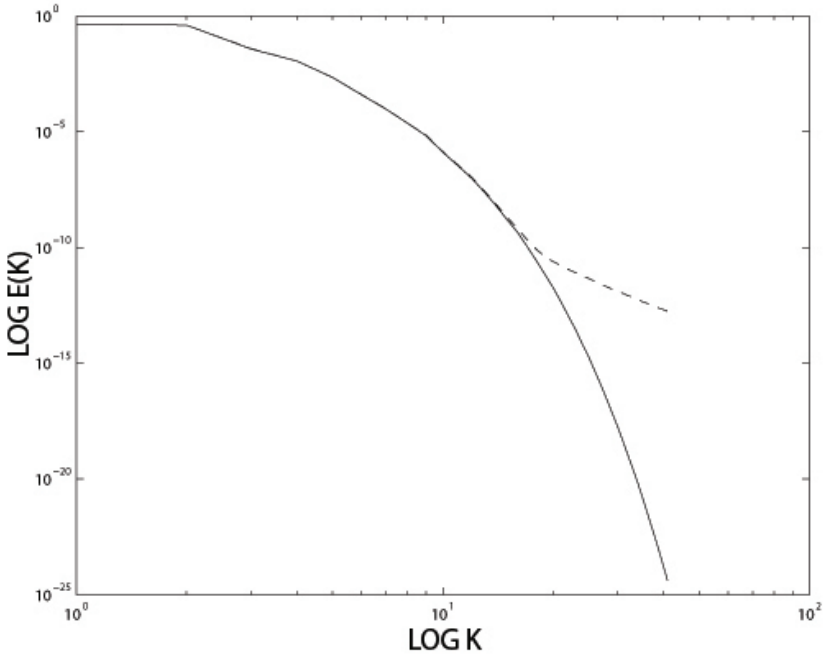

Navier-Stokes equations, via testing against the case of laminar flow, and found to be so up to negligible scales. Furthermore, the discussion of section 2.2.2, predicating this outcome on the basis of the behavior of $D_h(x,t)$ in regions of local smoothness of u_h, has been vindicated in the process.

2.3.3 Energy spectra and the Kolmogorov −5/3 law

2.3.3.1 Background

The Kolmogorov $-5/3$ law refers to a particular expected trend in the energy spectra of flow. An excellent introduction to the law, with subsequent detail regarding current theoretical and empirical work, is given in [51]; we paraphrase their introduction here for posterity. The *scales* of a flow can be thought of as constituting a dichotomy of large and small scale flow; the large scales being on the order of the flow width while the small scales include the inertial range and the Kolmogorov length scale. The inertial range of the flow constitutes, loosely, the scales which are small compared to the large scale but large compared to the small scale. The roles played in the dynamics of the flow by the scales are thus : the large scale commands the transport of mass, momentum and heat while the small scales of the flow dominate with respect to the dissipation of energy. The quantities involved in defining precisely these scales of motion, such as energy dissipation, the two-point velocity correlation tensor, etc are laid out in conjunction with rigorous definitions of the scales in [44] (see §6.5); a belaboring of these quantities, however, is not a necessary facet of describing the Kolmogorov $-5/3$ law. Kolmogorov put forth a hypothesis of *universality* for the phenomena of turbulence at small scales; his hypothesis, as summarized by [51], has two constituent portions:

- When the fluid viscosity, ν, is small the average energy dissipation rate, $\langle\epsilon\rangle$, is independent of ν.

- In a sufficiently high Reynolds number flow regime, turbulent phenomena on the order of the small scales is homogeneous, isotropic, steady and statistically independent of the large scales.

The primary consequences, of concern here, of the Kolmogorov hypothesis are that, statistically, the properties of the dissipation scales are determined by ν and $\langle\epsilon\rangle$ and that properties of the inertial range are determined by $\langle\epsilon\rangle$ alone. Hence, the Kolmogorov hypothesis constitutes a broad reduction in complexity for the statistical analysis of turbulence on the small scales; to see the implications of this reduction in complexity consider a *velocity increment* of the flow. Given a value of r on the order of the scale of the inertial range and a value of $\mathbf{x}$ a velocity increment can be defined by

$$\Delta u_r(\mathbf{x}) = u(\mathbf{x}+r) - u(\mathbf{x}) \tag{2.1}$$

Where u is the velocity *in the direction of* $\mathbf{x}$. For a given value of r define the normalized velocity increment by $\Delta\mathbf{u}_r(\mathbf{x})(r\langle\epsilon\rangle)^{-\frac{1}{3}}$. A result following from the Kolmogorov hypothesis is that the following statements are equivalent [51]:

- The probability density function of a normalized velocity increment is universal; that is, it is independent of $\mathbf{x}$, r. or the Reynolds number. E.g. a normalized velocity increment, regarded as a random variable, has a probability density function independent of its constituent parameters: r, $\mathbf{x}$ and Re.

- The moments of the velocity increment, also referred to as *longitudinal structure functions*, satisfy $\langle\Delta\mathbf{u}_r^n\rangle = \mathbf{C}_n(r\langle\epsilon\rangle)^{n/3}$ where $\mathbf{C}_n$ are universal constants.

According to [51] the value of $\mathbf{C}_n$ is currently only known for the third-order longitudinal structure function; the relation, called the *Kolmogorov -4/5 law*, is given by

$$\left\langle\Delta u_r^3\right\rangle = -\frac{4}{5}r\langle\epsilon\rangle \tag{2.2}$$

Kolmogorov derived this relation by assuming an isotropic, homogeneous regime of turbulent flow. Finally, from [51], if one considers the the spectral equivalent for the

expression $\langle \Delta \mathbf{u}_r^n \rangle = \mathbf{C}_n (r \langle \epsilon \rangle)^{n/3}$ in the case of $n = 2$ the retrieved result is

$$\phi(\kappa) = C \langle \epsilon \rangle^{2/3} \kappa^{-5/3} \tag{2.3}$$

Where $\phi(\kappa)$ is the one-dimensional spectrum of energy in the wavenumber component κ in the direction of $\mathbf{x}$.

2.3.3.2 Verification

In this section a foray into verifying the Kolmogorov $-5/3$ relation, (2.3), is laid out; the implementation details for the spectral codebase and entropy-viscosity were given in section 2.3.1. The approach for verification that the EV-LES model produces the expected $-5/3$ energy spectrum was:

- In the absence of the EV-LES closure term: find a physical viscosity, ν_{256}, at which a simulation with the number of grid points given by $N = 256^3$ is a DNS simulation, e.g. the full range of scales are suitably resolved, but for which simulations consisting of $N = 128^3, 64^3$ and 32^3 are not resolved.

- Add the EV-LES closure term to the simulated equations; the expected behavior is not only a stabilization to resolution, with clear inertial range and attenuation of the energy spectrum at high wave modes, but also the qualitative appearance of the $-5/3$ slope in the inertial range of the energy spectrum.

The results are shown in the following figures; $\nu_{256} = 0.0002$ was found, through trial and error, to accomplish the stated goal. In each figure the 256^3 DNS simulation, without the EV-LES term, is shown as a solid black line. The dashed lines in each figure show the results of a particular resolution, changing by figure, without EV-LES and the dot-dashed lines show that same resolution with the EV-LES term modeled. The thicker solid black line, present in all figures, demonstrates the $-5/3$ slope for

comparison of the inertial range. A few things to keep in mind : as the resolution decreases so does the range of wave-modes present in the energy spectrum. Hence, the case of the 256^3 DNS is expected to have a 'longer' spectrum whereas those cases with lower resolution will have progressively 'shorter' spectra. Each simulation was run for a total time of $T = 3$ seconds with iso-12 forcing; the DNS simulation $N = 256^3$ was stopped at $T = 2.1$ seconds as it had achieved steady state well before and was a costly computation. These ending times were more than adequate for the appearance of isotropic turbulence.

Figure 2.4: The $N = 128^3$ resolution case is shown without (dashed line) EV-LES modeling and with (dot-dashed line) EV-LES modeling. The "No Model" 256^3 DNS simulation (solid line) and Kolmogorov $-5/3$ (thick solid line) slope are included for comparison.

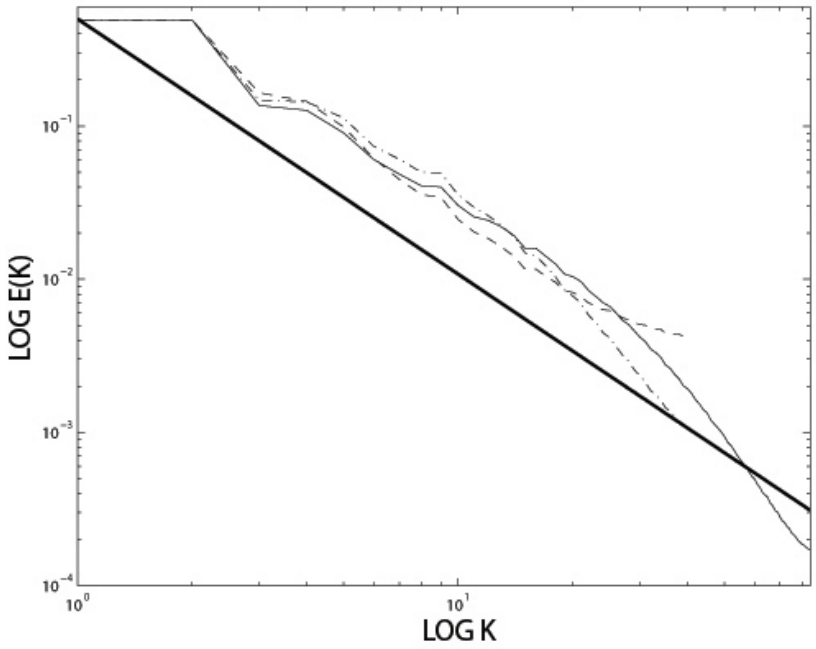

Figure 2.5: The $N = 64^3$ resolution case is shown without (dashed line) EV-LES modeling and with (dot-dashed line) EV-LES modeling. The "No Model" 256^3 DNS simulation (solid line) and Kolmogorov $-5/3$ (thick solid line) slope are included for comparison.

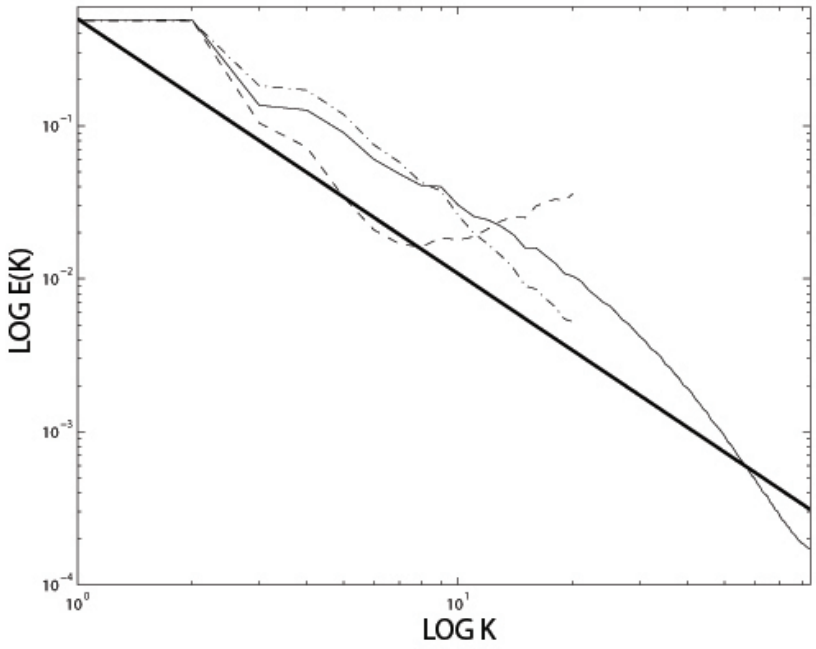

There are a few facets of interest in figure 2.4 which warrant mention; first, notice that the solid line, representing the $N = 256^3$ DNS case, shows a clear inertial range with a strongly damped high wave-mode range. This behavior indicates that the resolution of $N = 256^3$ properly represents all scales of the flow as we see the smaller scales, corresponding to higher wave numbers, being dominated by the energy dissipation induced by the choice of viscosity $\nu_{256} = 0.0002$. Secondly, the 'up-tick' in the $N = 128^3$ spectrum which lacks the EV-LES term (dashed line) is precisely the 'accumulation of energy at the grid scale' mentioned by [15] and referenced in section 2.2.2. The expectation is that, given enough time, the non-regularized $N = 128^3$ case

Figure 2.6: The $N = 32^3$ resolution case is shown without (dashed line) EV-LES modeling and with (dot-dashed line) EV-LES modeling. The "No Model" 256^3 DNS simulation (solid line) and Kolmogorov $-5/3$ (thick solid line) slope are included for comparison.

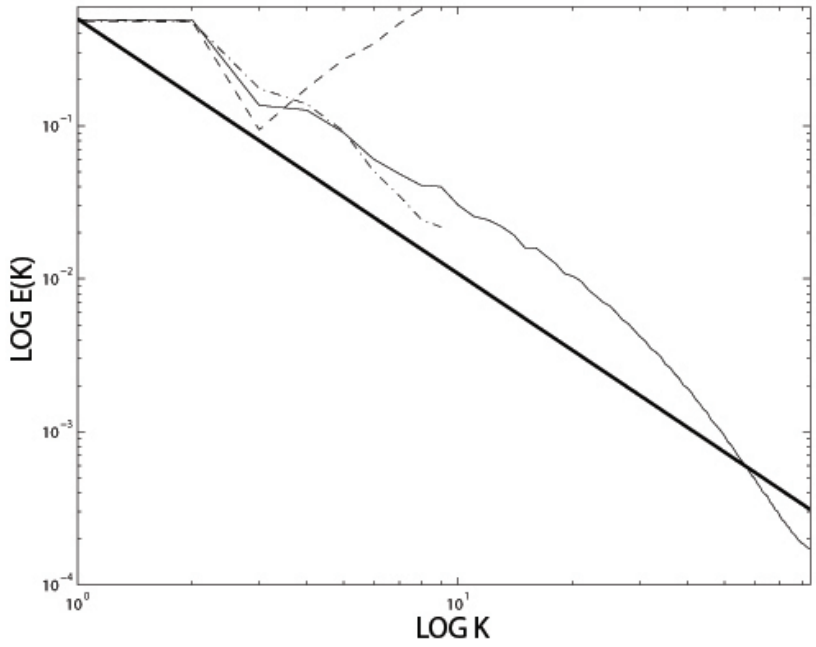

would accumulate the energy introduced by the forcing in increasing amounts until it produced a numerical blow-up.

Figure 2.5 offers increased insight into the efficacy of the EV-LES closure model; in particular the 'up-tick' on the non-regularized (dashed line) spectra is more pronounced. This is entirely expected; the lower the resolution, the more quickly the simulation accumulates energy in its latter wave modes due to the inability to resolve even more gradual gradients of the velocity. The pronounced effect that the EV-LES term presents is encouraging; notice that the introduction of the term presents a spectrum which, topologically, more closely resembles the spectrum of the 256^3 case

and exhibits the expected $-5/3$ behavior in the inertial range.

Finally, figure 2.6 is even more dramatic. The non-regularized (dashed line) flow is egregiously under-resolved; the 'up-tick' in the higher wave modes accumulates with a rapidity such that it is near the blow-up state after only $t = 3$ seconds. The impact of the EV-LES term is striking in this regard; not only does the flow exhibit facets of the resolved DNS simulation (solid line) but it appears to track the $-5/3$ Kolmogorov line as well. At the current time verification of the production of the $-5/3$ behavior of the EV-LES term is the only facet of the structure functions that has been undertaken; more results in this direction are forthcoming.

2.3.4 Behavior of the enstrophy

Enstrophy is defined as the euclidean magnitude of the vorticity one-tensor $\omega = \nabla \times \mathbf{u}$; the characteristics of enstrophy structures in turbulent flow is a well studied phenomena. Vorticity (enstrophy) tubes appeared, as predicted by some turbulence theories of the time, in the landmark simulation of [27]. Since then the presence of vorticity tubes has been studied and noted by other authors in the field [6, 37, 51]; more recent advances have shown that such vorticity structures appear in quantum turbulence generated in superfluid helium [3]. A primary concern for the proposal of the EV-LES model is the reproduction of known effects; to this end the requisite vorticity filaments produced in past simulations and experiments should be a manifest occurrence in the EV-LES model.

The qualitative investigation into the presence of vorticity filaments, at this stage, was tested in the context of two different regimes; a fully resolved DNS flow and an under-resolved flow. In both cases a test was run without EV-LES and, subsequently, with EV-LES active. It is expected that the vortex filaments should surface in the context of DNS with the addition of the EV-LES term as this term is expected to

Figure 2.7: Vortex filaments at a resolution of $N = 256^3$ mesh points

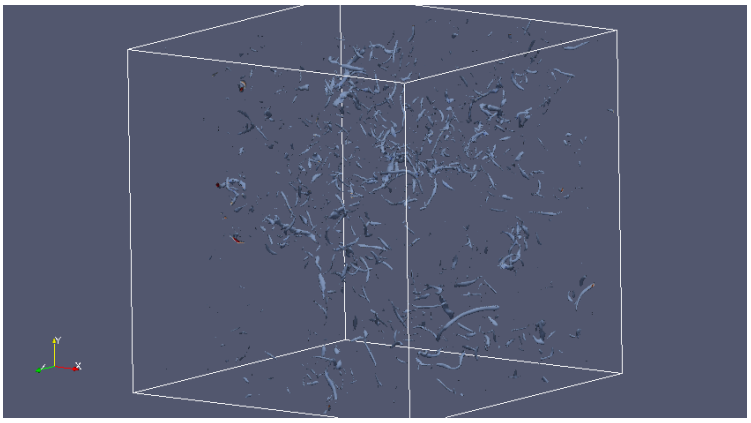

(a) DNS

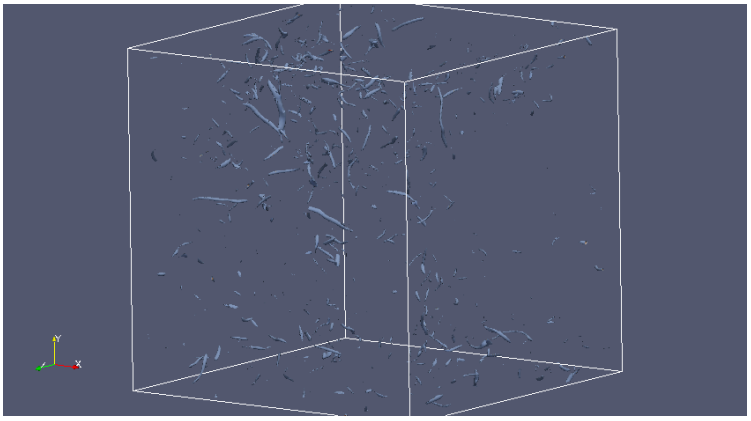

(b) EV-LES

be, and according to numerical tests actually is, consistent with the Navier-Stokes equations; at least in the discreet case. The results of the DNS run can be seen in figure 2.7. Quantitative properties, such as the mean radius of vortex filaments, have not yet been measured. Of more interest, however, is the case of an under-resolved flow (without EV-LES) and a flow resolved with the assistance of the EV-LES term; the operative query being whether or not the EV-LES term would "clear up" the excessive accumulation of energy, due to under-resolution, at the grid scales and "reveal" the presence of vorticity filaments at all. Figure 2.8 shows a clear display of

Figure 2.8: Surfaces of constant enstrophy. $N = 64^3$, $\nu = Re^{-1} = 2 \times 10^{-4}$

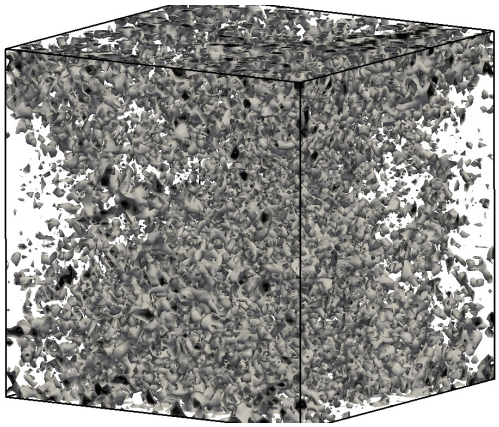

(a) DNS

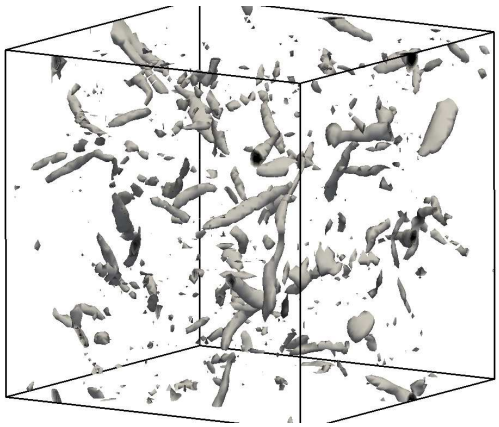

(b) EV-LES

the action of the effect of under-resolution and the subsequent effect of EV-LES. In the DNS case the accumulation of energy in the high wave modes causes subgrid-scale 'noise' pollution of the simulation whereas, when EV-LES is utilized, the sub-grid scale 'noise' has been suitably dissipated by the turbulence model term to evince the appearance of vortex filaments. The result is a visual manifestation of the enforcing of the defining inequality underlying definition 2.1.

3. A ONE-STAGE LEVEL SET METHOD WITH ENTROPY-VISCOSITY

3.1 Overview

In this section a brief outline of the current state of motion tracking for evolving interfaces in two-phase (or multi-phase) flows is discussed; among such techniques is the so-called *level set method*. Early iterations of the level set technique are mentioned in brief followed by mention of a proposed, novel one-stage technique based on the seminal works of [17] and [40]. The novelty of our technique arises from the fact that it is a one-stage procedure which captures well the full space level set function; whereas other recent iterations of the technique discussed involve at least two stages to achieve the same goal. One-stage methods for level set techniques are not entirely new; It should be noted that the work of [57] is an impressive one-stage technique for tracking a single (interface) level set, based on a one-stage re-distancing technique. Such an approach has implications for problems such as fluid buckling or other regimes where quantities are computed based only on a single (interface) level set.

A two-phase flow regime refers to a system containing a gas and a liquid; the phases are generally considered separated by an interface, called a meniscus, whereby relative physical quantities, such as density or viscosity, across the interface are considered to be discontinuous. A multi-phase flow refers to the obvious generalization of the notion of a two-phase flow. One of the main issues when constructing a numerical approach to the solution of such flows is the issue of tracking the motion of the evolving interfaces in the system; the approaches to this problem in the literature are varied. [46] offers an introduction of several methods; the survey categorizes the methods via the dichotomy of *fixed grid* and *moving-grid / adaptive-grid* but

focuses on the former with mention of sources for the latter. Within the family of *fixed grid* methods two popular approaches are *marker* and *volume of fluid* methods. Within the *marker method* category are surface and volume markers; the former utilizes markers located only on the fluid interface(s) while the latter utilize markers throughout the domain. [41] comments that the marker method incurs difficulty in regimes embodying large, complex motion. For instance, coalescing markers in regions of building curvature can introduce instabilities in the absence of re-gridding whereas regridding can introduce local error; marker methods can also suffer from topological issues such as the necessity to resort to ad-hoc methods to determine connectivity when regions coalesce. [46] cites [11] as well as [56] for further reading on the marker method.

Volume of fluid methods are also discussed in the survey; such methods entail the assignment of a *fraction of fluid* quantity to each cell in the mesh and the interface is constructed via a reconstruction technique. Due to the reconstruction of the interface the actual boundary of the advancing front is, in fact, not tracked; instead the interior of the region is tracked while advected and the boundary is reconstructed as a best-fit approximation. The reconstruction technique is by no means unique and [46] cite several options (ELVIRA, PY, least squares, etc); the reconstructed interface is then advected according to the underlying flow field. Conservation law implementation based such volume-of-fluid methods are thereby two-stage, advect-reconstruct, methods; furthermore, the curvature of the interface can be difficult to ascertain from the reconstruction. The inability to reliably reconstruct the curvature of the interface, especially for complex flows, can have an impact on the underlying physics of the model; for example, correctly prescribing surface tension, encountered in rising bubble problems, relies on the curvature of the interface.

Another popular method for the advection of fluid interfaces is the level set

method introduced in [41]. Our interests regarding the level set technique is the treatment of a front propagating with respect to an underlying vector field, $\mathbf{U}$; this particular case is treated in by the author as an auxiliary problem after the development of a more general theory. The poignant details, for our concern, is that a family $\gamma(t)$ of smooth, closed parametric curves can be considered to be generated by advecting an initial smooth curve, $\gamma(0)$; the interior of the region enclosed by the front is denoted Ω. The authors consider the front to be level sets of a function $\phi(x, y, t) = C$ (or $\phi(x, y, z, t) = C$ in three dimensions) where C is an arbitrary but fixed constant and ϕ satisfies the conditions

$$\phi(\mathbf{x}, 0) = \begin{cases} > 1, & x \in \Omega \\ \quad 1, & x \in \partial\Omega \\ < 1, & x \in \Omega^c \end{cases}$$

The equation satisfied by by ϕ is shown to be

$$\begin{aligned} \phi_t + \mathbf{U} \cdot \nabla\phi &= 0 \\ \phi(\mathbf{x}, 0) = (1 - d(\mathbf{x}, \Omega))^+ &+ d(\mathbf{x}, \Omega^c) \end{aligned}$$

Where $x^+ := \max\{\mathbf{x}, 0\}$. In practice, see for instance [52], the initial data for ϕ is taken to be the signed distance to the interface; hence the interface is zero level set of ϕ. One issue with the level set method, as pointed out in both [52] and [40], is that proceeding an advective step (or steps) the function ϕ is no longer a distance function and therefore requires a *re-distantiation* procedure; furthermore, the method in which this procedure is typically carried out is not conservative. The non-conservative nature of the canonical re-distancing incurs a loss of area; this issue is corrected in [40] where a conservative re-distantiation technique is introduced.

Consider a hyperbolic conservation law regularized with a first order viscosity $-\epsilon\Delta\phi$:

$$\phi_t + u \cdot \nabla\phi - \epsilon\Delta\phi = 0$$

Where ϕ is a discontinuous phase function in a two-phase flow having $\phi = 1$ in the first phase and $\phi = 0$ in the second phase. In the literature such a phase function is generally approximated and the advection takes place without the use of regularization; [52] utilize a mollified delta function with thickness in proportion to the spatial mesh size while [40] utilize a smeared Heaviside function. Long-time numerical solutions of this problem are known to introduce dispersion error. Towards this end we consider the addition of a term of the form $C = \epsilon\nabla \cdot (\phi(1-\phi)\frac{\nabla\phi}{|\nabla\phi|})$ to offset these dispersive effects; the term C is called an *artificial compressive flux*. We will build both our regularization term, R, and compression term, C on the foundation of the *entropy-viscosity* introduced in [14]; the forms of these terms will given respectively by

$$\mathbf{R} = -\nabla \cdot (\nu_E \nabla\phi) \quad \mathbf{C} = \nabla \cdot \left(\frac{\nu_E}{h}\phi\,(1-\phi)\,\frac{\nabla\phi}{|\nabla\phi|}\right)$$

This is not altogether a new concept; [17] introduces the concept of an artificial compressive flux and applies it in the context of monotonic finite difference schemes for hyperbolic conservation laws with Riemann initial data; it is shown that the monotonic schemes induce dispersion and that the compressor term acts to correct this error and maintain the fidelity of the propagation front. The author relies on the monotonic scheme to act as the regularization term whereas we make no such assumption and include an explicit regularization; furthermore, our regularization also has natural localization due its dependence on the entropy viscosity and we there-

fore expect the formulation to be somewhat independent of the chosen discretization. Towards this end we will utilize a finite element discretization. Further, the entropy-viscosity offers a natural method of constructing a compressor; where [17] builds an artificial compressor at each time step, when the location of shocks is unknown, we may utilize the entropy-viscosity from the regularization which embodies the knowledge of shock locations. Since the entropy-viscosity is based upon entropy production it carries with it the 'knowledge' of the locations of the shock fronts (as mentioned in section 1.2: see [45]); it therefore lends itself naturally to this venture.

3.2 One-dimensional heuristics

The objective of this section is to analyze in detail the one-dimensional setting as an impetus for a general formulation; the viewpoints herein are not new but are presented to aid in the conceptualization of the general formulation. Consider the one-dimensional transport equation in the whole space domain $\Omega = \mathbb{R}$:

$$\partial_t u + \beta \partial_x u = 0, \quad (x,t) \in \mathbb{R} \times \mathbb{R}_+, \quad u(x,0) = u_0(x) \tag{3.1}$$

It is further assumed that $\beta > 0$ is constant for simplicity; the solution is simple transport along the one-parameter family of characteristic lines in the (x,t) plane, with slope $\frac{1}{\beta}$, given by $x = \beta t + x_0$.

$$u(x,t) = u_0(x - \beta t) \tag{3.2}$$

For later comparison it is briefly recalled how this is established; if we consider a frame of reference moving in the (x,t) plane along the characteristics of equation (3.1), given by the coordinate transformation $\hat{x} = x + \beta t$, then equation (3.1) is

expressed in this frame as

$$\frac{d}{dt}\hat{u} = 0, \quad (\hat{x}, t) \in \mathbb{R} \times \mathbb{R}_+, \quad u(\hat{x}, 0) = u_0(x) \tag{3.3}$$

Where $\hat{u}(\hat{x}, t) = u(x + \beta t, t)$. In the case when the transported quantity is a physical variable, such as density or other material property, the initial data is often piece-wise constant and discontinuous; under such circumstances the function u is referred to as *multi-phase*. The discrete values of the range are referred to as the *phases* of u. High order numerical techniques for solving (3.1), such as continuous finite element and Lax-Wendroff schemes, can introduce spurious oscillations at discontinuities or, in the case of Lax-Friedrichs, damp high wave-number contributions and result in excessive smoothing. (see, e.g. [2]). In order to address such issues a perturbation of (3.1) is considered

$$\partial_t u + \beta \partial_x u - \epsilon \partial_{xx} u = 0, \quad (x, t) \in \mathbb{R} \times \mathbb{R}_+, \quad u(x, 0) = u_0(x) \tag{3.4}$$

The dissipation term, $-\epsilon \partial_{xx} u$ has a regularizing effect on the solution; more specifically, employing the aforementioned moving frame via the change of variables $\hat{x} = x + \beta t$, equation (3.4) becomes the heat equation for $\hat{u}(\hat{x}, t) = u(x + \beta t, t)$.

$$\frac{d}{dt}\hat{u} - \epsilon \partial_{\hat{x}\hat{x}} \hat{u} = 0, \quad (x, t) \in \mathbb{R} \times \mathbb{R}_+, \quad \hat{u}(x, 0) = u_0(x) \tag{3.5}$$

The solution $\hat{u}(x, t)$, and by a linear change of variables $u(x, t)$, is therefore smooth for all times $t > 0$ and given by the formula

$$\begin{aligned}\hat{u}(x,t) &= \frac{1}{\sqrt{4\pi\epsilon t}}\int_{-\infty}^{\infty} e^{-\frac{(x-\xi)^2}{4\epsilon t}} u_0(\xi)d\xi \to u(x,t) \\ &= \frac{1}{\sqrt{4\pi\epsilon t}}\int_{-\infty}^{\infty} e^{-\frac{(x-\beta t-\xi)^2}{4\epsilon t}} u_0(\xi)d\xi \end{aligned} \tag{3.6}$$

This regularity inducing effect is not limited to linear conservation equations; the addition of a viscous regularization term, $\epsilon\partial_{xx}u$, to the right hand side of the nonlinear in-viscid burgers equation

$$\partial_t u + u\partial_x u = 0, \quad (x,t) \in \mathbb{R}\times\mathbb{R}_+, \quad u(x,0) = u_0(x) \tag{3.7}$$

allows for linearization by a Cole-Hopf transformation $u = -2\epsilon\phi^{-1}\partial_{xx}\phi$.

$$\begin{aligned} \partial_t u + u\partial_x u - \epsilon\partial_{xx}u = 0 \quad &\to \quad \partial_x(\phi^{-1}\partial_t\phi) = \epsilon\partial_x(\phi^{-1}\partial_{xx}\phi) \\ \partial_x\left(\phi^{-1}\partial_t\phi\right) = \epsilon\partial_x\left(\phi^{-1}\partial_{xx}\phi\right) \quad &\to \quad \partial_t\phi - \epsilon\partial_{xx}\phi = \phi f(t) \end{aligned} \tag{3.8}$$

The resulting equation for ϕ, after substitution of $u = -2\epsilon\phi^{-1}\partial_{xx}\phi$ into (3.8), is once more the heat equation, choosing the arbitrary function $f(t)$ to be zero, and the solution is thereby smooth. A brief historical perspective on the introduction of an artificial *numerical viscosity* to systems of conservation equations is offered in the introduction of [17]. In addition, existence and uniqueness results of solutions to more general systems of such viscous perturbations of hyperbolic conservation equations, their regularity, requirements on initial data and the convergence of the method of vanishing viscosity ($\epsilon \to 0$) is put forth in [9]; see for instance §7.3.2(b).

In both the linear and nonlinear cases put forth the addition of dissipative regularization facilitates a reduction to solving the heat equation. The Gibb's phenomena, which can be excessive when solving (3.1), or likewise (3.7), with discontinuous ini-

tial data and high order numerical schemes, is eased when those schemes are applied instead to the regularized equations (3.4), likewise (3.8); a cost is paid in the loss of numerical accuracy for long-time solutions due to accumulation of dissipation effects. The original intent being the solution to equation (3.1), likewise (3.7), a logical next step is the introduction of a counter-balancing term to offset the dissipative effects of the viscous regularization. This is precisely the underlying context first proposed by [17], embodied by the concept of an *artificial compressor* for dissipative finite difference schemes applied to Riemann problems, again by [41] for propagating flame fronts where the balancing depends on the local curvature of the front and once more by by [40] in the context of the level set method applied to two-phase transport; subsequent coupling of level set methods with conservation laws was also discussed in [38]. Each of the aforementioned papers applied their respective corrective procedures for the dissipative effects of the utilized regularization as a 'second phase' of their numerical procedure; thus these methods can be classified as two-step procedures.

It is the theme of this paper to utilize the addition of a counter-dissipation term, $g(u)$, allowing for the advent of a novel one-step procedure which achieves similar effects as the pre-existing two-step approaches. We motivate the regularization heuristically in two ways : one physical impetus is given and one heuristic impetus, based on the Harten artificial compressor approach, is given; both a one-dimensional and general formulation is presented in section 3.2.3.

3.2.1 Physical motivation

Consider two perfectly conducting, thin metal rods each of infinite length and of uniform initial temperature. Assume that, with respect to a reference temperature $K > 0$, the leftward rod is fixed at temperature $T = 1$ while the rightward rod is fixed at temperature $T = 0$. Suppose further that these two rods are then brought

together; inducing seamless contact at the origin. Let $V = [-L, L]$ be an interval in $\mathbb{R}$ with $L >> 0$ and let $u(x,t)$ represent the heat per unit volume contained in the adjoined rods at the point x and time t. It is known that the change in total heat in the region V is governed by the relation

$$\frac{d}{dt}\int_V u dx = -\int_{\partial V} F \cdot n dS \rightarrow \frac{d}{dt}\int_V u dx = -\int_V div(F) dx \tag{3.9}$$

Where F is the flux density through the boundary of V and the divergence theorem has been applied to achieve the right-hand relation. Furthermore, in the case of many physical quantities such as heat, we have the relation that $F = -\lambda \partial_x u$ for some $\lambda \in \mathbb{R}$. Continuing un-abetted in this direction will lead to a derivation of the canonical heat equation; instead, suppose that it is desirable to maintain, as much as possible, the original temperatures of the two rods. That is we seek to approximate, with a smooth function, the initial state of

$$u_0(x) = \begin{cases} 1 & : x < 0, \quad \forall t \geq 0 \\ 0 & : x > 0, \quad \forall t \geq 0 \end{cases} \tag{3.10}$$

In order to accomplish this suppose a distribution, tightly packed with uniform spacing $0 < h << 1$ from each other, of infinitesimal warming and cooling sensors are placed perfectly on the surface of the conjoined rods in the regions $x < 0$ and $x > 0$, respectively. These theoretical sensors are designed to counteract the canonical heat-flux field induced by the joining of the rods. At the moment the rods touch, heat begins to flow and the distribution of heat is smoothed; the sensors are then activated by their measuring of the heat distribution, $u(x,t)$, at some positive time $t_0 \approx 0$. Given the physical paradigm, what is known regarding the behavior of heat, and the desired affect of the counterbalancing term it is reasonable to set for the following

requirements for $g(u,t)$:

- In order to counteract the flow of heat the counterbalancing term, induced by the sensors, at time $t_0 > 0$ should be supported in the region given by the set $\{x \in \mathbb{R} | u(x,t) \in (0,1)\}$

- The sensors which generate the counterbalancing term sample the current heat distribution; therefore the counterbalancing term should depend only on u. E.g. $g(u,t) = g(u)$. Furthermore, the heat distribution is continuous and therefore, since $g(u)$ should not introduce discontinuity, $g(u)$ should be continuous in u.

- Since the initial state was given by equation (3.10) the state at time $t_0 > 0$ will satisfy $\partial_x u \in [-C, 0]$ for some $C > 0$. That is, the heat flux ($F = -\partial_x u$) is positive and hence directed from the hot leftward region towards the cold rightward region.

- Since $F = -\lambda \partial_x u$ is the the flux to be balanced the sign of the counterbalancing term, $g(u)$, should be equal to the sign of $\partial_x u$. As $h \to 0$ the counterbalancing term should exactly oppose the heat flux; it is therefore reasonable to assume that the counterbalancing term is in proportion to the heat flux and the proportionality constant is a function of h.

- Physically, the temperature should decrease in the hot region at the same rate as it increases in the cold region; therefore the counterbalancing term should be symmetric about the point of contact of the rods and the temperature there should be the average of the initial condition extremities. Since $g(u)$ depends on u alone this implies that the function $\tilde{g}(u) = g(u + T_0)$ should be an even function of u where T_0 is the temperature at the point of contact of the rods. In this case, $T_0 = \frac{1}{2}$

- Since the rods are infinite in length and heat propagation distance is finite for finite times it follows that the far extremities of the leftward rod should have temperature $T \approx 1$ and the far extremities of the rightward rod should embody temperatures $T \approx 0$.

From these items an equation, as well as boundary conditions, can be extracted as well as properties of $g(u)$; see equations (3.11), (3.12) and (3.13). The approximation of

$$-\lambda\partial_x u + C(h)g(u) = 0 \quad C(h) \geq 0, \quad lim_{h\to 0}C(h) = 1 \quad 0 < h << 1 \tag{3.11}$$

$$\begin{aligned} &u(0,t) = \tfrac{1}{2}, && \forall t > 0 \\ &\lim_{x\to\infty} u(x,t) = 0, && \forall t \in [0,\infty) \\ &\lim_{x\to-\infty} u(x,t) = 1, && \forall t \in [0,\infty) \end{aligned} \tag{3.12}$$

$$\begin{aligned} &g(u) \in C^1(\mathbb{R}) \\ &g\left(-\left(u+\tfrac{1}{2}\right)\right) = g\left(u+\tfrac{1}{2}\right) && \forall u \in \mathbb{R} \\ &g(u) < 0 && \forall u \in (0,1) \\ &g(u) = 0 && u \in \{0,1\} \end{aligned} \tag{3.13}$$

Resuming the derivation (3.9) and employing the notion of the balancing flux, $g(u)$, the flux field F, now comprised of the concentration dissipation term and the counterbalancing term, is given by $F = -\lambda\partial_x u + C(h)g(u) = 0$ so that, for $t > t_0$, we have the integral relation

$$\frac{d}{dt}\int_V u dx = -\int_V div(F)dx \to \int_V \partial_t u - \lambda\partial_{xx}u + \partial_x g(u)dx = 0 \tag{3.14}$$

Letting $V = [-L, L]$ denote an arbitrary symmetric sub-domain of $\mathbb{R}$ yields that the equation to consider for time $t \geq t_0 > 0$ is given by

$$\partial_t u - \lambda \partial_{xx} u + \partial_x \left[g(u) \right] dx = 0, \quad u(x, 0) = \tilde{u}(x, t_0), \quad t > 0 \tag{3.15}$$

Where $\tilde{u}(x, t_0)$ denotes the solution to the usual heat equation with discontinuous initial data at time t_0; e.g. this represents the solution before the counterbalancing sensors are activated. As per previous mention equation (3.15) is augmented with boundary values given by (3.12); furthermore $g(u)$ should be selected such that the conditions (3.13) also hold.

3.2.2 Motivation via an artificial compression

In this section the artificial compression method (ACM) of [17] is first briefly outlined; the level set method, a popular front capturing scheme, is then shown to be in the spirit of an ACM. A conservative level set method proposed by [40] is, in particular, discussed for the artificial compression flux (ACF) it employs; these two perspectives provide the foundation for another route of motivation for our proposed one-step method.

3.2.2.1 An overview of Harten's artificial compression method (ACM)

The concept of an *artificial compressor* and the resulting *artificial compression method (ACM)* was proposed first by [17]; Harten begins by outlining a need for the ACM, via a class of dissipative finite difference schemes, and then proceeds to present the ACM as a correction technique. In this seminal work, non-linear conservation laws of the form (3.16) were considered.

$$\partial_t u + \partial_x \left[f(u) \right] = 0, \quad u(x, 0) = u_0(x), \quad -\infty < x < \infty \tag{3.16}$$

In the case of intersecting characteristic lines classical solutions fail to exist; hence weak solutions to (3.16) are considered and are defined by their satisfaction of the integral relation

$$\int_0^\infty \int_{-\infty}^\infty \left[\phi_t u + \phi_x f(u)\right] dxdt + \int_{-\infty}^\infty \phi(x,0)u_0(x)dx = 0 \tag{3.17}$$

Where $\phi(x,t)$ is any smooth compactly supported test function. The weak formulation (3.17) admits piecewise continuous solutions of the original equation (3.16) which satisfy the Rankine-Hugoniot condition (3.18) where (u_L, u_R, S) are the values of u to the left and right, respectively, of the discontinuity and S is the speed of propagation of the point of discontinuity.

$$f(u_R) - f(u_L) = S(u_R - u_L) \tag{3.18}$$

In general equation (3.17) is not well posed in the sense that uniqueness cannot be established in the class of all weak solutions; hence one approach for determining physically relevant weak solutions is to consider those solutions obtainable as the limit of the viscous problem (3.19) as $\epsilon \to 0$ [17]; the maximum principle allows for only a single solution.

$$\partial_t u^\epsilon + \partial_x \left[f(u^\epsilon)\right] = \epsilon \partial_x \left[\beta(u^\epsilon)\partial_x u^\epsilon\right], \quad \epsilon > 0, \quad \beta > 0 \tag{3.19}$$

To utilize the vernacular of Harten's treatise: a discontinuity (u_L, u_R, S) is said to possess a *viscous profile* if a solution to (3.19) exists of the form $u^\epsilon(x,t) = V(\frac{x-St}{\epsilon})$ with $lim_{x-St\to\infty} = u_R$ and $lim_{x-St\to-\infty} = u_L$. Condition (3.20) then characterizes when a viscous profile exists for a discontinuity (u_L, u_R, S); the condition is equivalent to an entropy condition first presented by [39], cited by Harten, which characterizes

the types of discontinuities (u_L, u_R, S) that can arise in the limit solution of (3.19).

$$\begin{aligned} [g_0(u) - C]\, sgn(u_R - u_L) > 0, \qquad & \forall u \in (u_L, u_R) \\ g_0(u) := f(u) - Su, \qquad & C := g_0(u_L) = g_0(u_R) \end{aligned} \tag{3.20}$$

Harten discusses a class of numerical schemes, called *monotone schemes*, and cites several results pertaining to them; among the most notable is that discrete solutions to monotone schemes behave in similar fashion to solutions of a corresponding modified parabolic equation (see [19]) given by

$$\partial_t w + \partial_x \left[f(w) \right] = \Delta t \partial_x \left[\beta(w, \lambda) \partial_x w \right], \quad \beta(w, \lambda) \geq 0 \tag{3.21}$$

and that (see [25]) monotone schemes which are also in *conservation form* posses steady advancing fronts which are discrete versions of viscous profiles that arise in the solution of the viscous limit problem (3.19) as $\epsilon \to 0$

Finally Harten cites a now famous result of [31] which states that finite difference schemes in conservative form which converge boundedly almost everywhere do so to weak solutions of (3.16). The quintessential conclusion here is two-fold : namely that monotonic schemes, by way of equation (3.21), act as a method of regularization and that monotonic schemes in conservation form yield weak solutions which satisfy the entropy condition (3.20) characterizing limit discontinuities. Harten then introduces *artificial compressors* as a method of correcting the dissipation introduced in solving (3.21), e.g. solving (3.16) with a monotonic finite difference scheme, and details an implementation of an artificial compressor in a two-phase approach. The theoretical motivation is to consider the original problem, equation (3.16), and supposing a solution is obtained which possesses a shock, or contact discontinuity, given by $(u_L, u_R, S(t))$; the speed of propagation is therefore $S(t)$ and across the discontinu-

ity the solution u jumps from u_L to u_R. Instead of solving the original problem, (3.16),Harten proposes to solve a problem of the form

$$\partial_t u + \partial_x \left[f(u) + g(u,t) \right] = 0, \quad u(x,0) = u_0(x), \quad -\infty < x < \infty \tag{3.22}$$

Where $g(u,t)$, the *artificial compressive flux (ACF)*, is any function satisfying properties (3.23) and (3.24)

$$g(u,t) = 0, \ \forall u \notin (u_L, u_R) \tag{3.23}$$

$$g(u,t) sign \left[u_R(t) - u_L(t) \right] > 0, \ \forall u \in (u_L, u_R) \tag{3.24}$$

After presenting the definition of an artificial compressive flux (ACF) Harten then proves compatibility for the modified equation with ACF; the proof can be found in [17].

Theorem 3.1 [*Harten*] *Suppose $u(x,t)$ is a solution to equation* (3.16)*; then if $g(u,t)$ is an ACF, $u(x,t)$ solves* (3.22)*. Furthermore, the entropy condition for the modified equation,* (3.22)*, is also satisfied.*

The remainder of the paper is focused on an analysis of certain numerical schemes applied to (3.16) and (3.22); it is shown that the same numerical scheme produces better results, having more resolved shocks and contact discontinuities, when applied to the latter equation. The refined results are therefore attributable to the presence of the ACF; numerical results are given.

3.2.2.2 A conservative level set method as an ACM

In the conclusion of [17] a generalized description of a method for augmenting a pre-existing numerical scheme with a *compression phase* is outlined. Furthermore, a particular conservative level set method, proposed by [40], can be seen as an application of Harten's approach to the area of *front tracking methods*.

Not every level set method is an ACM; in general a level set method refers to some method in which a *level set function*, usually a distance function, is used to represent a boundary or front between two or more regions. For example [41] employs a level set technique for modeling curvature-dependent front propagation, [38] to that of gas dynamics, and [52] to two-phase flow. Letting Γ denote the boundary of transition from one area of interest to another a canonical level set approach is to utilize a a level set function, $|\phi(x,t)| = \min_{y\in\partial\Gamma}|y-x|$; e.g. a signed distance function such that $\phi(x,t) > 0$ on one side of Γ and $\phi(x,t) < 0$ on the other. In such a case, the level set $\phi = 0$ is the interface in question and, at some point, is acvected via a conservation equation; in [52] $\partial_t\phi + (u\cdot\nabla)\phi = 0$ is utilized whereas in [38] a Hamilton-Jacobi like equation, $\partial_t\phi + F(\mathbf{x})|\phi|$, is employed where $F(\mathbf{x})$ is the magnitude of the normal direction to the (level set) front at $\mathbf{x}$.

[24] clearly describe the historical difficulty inherent in the canonical level-set approach; essentially, mass conservation is generally not enforced when advecting the level-set function, ϕ, and the level set function can therefore lose its initial status as a distance function as advection transpires. With the advantage that particular schemes employed to advect the level-set function can automatically handle topological changes, such as merging fronts etc, comes the disadvantage that with enough advection the level set function loses its defining characteristic of being a distance function all-together. At some point a *re-distancing* procedure must be carried out

to re-imbue ϕ with this property; [52] offer many first-generation type details on re-initializing the distance function as well as the loss of mass conservation incurred by failure to do so.

The re-initialization procedure, necessitated by the lack of conservation of mass when advecting a level set function, is costly; [52] mentions that initial efforts at such incurred $O(n^3)$ time complexity, where n is the number of spatial grid points, and offers an iterative approach based on solving an intermediate problem to steady state after every time-step to re-initialize ϕ as a distance function. For sizable physical problems, considered as being solved in the context of large parallel computations, the sheer number of communications that would arise in the re-distancing procedure, stemming from a complex boundary, is conceivably quite daunting. [43] put forth a localized method of re-distancing which alleviates the necessity for a global computation; while more palatable the approach is a four-step method, albeit on a significantly reduced portion of the grid. One method of avoiding the need to re-distance all-together is to introduce some mechanism for mass conservation; it was the novel approach of [40] to propose a conservative method for this process by adapting the work of Harten.

The remainder of this sections is dedicated to describing the method of [40] and explicating its link to the the ACM of [17]. A smoothed Heaviside function is utilized, $\phi(x) := H_\epsilon(x)$, as an approximation to a level set function; this outlook acts analogously to the smoothing affect espoused by Harten's proposed monotonic schemes. Assuming a divergence free velocity field, $\nabla \cdot \mathbf{u} = 0$, the level set is advected by the standard conservation law

$$\partial_t \phi + \mathbf{u} \cdot \nabla \phi = 0 \quad \rightarrow \quad \partial_t \phi + \nabla \cdot (\mathbf{u}\phi) = 0 \tag{3.25}$$

Following this advection a corrective step, an artificial compressor-like phase, is then solved via equation (3.26); Kreiss utilizes a bit of extra, constant viscosity which is not utilized explicitly by Harten's formulation. The function $f(\phi)$ is defined by be $f(\phi) = \phi(1-\phi)\frac{\nabla\phi}{|\nabla\phi|}$

$$\partial_\tau \phi + \nabla \cdot f(\phi) = \epsilon \Delta \phi \quad \rightarrow \quad \partial_\tau \phi + \nabla \cdot \tilde{f}(\phi) = 0 \tag{3.26}$$

The right hand side of equation (3.26) is the recasting into conservative form where $\tilde{f}$ is defined by $\tilde{f}(\phi) = f(\phi) - \epsilon \nabla \phi$. Equation (3.26) is then solved to steady state before the next advection; the parameter τ is utilized in lieu of t to signify a false time and appropriate boundary conditions are prescribed. The choice of the level set function $\phi(x) = H_\epsilon(x)$, in the context of Harten, signifies that $u_L = 0$ and $u_R = 1$. Therefore an application of conditions (3.23) and (3.24) shows directly that $\tilde{f}(\phi)$ is an ACF for the modified equation (3.22) with initial data $u_0(x) = H(x)$. After reaching a steady state the compressed result is utilized as the initial data for the next advection; the conservation of the interface level set avoids the need to reinitialize the level set 'distance' function.

3.2.3 A proposed one-step approach

The conclusion of [40], pertinent to our proposal, is that the utilization of the Harten ACM technique allowed for the creation of a conservative level-set adaptation which avoids the need for the canonical re-initialization of the distance function. The primary drawback being that the general ACM method, as described in [17] and utilized in [40], requires an intermediate compression phase solved to steady state; to its credit, however, the method should be lauded for its accomplishments regarding the abdication of re-distancing which, at best, was a four-step procedure (see [43]). We seek to alleviate this two-phase facet of the approach via proposition

of a one-step method taking motivation from the discussions in sections 3.2.1 and 3.2.2; furthermore utilization of an entropy based viscosity in the formulation will be leveraged for its natural efficacy in front-tracking methods. The formulation of the proposed one-step approach is first broached without the entropy-viscosity for clarity; entropy-viscosity is then briefly explained and introduced into the model.

3.2.3.1 The one dimensional case with constant viscosity and compression coefficients

give you control over the gradient of u via modification of the compression function. This can act as a segue into the entropy-viscosity. Maybe recast this discussion in that light.

For the time being, attention is still restricted to the one-dimensional case; recall that the original problem we wish to solve is of the form given in equation (3.1) with piecewise linear, discontinuous initial data $u_0(x) = 1 - H(x)$. In order to abet issues arising from high order methods introducing spurious oscillations at shock fronts a small viscosity is added to (3.1) yielding (3.4) which facilitates a reduction to equation (3.5). As outlined in the motivation sections, 3.2.1 and 3.2.2, the addition of a term $\nu\partial_x g(u)$ is considered to counter-balance the dissipation. The resulting equation therefore has the form (3.15) and, for the time being, we assume the initial data is a smoothed step function as given in equation (3.15); contrary to the more general formulation, equation (3.22), we consider the compressive term to depend only on u.

Based on the discussion in the physical motivation section the desired goal is to approximate the solution to (3.1), with the initial step data $u_0(x) = 1 - H(x)$, via the use of the artificial compressive flux $g(u)$ such that the result approaches a smoothed-step configuration of $u_0(x)$ with small transition region. The boundary

conditions (3.12) are assumed to augment equation (3.15) and the conditions on $g(u)$ are assumed given by (3.13). Under these assumptions the following small lemma is proved quite easily:

Lemma 3.1 *Suppose that u is a classical solution to* (3.15) *with boundary conditions* (3.12) *and let* $g := g(u)$ *satisfy the properties given by* (3.13)*. If u reaches a steady state, e.g.* $\partial_t u = 0$*, then there exists* x_0 *such that* $[\nu g(u) - \lambda \partial_x u](x_0) = 0$

Proof. Suppose $\partial_t u = 0$ but no such x_0 exists; therefore by assumption

$$\forall x, \quad [\nu g(u) - \lambda \partial_x u](x) = f(x)$$

Furthermore, the function $f(x)$ is always non-zero. To rule out that, possibly, $f(x) = C$ for some $C \in \mathbb{R}$ assume that $f(x)$ is constant. It follows from (3.12) and (3.13) that

$$\lim_{x \to \pm\infty} [\nu g(u) - \lambda \partial_x u](x) = \lim_{x \to \pm\infty} \lambda \partial_x u(x) = C$$

Suppose without loss of generality that $C > 0$, a similar line of argument will hold for $C < 0$, then this implies that there exists $L > 0$ such that on the complement of the set $[-L, L]$ the function u is strictly increasing in x. This contradicts the limiting assumptions of (3.12). It therefore follows that $C = 0$ which contradicts $f(x) = C$ nonzero. Therefore the function $f(x)$ is non-constant and hence $\partial_x f(x) \neq 0$. Since u, by hypothesis, solves (3.15) it follows that

$$\partial_t u + \nu \partial_x g(u) - \lambda \partial_{xx} u = 0 \to \partial_t u + \partial_x [\nu g(u) - \lambda \partial_x u] = 0$$

$$\partial_t u + \partial_x [\nu g(u) - \lambda \partial_x u] = 0 \to \partial_t u + \partial_x [f(x)] = 0$$

$$\partial_t u + \partial_x [f(x)] = 0 \to \partial_t u = -\partial_x f(x) \neq 0$$

So that $\partial_t u \neq 0$ and u has not reached steady-state; this contradiction proves the claim. □

The effect of this small result is that, under a steady-state assumption, it can be precisely demonstrated what the solution to certain compression cases will be and judge the impact of the parameters ν and λ. For our choice of initial data the shock discontinuity in the non-smoothed initial data, $u_0 = 1 - H(x)$, is characterized by $(u_L, u_R, S) = (1, 0, \beta)$; in light of the Harten ACF requirements, equations (3.23) and (3.24), and motivated by the ACF of [40] the compression term is selected as

$$\nu g(u) = \nu u(u-1), \quad \nu > 0 \tag{3.27}$$

Note immediately that the compression (3.27) satisfies all three of the base criterion given by (3.13); ν is a positive constant which, as we discuss later, is chosen to posses the necessary units to ensure dimensional consistency. Inspired by [40] assume that u is a steady-state solution to (3.15), (3.12) with ACF (3.27). Equation (3.28) follows where $k(t)$ is, for each t, the constant of integration; by lemma 3.1 it follows that $k(t) = 0$.

$$\nu \partial_x g(u) - \lambda \partial_{xx} u = 0 \rightarrow \quad \nu g(u) - \lambda \partial_x u = k(t) \tag{3.28}$$

$$\nu g(u) - \lambda \partial_x u = \rightarrow \quad \kappa = \frac{1}{g(u)} \partial_x u \tag{3.29}$$

Where $\kappa = \frac{\nu}{\lambda}$, in tribute to Harten's vernacular, is termed the *artificial compression coefficient* (ACC); solving an equation of the form (3.29) is straightforward if the function $(g(u))^{-1}$ is integrable in u. Assuming this is the case (3.29) can be recast as $G`(u)\partial_x u = 1$, where $G`(u) = (g(u))^{-1}$; integrating both sides with respect

to x will yield an implicit equation for u which can then be solved algebraically or by other means. With $g(u)$ given by equation (3.27) the resulting equation is (3.30) which yields equation (3.31) for u; differentiation, with respect to x, also yields (3.32)

.

$$ln\left(\frac{1-u}{u}\right) = \kappa x + c(t) \tag{3.30}$$

$$u\left(x,t\right) = \left(1 + e^{\kappa x + c(t)}\right)^{-1} \tag{3.31}$$

$$\partial_x u\left(x,t\right) = \frac{-\kappa e^{\kappa x}}{(1+e^{\kappa x})^2} \tag{3.32}$$

Figure 3.1: Steady state solutions, $u(x,t)$, for various κ

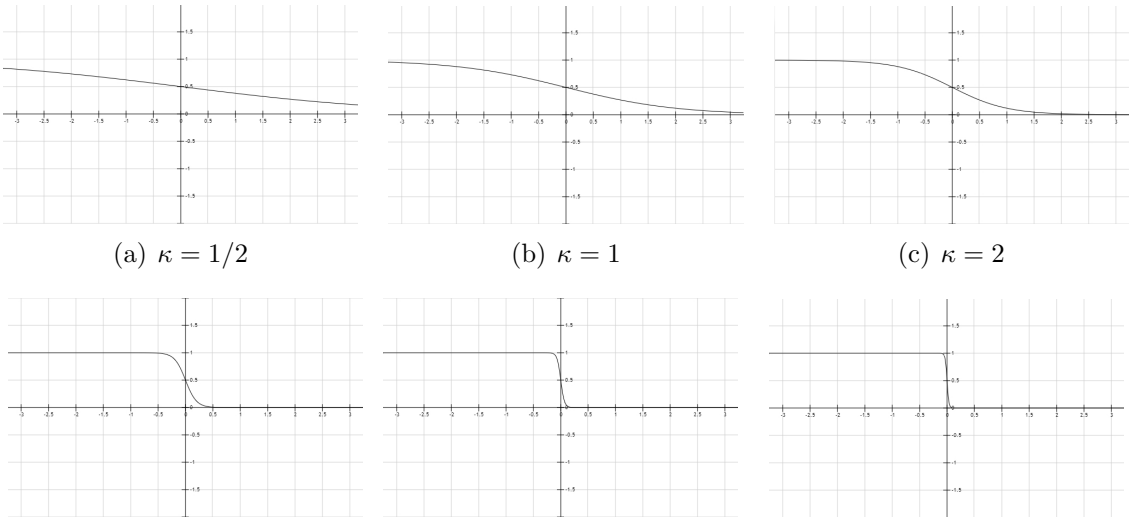

(a) $\kappa = 1/2$ (b) $\kappa = 1$ (c) $\kappa = 2$

(d) $\kappa = 10$ (e) $\kappa = 30$ (f) $\kappa = 60$

Applying the boundary conditions (3.12) yields $c(t) = 0$; the limiting boundary conditions, as $x \to \pm\infty$, are seen to be satisfied. The effects of varying the ACC,

$\kappa = \frac{\nu}{\lambda} > 0$, on the solution are shown in figure 3.1. If the steady state solutions for various κ are considered then a description of the width of the transition region, which from figure 3.1 clearly depends on κ, can be endeavored utilizing the closed form in equation (3.31) with $c(t) = 0$. Intuitively, the transition region is *where the level set function undergoes the most pronounced phase change* or, equivalently, where the change from $u \approx 1$ to $u \approx 0$ is most noticeable. From figures 3.1 and 3.2 it is evident that as $k \to \infty$, the derivative, $\partial_x u$ tends to a negative delta function, $-\delta_0(x)$, at zero. Hence $|\partial_x u| = ke^{kx}(1+e^{kx})^{-2}$ approximates a delta function at zero as $k \to \infty$; in addition a quick computation shows that $\int_{\mathbb{R}} |\partial_x u||dx = 1$ for all $\kappa > 0$. Therefore, since $|\partial_x u|$ approximates a delta function as $\kappa \to \infty$ and the region of transition is, intuitively, where the derivative is nonzero, a region of transition can conceptualized as a set E such that the integral over that set of $|\partial_x u|$ nearly coincides with unity.

Figure 3.2: Steady state graphs of $|\partial_x u(x,t)|$ for various κ

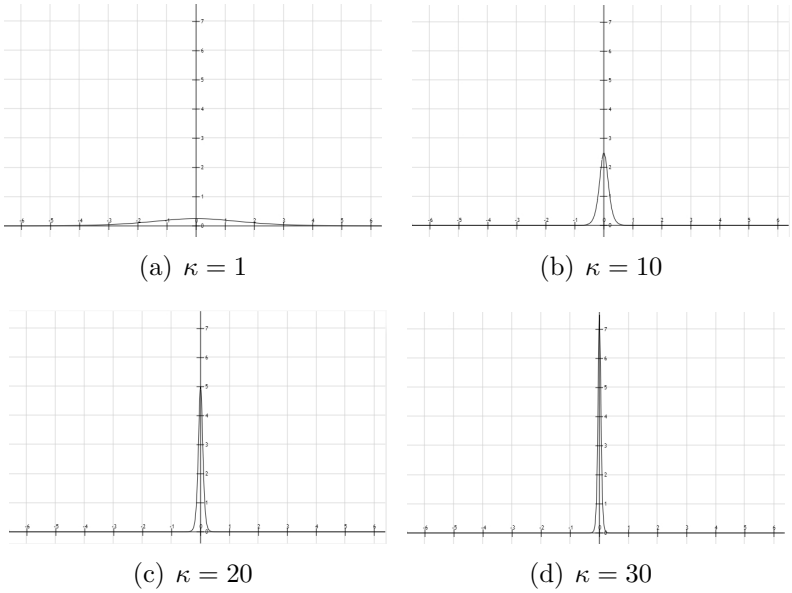

(a) $\kappa = 1$ (b) $\kappa = 10$

(c) $\kappa = 20$ (d) $\kappa = 30$

Definition 3.1 *Suppose that $u(x,t)$ is a steady-state solution to equation* (3.15) *with boundary conditions* (3.12). *Let $0 \leq \gamma < 1$ be a fixed quantity. Then the region of transition associated to γ is defined by the set $E_\gamma = [-L, L]$ satisfying*

$$\int_{-L}^{L} |\partial_x u(x,t)| dx = \gamma \tag{3.33}$$

(3.32) provides the following small result

Corollary 3.1 *If the ACF is selected as given in equation* (3.27) *then transition regions E_γ for a steady state solution to* (3.15), *with boundary conditions* (3.12), *satisfy $E_\gamma = [-L, L]$ where $L = \kappa^{-1}\left(ln\left(\gamma+1\right) - ln\left(1-\gamma\right)\right)$*

Proof. Definition 3.1 and equation (3.32) give

$$\gamma = \int_{-L}^{L} |\partial_x u(x,t)| dx = \left(1 + e^{-\kappa L}\right)^{-1} - \left(1 + e^{\kappa L}\right)^{-1}$$

After algebraic manipulation this leads to the equation

$$e^{\kappa L} - e^{-\kappa L} = 2\gamma + \gamma e^{\kappa L} + \gamma e^{-\kappa L}$$

Letting $\mu = e^{\kappa L}$ and gathering like terms leads to a quadratic equation in μ

$$\left(1-\gamma\right)\mu^2 - 2\gamma\mu - \left(\gamma+1\right) = 0 \quad \rightarrow \quad \mu \in \left\{\tfrac{\gamma+1}{1-\gamma}, -1\right\}$$

Since $\kappa \geq 0$ and $L \geq 0$ it follows that $\mu = e^{\kappa L} \geq 1$ therefore $\mu = \frac{\gamma+1}{1-\gamma}$. Taking logarithms and using $\mu = e^{\kappa L}$ yields the result.□

The final conclusion presented by corollary 3.1 is that for any fixed $0 \leq \gamma < 1$ the transition region $E_\gamma = [-L, L]$ has the property that $L \to 0$ as $\frac{1}{\kappa}$; that is $L = O(\frac{\lambda}{\nu})$

so that the width of the transition region is inversely proportional to the ACC with proportionality constant determined by γ.

typical approach for level set methods is to begin with a smoothed level-set function, with smoothing on the order of several grid spaces, in order to avoid excessive spurious oscillation in the resulting solution. Ideally a piece-wise discontinuous level set function would be preferred as this paradigm is more representative of multi-phase flow; one advantage of considering equation (3.15) is that a smoothing step is essentially 'built in' and such initial data are thereby permissible. It is quite straightforward to see the action of the smoothing heuristically; suppose that $u_0(x) = 1 - H(x)$ is the backwards facing Heaviside step function. It follows that $\partial_x u_0(x) = 0$ almost everywhere so that equation (3.15), with $g(u) \in C^1(\mathbb{R})$, reduces to the heat equation at time $t = 0$. Another way to see this is numerically; if one were to utilize, say, an explicit time-stepping scheme to solve equation (3.15) the first evaluation of the spatially discretized right-hand side will not have the compression term present

3.2.3.2 The general case and the utilization of an entropy-viscosity based ACC

In section 3.2.3.1 the case of constant λ and ν, thus a constant ACC $\kappa = \frac{\nu}{\lambda}$, was considered. In this section we consider $\nu = \nu(\mathbf{x})$ and $\lambda = \lambda(\mathbf{x})$ constructed based off of an *entropy residual*. Consider a brief dimensional analysis of equation (3.15) with $g(u)$ given by equation (3.27).

$$\partial_t u + \nu \partial_x \left(u \left(u - 1 \right) \right) - \lambda \partial_{xx} u = 0$$

Comparing the units of each term, specifically the viscous and compression terms, we have $\frac{\nu u}{h} = \frac{\lambda u}{h^2} \rightarrow \nu = \frac{\lambda}{h}$. Comparing the first and third term yields $\frac{u}{t} = \frac{\lambda u}{h^2}$ so that, as expected, $\lambda = \frac{h^2}{t}$ has units of viscosity. Therefore $\nu = \frac{\lambda}{h} = \frac{h^2}{t}\frac{1}{h} = \frac{h}{t}$ has units of *velocity*. If we consider equation (3.15) with smooth initial data it is evident

that the presence of the viscosity λ is not needed except to prevent the ACF term, $\partial_x g(u)$, from creating a shock; therefore if the viscosity, λ, were somehow able to be localized around the region of transition, E_γ, the introduction of unnecessary dissipation could be avoided. A simple, first-attempt, ad-hoc localization might be procured by considering (3.15) with a space-time viscosity defined in terms of $E_\gamma = [-L, L]$ by

$$\lambda(x) = \begin{cases} 0 & L > L_0 \text{ or } x \notin [-L, L] \\ \lambda_0 & L < L_0 \text{ and } x \in [-L, L] \end{cases} \tag{3.34}$$

This approach would avoid dissipation outside of a particular transition region. If, instead, a piece-wise linear initial data, such as the backwards step $u_0 = 1 - H(x)$, were considered in lieu of smoothed data then the transition region would be the degenerate set $E_\gamma = \{0\}$; this would force the use of some approximate transition region $\tilde{E}_\gamma = [-\epsilon, \epsilon]$. However, any $\epsilon > 0$ would technically introduce 'too much' viscosity; the appropriate viscosity to introduce in this case would be a delta measure. The concept of a transition region is essentially an attempt at *shock capturing*; in turn, equation (3.34) is therefore a viscosity constructed from a shock-capturing technique. One particularly efficacious method of shock capturing, utilized for systems of hyperbolic conservation laws, is *entropy production*; entropy production is measured in terms of an *entropy residual*. [45] has shown, numerically, that entropy production in this context is concentrated at shocks and contact discontinuities for certain central-difference discrete schemes and that the extent of the concentration intensifies as the spatial grid spacing tends to zero. The numerical usage of entropy production is not new;[1] utilize spurious entropy production to produce *a posteriori* error estimations and applies these estimates to adapt local mesh refinements while [45] utilizes this quantity to track shocks and to provide local scheme adaptations

(e.g. linear versus nonlinear terms).

Drawing attention once more to the simplistic model viscosity (3.34) it is seen that the shock capturing artifact, E_γ, is utilized to construct a localized viscosity. Based on this attempt at introducing viscosity in the neighborhood of a shock, the natural 'shock capturing' behavior of entropy production is suggestive of good candidacy for the foundation of the construction of a local viscosity for use in numerical schemes. This novel, but evolutionary, concept was put forth in [14]; at each step a (variable) viscosity is computed by evaluating a residual based on the entropy and this viscosity is utilized in the (stabilized form of the) Galerkin formulation to evince the solution method. The entropy production is expected, as in [45], to tend to zero in regions where the solution in smooth, on the order of the local truncation error, and become pronounced at shocks. [14] perform copious tests of entropy-viscosity applied to both linear and nonlinear conservation laws for known model problems; the entropy-viscosity performs quite well. It is worthwhile to note that the construction of a localized entropy based on a residual is not a novel concept; e.g. in [26] a PDE residual is utilized as a foundation for a localized viscosity. The original contribution of [14] is the formation of a localized viscosity based on an entropy residual; as discussed in [14], in the context of Burger's equation, the entropy residual can be non-zero even when the PDE residual vanishes in a distributional sense.

The essential details of the entropy-viscosity formulation are as follows : an entropy function, E, is selected, an entropy pair, (E, F), is constructed, a discreet entropy residual, $D_h(x,t)$, based on that pair is measured, numerically, and from this residual, at each time step, a viscosity, to be utilized for the next time step, is constructed. The reader is referred to [14] for a more involved discussion as well as numerical results. For posterity the equation of the entropy-viscosity can be considered as

$$\nu_E = \min\left(c_E h^2 |D_h(x,t)|/||E(u_h) - \overline{E}(u_h)||_{\infty,\Omega} \ , \ c_{max} h |u|\right) \tag{3.35}$$

Where h represents the local grid size, c_E and c_{max} are tunable constants, which depend on the approximation technique and the domain, and single vertical bars represent absolute value. It is expected that $D_h(x,t) \approx 0$ for smooth solutions or in regions of smooth solution; see for instance [14, 45]. Returning to the initial problem, linear transport of discontinuous data, discussed in section 3.2 the entropy viscosity method, in arbitrary dimension proceeds by augmenting the model problem with the entropy-viscosity regularization term; see equation (3.36).

$$\partial_t u + \beta \cdot \nabla u = 0 \quad \rightarrow \quad \partial_t u + \beta \cdot \nabla u = \nabla \cdot (\nu_E \nabla u) \tag{3.36}$$

Before giving the multi-dimensional analogue of equation (3.15) we make mention of a detail which, while not neglected, has been obscured somewhat. In section 3.2.1 a physical motivation was put forth which, among other things, detailed that the counterbalancing compressive flux should be directed opposite the dissipation. Furthermore, the dissipation in section 3.2.1 was determined by $-\partial_x u$ and hence directed towards $-\frac{\partial_x u}{|\partial_x u|}$; it follows that the counterbalancing compressive flux should act in the direction $\frac{\partial_x u}{|\partial_x u|}$. Re-examining the ACF requirements of [17] note that the requirements put forth by equations (3.23) and (3.24) is precisely a codification of this detail. In one dimension dispersion acs in the direction sign$[u_L - u_R]$; hence (3.23) says that compression only acts where dispersion is active and (3.24) dictates the direction that the compression acts. Figure 3.3 provides an illustration of the compressive flux direction for each case.

In higher dimensions the direction of dispersion and compression require the use of a unit vector to control their action; a sign is no longer sufficient on its own;

Figure 3.3: Compressive flux directions

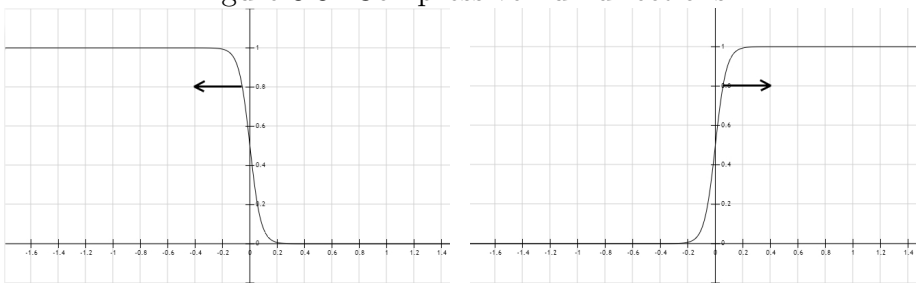

(a) $u_L > u_R$; leftward compression (b) $u_L < u_R$; rightward compression

in high dimension the compression is, in analogy with the one-dimensional case, directed along the unit vector $-\frac{\nabla u}{|\nabla u|}$. The compression should therefore be directed along the negative direction, $\frac{\nabla u}{|\nabla u|}$. This motivation fully explicates the appearance of such a term in the conservative level set method proposed by [40]; more specifically the version of the ACF selected therein is

$$g(\phi) = \nabla \cdot \left(\phi (1 - \phi) \frac{\nabla \phi}{|\nabla \phi|} \right). \tag{3.37}$$

There is no concern as to whether or not the function to be compressed resembles a forwards or backwards step; the sign of the unit normal in (3.37) handles the issue. Our aim is to incorporate this term into the proposed single-phase method; thus far the single-phase method has the form of equation (3.36). to do so it is necessary to balance the units of equation (3.37) with those of equation (3.36). This procedure was carried out at the beginning of the section and carries through in the exact same manner so that in order to incorporate the full-dimensional compression term (3.37) into the entropy-viscosity transport equation (3.36) the compression term must be pre-multiplied by units of *velocity*. A local velocity is constructed from the entropy-viscosity via $\frac{\nu_E}{h}$ where $h = h(x)$ is the local grid size. Finally, the fundamental

n-dimensional form of the one-stage advection-diffusion-compression equation is

$$\partial_t u + \beta \cdot \nabla u + \nabla \cdot \left(\nu_E h^{-1} \left[u \left(1 - u \right) \right] \frac{\nabla u}{|\nabla u|} \right) - \nabla \cdot \left(\nu_E \nabla u \right) = 0 \tag{3.38}$$

Note that the artificial compression coefficient (ACC) for the compressive action of equation (3.38) is $\kappa = \frac{\nu_E h^{-1}}{\nu_E} = h^{-1}$; corollary (3.1) sets the expectation that as $h \to 0$ the width of the transition region also goes to zero for smooth steady-state solutions of (3.38).

3.2.4 Controlling compressive behavior

In the course of numerical application some minor modifications to the general form of equation (3.38) have been formulated in order to produce some impact on various paradigms and difficulties that arise in practice. This section details three minor modifications to the general equation:

- A *steady-state* or *minimum* compression is introduced and a corresponding first-order *steady-state* or *minimum* viscosity is added
- A *compression strength* coefficient is added
- A small parameter $\epsilon \approx 0$ is introduced into the gradient residing in the denominator of the compressive in order to prevent the presence of removable singularities; these cause *division by zero* computational errors.

These three facets are addressed in the order they are presented; beginning with the steady-state, or minimum, compression term. Let $\alpha_{min} > 0 \in \mathbb{R}$ and $g(u) :=$

$u(1-u)$; consider the modification to the compressor given by

$$\nabla \cdot \left(\nu_E h^{-1} g\left(u\right) \frac{\nabla u}{|\nabla u|} \right) \quad \rightarrow \quad \nabla \cdot \left(\left(\nu_E h^{-1} + \alpha_{min} \right) g\left(u\right) \frac{\nabla u}{|\nabla u|} \right) \tag{3.39}$$

Since, by (3.35), $\nu_E \geq 0$ equation (3.39) ensures, even for smooth quantities in the absence of any advection, there is a minimal compression α_{min} present in the system for all time. In order to prevent the formation of singularities, and to preserve the form of the ACC $\kappa = \frac{1}{h}$, a corresponding first-order viscosity is added to augment the viscous term in (3.38)

$$-\nabla \cdot \left(\nu_E \nabla u \right) \quad \rightarrow \quad -\nabla \cdot \left(\left(\nu_E + h\alpha_{min} \right) \nabla u \right) \tag{3.40}$$

The next adaptation is the introduction of a *compression strength*; this is a parameter which can be adjusted to modify the ACC directly; let $\mathcal{C} > 0$ and modify equations (3.39) and (3.40) by introducing $\mathcal{C}$ as follows

$$\nabla \cdot \left(\mathcal{C} \left(\nu_E h^{-1} + \alpha_{min} \right) g\left(u\right) \frac{\nabla u}{|\nabla u|} \right) \tag{3.41}$$

$$- \nabla \cdot \left(\left(\nu_E + h\mathcal{C}\alpha_{min} \right) \nabla u \right) \tag{3.42}$$

The change allows more direct control over the artificial compressive coefficient, κ, in regions of shock. In regions where $\nu_E \approx 0$, κ behaves as $\frac{\mathcal{C}\alpha_{min}}{h\mathcal{C}\alpha_{min}} = \frac{1}{h}$ and is thus unchanged; whereas in regions where ν_E is large, such as in the vicinity of a shock, $\kappa \approx \frac{\mathcal{C}\nu_E}{\nu_E h} = \frac{\mathcal{C}}{h}$. The final modification to equation (3.38) that is proposed is the addition of a small positive constant $\epsilon \approx 0$ to prevent numerical division by zero. The directional portion of the compressor term, $\frac{\nabla u}{|\nabla u|}$, is augmented by ϵ to be $\frac{\nabla u}{|\nabla u| + \epsilon}$; in practice, $\epsilon = 1.1 \times 10^{-14}$ was utilized. The final one-stage compression-advection-

diffisuion equation that was implemented is therefore

$$\partial_t u + \beta \cdot \nabla u + \nabla \cdot \left(\mathcal{C} \left(\nu_E h^{-1} + \alpha_{min} \right) \left[u \left(1 - u \right) \right] \frac{\nabla u}{|\nabla u| + \epsilon} \right) - \nabla \cdot \left(\left(\nu_E + h \mathcal{C} \alpha_{min} \right) \nabla u \right) = 0 \tag{3.43}$$

3.3 Implementation and numerical results

3.3.1 Implementation details

Consider the equation (3.38) written as $\partial_t u = T(\beta, u)$. Time stepping is approached via the explicit SSP RK3 method with Butcher tableau given by (3.1); the operator (3.2) is discretized in space via finite differences utilizing the staggered-grid *Marker and Cell* distribution of unknowns. More specifically, scalar quantities are considered at the center of cells while vector quantities are located at the midpoints of faces; e.g., in two dimensions, scalar quantities are located at x_{ij} whereas the components of the velocity, $\mathbf{u} = (u, v)$, are located at $x_{i\pm\frac{1}{2},j}$ and $x_{i,j\pm\frac{1}{2}}$ respectively. An in-depth discussion of the *Marker and Cell* method can be found in the appendix of [16].

$$\begin{array}{c|ccc} 0 & 0 & 0 & 0 \\ 1 & 1 & 0 & 0 \\ \frac{1}{2} & \frac{1}{4} & \frac{1}{4} & 0 \\ \hline & \frac{1}{6} & \frac{1}{6} & \frac{2}{3} \end{array} \tag{3.1}$$

$$T\left(\beta, u\right) = -\beta \cdot \nabla u - \nabla \cdot \left(\mathcal{C} \left(\nu_E h^{-1} + \alpha_{min} \right) \left[u \left(1 - u \right) \right] \frac{\nabla u}{|\nabla u| + \epsilon} \right) + \nabla \cdot \left(\left(\nu_E + h \mathcal{C} \alpha_{min} \right) \nabla u \right) \tag{3.2}$$

In addition, when computing the compressive term, u is smoothed by local averaging before the directional component, $\frac{\nabla u}{|\nabla u|+\epsilon}$, is computed; this was due to small numerical errors in u causing large spurious gradients. Furthermore, for each of the Runge-Kutta iterates k_i, an intermediate entropy-viscosity is formulated for use with computation of the next iterate. In the presence of compression special care must be taken regarding numerical error; specifically low-order dispersive waves; the general reason for this is that the compression term seeks to compress these waves while the dissipation term seeks to subdue them. The end result of this duality is that dispersive errors which are too large, in the presence of over-compression, tend to persist in time and solidify as numerical artifacts; spurious dispersive waves cause numerical entropy production and therefore both the entropy-viscosity based compression and entropy-viscosity based dissipation are active in their locale. In order to abet the issue with low order dispersive waves it is sufficient to ensure that their order is much higher than the order upon which the compression term can act; e.g. dispersive error waves should only manifest at a sub-grid scale. The right-hand side of (3.2) is written in divergence form; therefore if second order central differences are utilized to treat first derivatives, at each step of computing an approximation to (3.2), the leading error is $\mathcal{O}\left(\frac{h^2}{6}\partial_{x_i x_i x_i} u_i\right)$. Thus solving $\partial_t u_i = T(\beta, u)$ on a uniform grid where $T(\beta, u)$ is in divergence form and the second order central finite difference is used to compute the derivatives, ∂_{x_i}, is similar to solving the same equation using $\mathbb{Q}^1$ finite elements and a lumped mass matrix (see [13]). In fact, [13] discuss a straight-forward technique for eliminating dispersive error by approximating the inverse to the consistent mass matrix for use as an error-correction term in an otherwise lumped mass matrix scheme. The authors go on to detail applications of their method in higher dimensions and with more general finite element spaces; however, since we desire to construct a finite difference scheme for a dispersion-free one-dimensional derivative,

for use in approximating the the operator (3.2) given in divergence form, their work in one-dimension motivates the following lemma:

Lemma 3.1 *Let ϕ_i be a discretization of a one-dimensional infinitely differentiable function ϕ on a uniform mesh of size h. Define $\tilde{\phi}_i = \phi_i + (\phi_{i+1} - 2\phi_i + \phi_{i-1})/6$. Then the usual central difference applied to $\tilde{\phi}$ approximates the derivative of ϕ and is free of low order dispersion; that is*

$$\frac{\tilde{\phi}_{i+1} - \tilde{\phi}_{i-1}}{2h} = (\partial_x \phi)_i + \mathcal{O}\left(h^4\right) \tag{3.3}$$

The obvious generalizations to higher space dimensions apply by considering each direction separately.

Proof. The proof follows by utilizing the definition of $\tilde{\phi}_i$, algebraic manipulation, and use of the Taylor expansion at x_i. The following expansions will be instrumental

$$\phi_{i+2} = \phi_i + 2h\left(\partial_x \phi\right)_i + \frac{4h^2}{2}\left(\partial_{xx}\phi\right)_i + \frac{8h^3}{6}\left(\partial_{xxx}\phi\right)_i + \frac{16h^4}{24}\left(\partial_{xxxx}\phi\right)_i + \mathcal{O}(h^5) \tag{3.4}$$

$$\phi_{i+1} = \phi_i + h\left(\partial_x \phi\right)_i + \frac{h^2}{2}\left(\partial_{xx}\phi\right)_i + \frac{h^3}{6}\left(\partial_{xxx}\phi\right)_i + \frac{h^4}{24}\left(\partial_{xxxx}\phi\right)_i + \mathcal{O}\left(h^5\right) \tag{3.5}$$

$$\phi_{i-1} = \phi_i - h\left(\partial_x \phi\right)_i + \frac{h^2}{2}\left(\partial_{xx}\phi\right)_i - \frac{h^3}{6}\left(\partial_{xxx}\phi\right)_i + \frac{h^4}{24}\left(\partial_{xxxx}\phi\right)_i + \mathcal{O}\left(h^5\right) \tag{3.6}$$

$$\phi_{i-2} = \phi_i - 2h\left(\partial_x \phi\right)_i + \frac{4h^2}{2}\left(\partial_{xx}\phi\right)_i - \frac{8h^3}{6}\left(\partial_{xxx}\phi\right)_i + \frac{16h^4}{24}\left(\partial_{xxxx}\phi\right)_i + \mathcal{O}\left(h^5\right) \tag{3.7}$$

Computing $(\partial_x \tilde{\phi})_i$ utilizing the central difference formula (3.3) and gathering terms then gives

$$\frac{\tilde{\phi}_{i+1} - \tilde{\phi}_{i-1}}{2h} = \frac{1}{2h}\left[\phi_{i+1} - \phi_{i-1}\right] + \frac{1}{12h}\left[\phi_{i-2} - \phi_{i+2} + 2\left(\phi_{i+1} - \phi_{i-1}\right)\right] \tag{3.8}$$

Utilizing expansions (3.4)-(3.7) in the right-hand side of (3.8) yields

$$\frac{1}{2h}\left[2h\left(\partial_x\phi\right)_i+\frac{2h^3}{6}\left(\partial_{xxx}\phi\right)_i+\mathcal{O}\left(h^5\right)\right]+\frac{1}{12h}\left[\frac{-12h^3}{6}\left(\partial_{xxx}\phi\right)_i+\mathcal{O}\left(h^5\right)\right] \tag{3.9}$$

The result is evident; namely

$$\frac{\tilde{\phi}_{i+1}-\tilde{\phi}_{i-1}}{2h}=\left(\partial_x\phi\right)_i+\mathcal{O}\left(h^4\right) \tag{3.10}$$

This concludes the proof; generalization to higher dimensions is direct. □

It bears mentioning that lemma (3.1) still has a leading error term which is dispersive; however, the order is not significantly higher: $\mathcal{O}(h^4)$ instead of $\mathcal{O}\left(h^2\right)$. The end result is that, in practice, the ACC can embody higher values, through the use of the compression strength $\mathcal{C}$, without preserving dispersive error waves.

In summary: however the reader chooses to implement a numerical method solving (3.38), for either smooth or discontinuous initial data, it is advised to select a numerical approach in which low-order dispersive error is corrected for. This consideration arises due to the action of the compression term in solidifying such numerical artifacts into the long-term dynamics of the numerical solution. Herein we see the primary 'drawback' of the proposed one-stage approach; i.e. previously mentioned approaches suffered from the need to re-initialize a distance function [52, 43] or falsely iterate an auxiliary problem to a steady state [17, 40] to enforce mass conservation. The canonical 'no-free-lunch' mantra applies: the burden of implementing (3.38) is one of suitably addressing low-order error correction. Typically this would could cost a matrix inversion at every time step, e.g. computing M^{-1} to correct dispersion or something of this nature, however the approximation technique of [13], reflected in lemma (3.1), has allowed for a methodology by which this consideration can be

somewhat relaxed.

3.3.2 Numerical results

This section details numerical results for the implementation of (3.43), using $\epsilon = 1.1 \times 10^{-14}$, with SSP RK3 time-stepping, a CFL of 0.5, a second order spatial discretization of (3.2) and dispersive error correction. We analyze a cadre of test cases in a bounded domain with initial value $\phi(x,t) = \phi_0(x)$; each boundary edge, or face, is considered an inflow and are therefore conditions of Neumann type. Finally, the entropy viscosity, ν_E, utilizes a choice of *entropy function*; for these tests the convex entropy function $E(\phi) = \left(\phi - \frac{1}{2}\right)^{40}$ was chosen. The choice of entropy function does indeed play a role here; it is the foundation of the entropy viscosity and hence plays a leading role in the compressive and diffusive behavior. For more on entropy functions see [14, 45]. Results from [40] as well as a particle level-set method of [24], where applicable, motivate the numerical tests chosen.

3.3.3 Rigid body rotation of Zaleska's disc

The first numerical foray is the advection of a circular level step function; the definition of the initial level-set function is quite simple and given by

$$\phi_0(x) = \begin{cases} 1 & : |x - x_0| \leq r_0 \\ 0 & : \text{ otherwise} \end{cases} \tag{3.11}$$

We solve equation (3.43) with stationary, in time, ambient vector field $\beta = (-2\pi(y - 0.5), 2\pi(x - 0.5))$; the center of the circle at time $t = 0$ is taken to be $x_0 = (0.75, 0.5)$ with radius $r_0 = 0.15$. The expected motion is therefore that the circle processes in a circumferential manner; a procession occurring for each time increment. In the spirit of the work of [40] we show contours of the level set function (3.11) initially and after various numbers of revolution; of note will be the explo-

ration of the compression strength factor $\mathcal{C}$ as the mesh size goes to zero. The first results shown are after a single revolution; the level sets $\phi = 0.05$, $\phi = 0.50$, and $\phi = 0.95$ are shown. Utilizing these contours one can compare this method to the results of [40] directly.

3.3.3.1 Short time results

Figure 3.4: Solid revolution: 100×100 mesh, one revolution

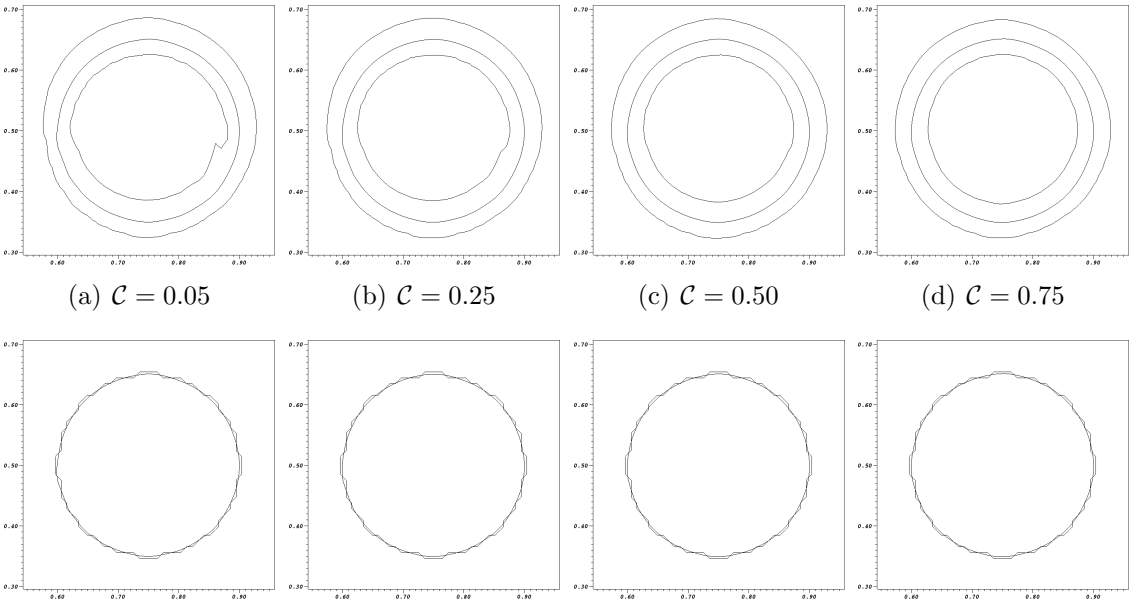

(a) $\mathcal{C} = 0.05$ (b) $\mathcal{C} = 0.25$ (c) $\mathcal{C} = 0.50$ (d) $\mathcal{C} = 0.75$

(e) $\mathcal{C} = 0.05$ (f) $\mathcal{C} = 0.25$ (g) $\mathcal{C} = 0.50$ (h) $\mathcal{C} = 0.75$

In this subsection short time, $T = 1$, results are reported; the circular level set function (3.11), having radius $r = 0.15$, completes one complete revolution within the $2D$ domain $[0, 1] \times [0, 1]$ and returns to its starting position. The first results are contour plots with various compression strengths shown; in the spirit of [40], three choice to show three contours per result has been made; in each of the three cases the constant compression, α_{min}, is identical and equal to 0.05. The first case

Figure 3.5: Solid revolution: 200×200 mesh, one revolution

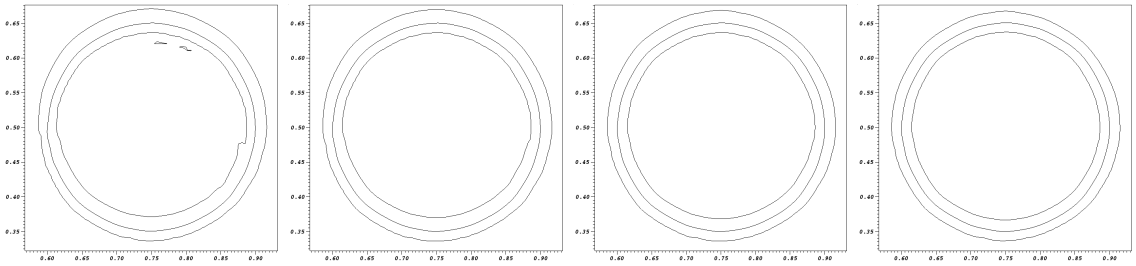

(a) $\mathcal{C} = 0.05$ (b) $\mathcal{C} = 0.25$ (c) $\mathcal{C} = 0.50$ (d) $\mathcal{C} = 0.75$

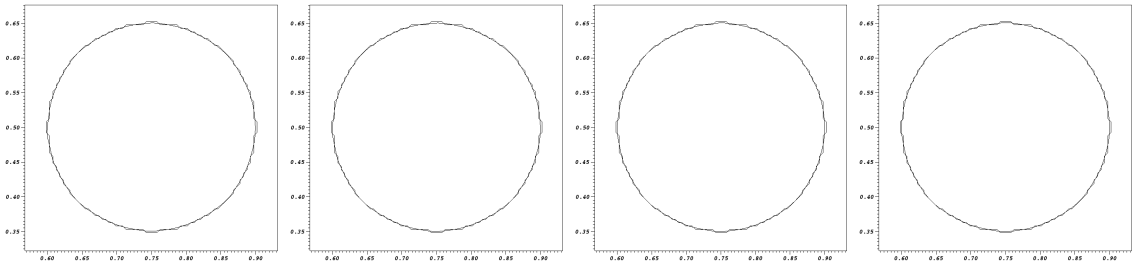

(e) $\mathcal{C} = 0.05$ (f) $\mathcal{C} = 0.25$ (g) $\mathcal{C} = 0.50$ (h) $\mathcal{C} = 0.75$

treated, shown in figure 3.4, is the 100×100 domain discretization of $[0, 1] \times [0, 1]$. Subsequently, figure 3.5 shows the result of utilizing a 200×200 discretization of same domain while figure 3.6 utilizes the finest discretization of 400×400 mesh points. The top rows of figures 3.4, 3.5 and 3.6 show the contours $\phi = 0.05, 0.5, 0.95$ for each of the values of the compression strength, $\mathcal{C}$, mentioned for the resolutions of 100×100, 200×200 and 400×400 respectively. Likewise, the bottom rows depict the interface level set, $\phi = 0.5$ following a single rotation, overlaid with the initial data. Particularly striking is the the preservation of this interface level set, $\phi = 0.5$, for every compression strength and resolution. Low compression strength, $\mathcal{C} = 0.05$, clearly introduces some level set perturbations after a single revolution whereas higher compression, $\mathcal{C} = 0.75$, preserves the overall structure very well. Despite the presence of the artifacts in the low-compression case the interface level sets are preserved quite well; in the case of 400×400 resolution the initial data and

Figure 3.6: Solid revolution: 400×400 mesh, one revolution

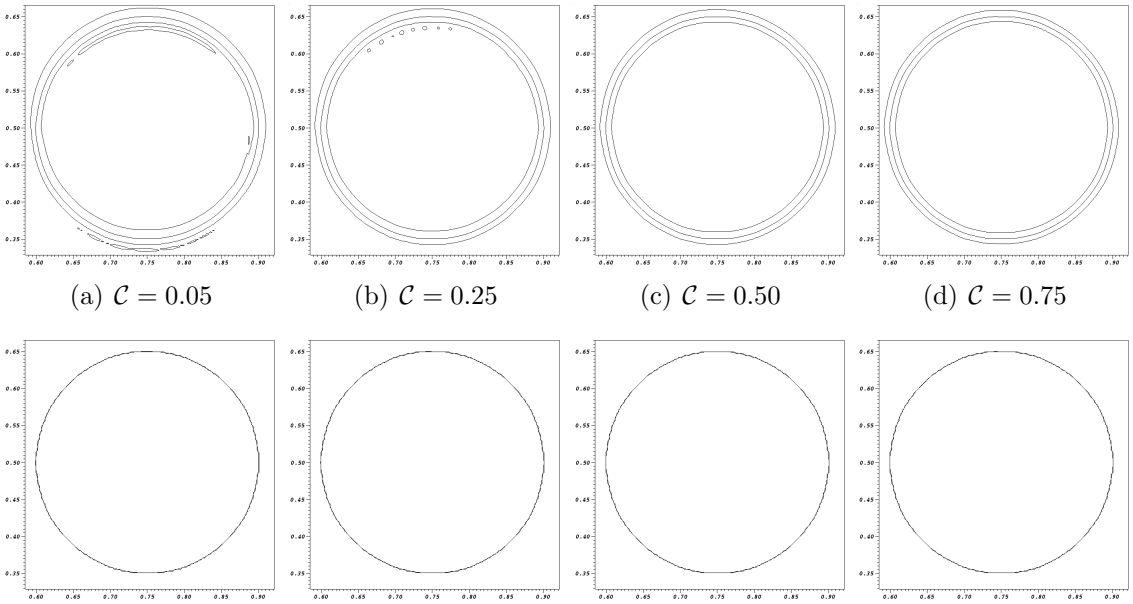

(a) $\mathcal{C} = 0.05$ (b) $\mathcal{C} = 0.25$ (c) $\mathcal{C} = 0.50$ (d) $\mathcal{C} = 0.75$

(e) $\mathcal{C} = 0.05$ (f) $\mathcal{C} = 0.25$ (g) $\mathcal{C} = 0.50$ (h) $\mathcal{C} = 0.75$

the interface level set are nearly indistinguishable.

In [40] several underlying methods were utilized to advect the level set function including total variation diminishing (TVD) methods (first proposed by Harten himself), second order non-TVD methods, central difference methods, and several more; the result is shown first without the intermediate compression phase and then, in the spirit of [17], with the compression problem 'tacked on' after each time step. [40] reports very good results; the results herein can be directly compared. Of note: when the compression strength, $\mathcal{C}$ is too low, such as in the $\mathcal{C} = 0.05, 0.25$ cases, the artifacting produced is comparable to the non-TVD method result, sans compression step, in [40].

Figure 3.7: Solid revolution: 100×100 mesh, twenty revolutions

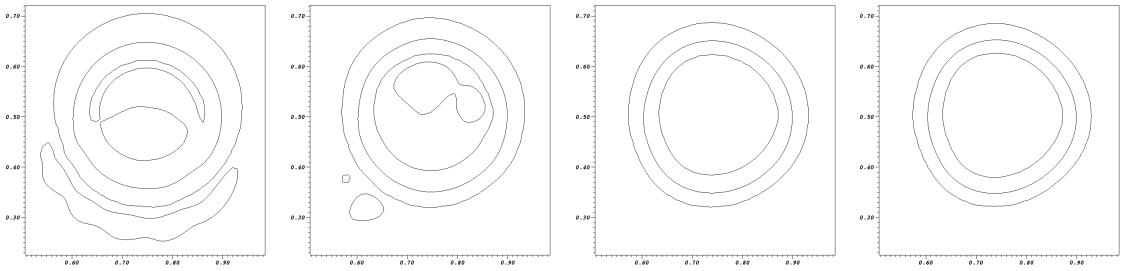

(a) $\mathcal{C} = 0.05$ (b) $\mathcal{C} = 0.25$ (c) $\mathcal{C} = 0.50$ (d) $\mathcal{C} = 0.75$

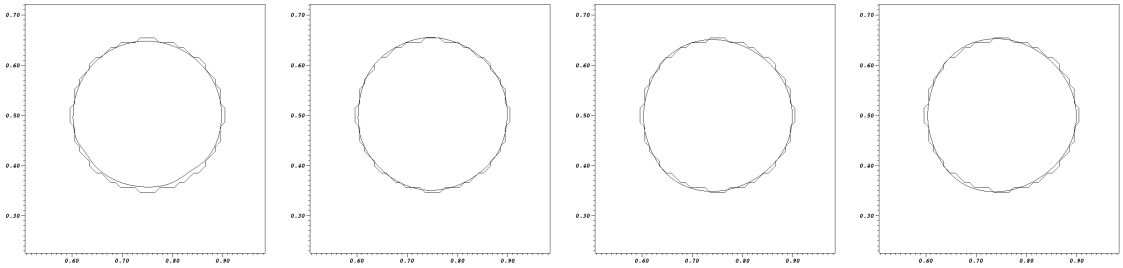

(e) $\mathcal{C} = 0.05$ (f) $\mathcal{C} = 0.25$ (g) $\mathcal{C} = 0.50$ (h) $\mathcal{C} = 0.75$

3.3.3.2 Long time results

In [40] only a single revolution of the circular step function is considered; this is justified as the authors are concerned mostly with displaying the efficacy of their two-stage compression approach when utilized with a bevy of different already-known methods. Of primary interest to us is the behavior of the compression parameter. In section 3.3.3.1 it was seen that, for low compression strength values $\mathcal{C}$, the result could appear quite disparate overall despite the amenable preservation of the interface level set.

In order to explore further the effect of the compression strength on the computed solution some long-time tests were performed. These tests had an ending time of $T = 20$ and, hence, twenty full revolutions of the initial data were made through the domain; theoretically, the result should coincide exactly with the initial data

Figure 3.8: Solid revolution: 200×200 mesh, twenty revolutions

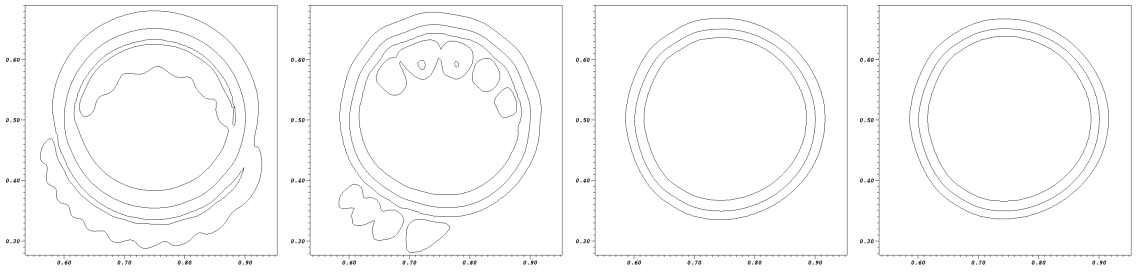

(a) $\mathcal{C} = 0.05$ (b) $\mathcal{C} = 0.25$ (c) $\mathcal{C} = 0.50$ (d) $\mathcal{C} = 0.75$

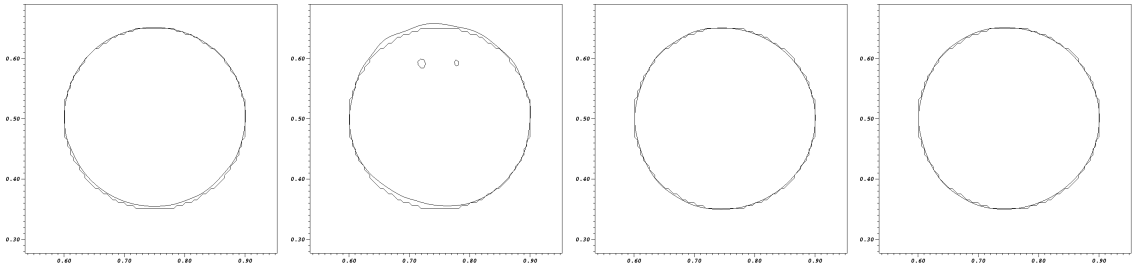

(e) $\mathcal{C} = 0.05$ (f) $\mathcal{C} = 0.25$ (g) $\mathcal{C} = 0.50$ (h) $\mathcal{C} = 0.75$

modulo some smoothing effect due the the viscosity being dominant at time $t = 0$. As in section 3.3.3.1 figure 3.7 shows the results arising from the discretization of $[0, 1] \times [0, 1]$ by a mesh of size 100×100, figure 3.8 by a mesh of size 200×200 and figure 3.9 by a mesh of size 400×400. The results serve to reinforce the findings of the single-revolution case as the presence of artifacts, in the context of low compression strength, are exacerbated though the coincidence of the interface level set, $\phi = 0.5$, after twenty revolutions is still high. The general presentation of the results mirrors that of the last section; the top row of figures 3.7, 3.8 and 3.9 show the contours $\phi = 0.05, 0.5, 0.95$ for the indicated values of the compression strength, $\mathcal{C}$, at resolutions 100×100, 200×200 and 400×400 respectively while the bottom row displays an overlay of the interface level set, $\phi = 0.5$, with the initial data.

Figure 3.9: Solid revolution: 400×400 mesh, twenty revolutions

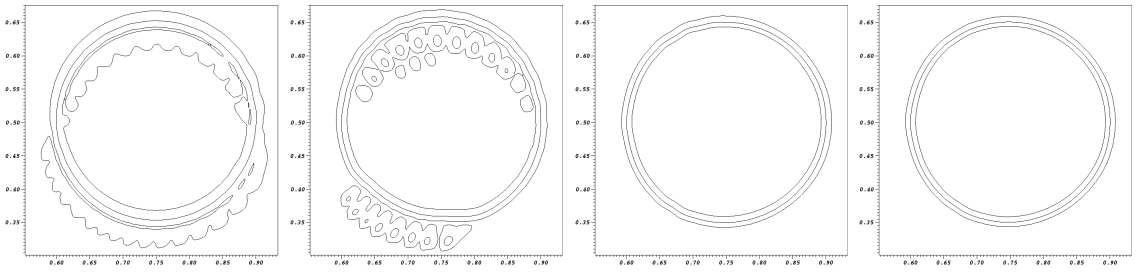

(a) $\mathcal{C} = 0.05$ (b) $\mathcal{C} = 0.25$ (c) $\mathcal{C} = 0.50$ (d) $\mathcal{C} = 0.75$

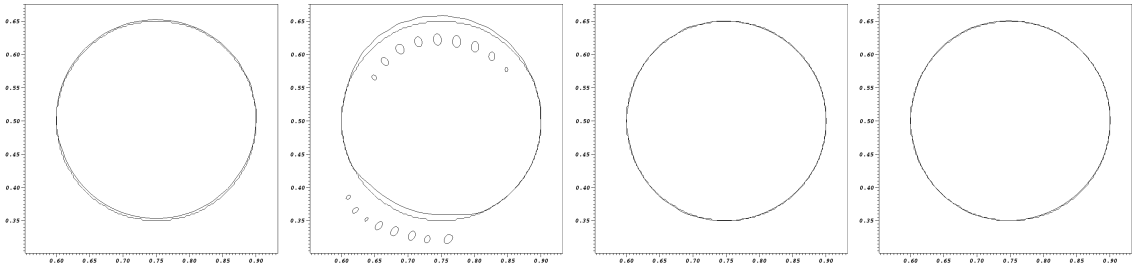

(e) $\mathcal{C} = 0.05$ (f) $\mathcal{C} = 0.25$ (g) $\mathcal{C} = 0.50$ (h) $\mathcal{C} = 0.75$

3.3.4 Periodic vortex test

This test appears in [40]; the underlying concept here is to test the one-stage compression in a slightly more complex regime. As in [40] the underlying vector field is periodic, in time, and produces a twisting vortex-like effect. The velocity field is given by

$$u(x,t) = sin\left(\pi x\right)^2 sin\left(2\pi y\right) cos\left(\frac{t\pi}{2}\right)$$
$$v(x,t) = -sin\left(\pi y\right)^2 sin\left(2\pi x\right) cos\left(\frac{t\pi}{2}\right)$$

The initial data is a circular level set function, as in section 3.3.3, with radius $r = 0.15$ and initial position $(0.5, 0.75)$; the choice of vector field dictates that the

Figure 3.10: Periodic vortex: 100×100, $\mathcal{C} = 0.75$ $\alpha_{min} = 0.05$

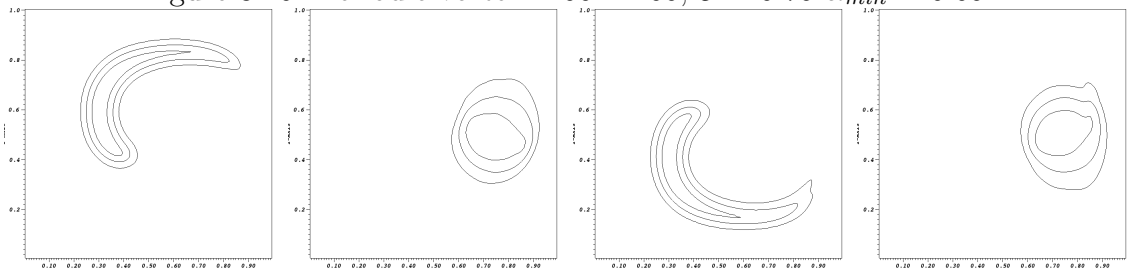

(a) $t = 1$ (b) $t = 2$ (c) $t = 3$ (d) $t = 4$

Figure 3.11: Periodic vortex: 100×100, $\mathcal{C} = 0.75$ $\alpha_{min} = 0.75$

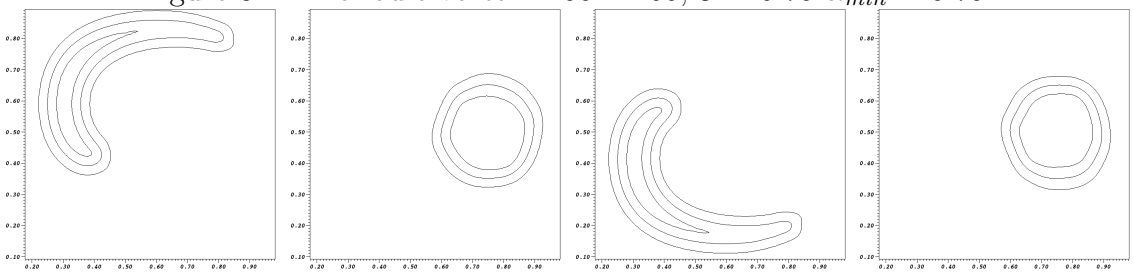

(a) $t = 1$ (b) $t = 2$ (c) $t = 3$ (d) $t = 4$

initial data should curl counter-clockwise, stop and return to its initial position at time $t = 2$ before curling clockwise and returning to its initial position at time $t = 4$. In the context of the vortex experiment we took the opportunity to also test the minimum compression parameter α_{min} more thoroughly. It was found that $\mathcal{C} = 0.75$ and $\alpha_{min} = 0.75$ yielded results on par with the vortex test of [40]; a low value, $\alpha_{min} \approx 0.05$, produced 'wobble' or 'smushed' effects in the non-interface level sets of ϕ. As in previous sections various discretizations are utilized to delineate the role of mesh resolution juxtaposed with the parameter α_{min}; the compression strength, $\mathcal{C}$, is kept at the constant value $\mathcal{C} = 0.75$ throughout. Each figure illustrates the results of the advected level set function, for the particular corresponding parameters, at

Figure 3.12: Periodic vortex: 200×200, $\mathcal{C} = 0.75$ $\alpha_{min} = 0.05$

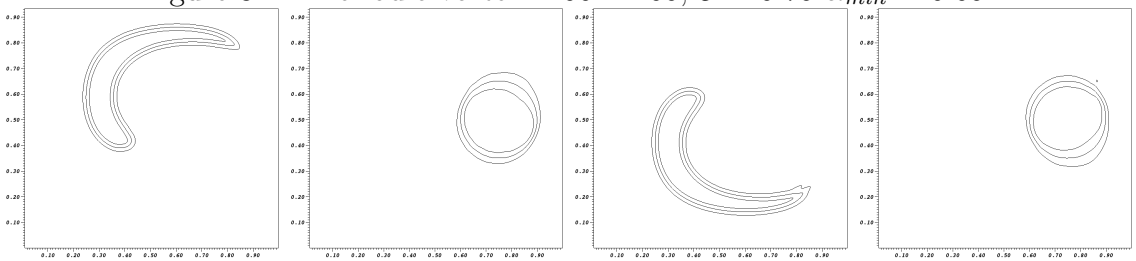

(a) $t = 1$ (b) $t = 2$ (c) $t = 3$ (d) $t = 4$

Figure 3.13: Periodic vortex: 200×200, $\mathcal{C} = 0.75$ $\alpha_{min} = 0.75$

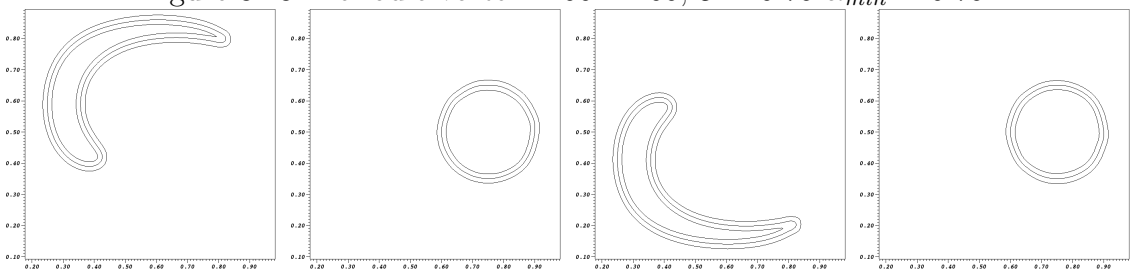

(a) $t = 1$ (b) $t = 2$ (c) $t = 3$ (d) $t = 4$

the four time positions $t = 1, 2, 3, 4$. Figures 3.10 and 3.11 correspond to the values $\alpha_{min} = 0.05$ and $\alpha_{min} = 0.75$, respectively, on a 100×100 mesh of the domain $[0, 1] \times [0, 1]$. Likewise figures 3.12 and 3.13 correspond to the same variation in α_{min} on with an underlying mesh of 200×200 grid points; figures 3.14 and 3.15 are also given in the same manner but correspond to an underlying mesh of 400×400 mesh points. In the $\alpha_{min} = 0.05$ cases it was found that the interface level set $\phi = 0.05$ coincided well with the initial data in the 200×200 and 400×400 case despite the other clearly egregious distortions; in the $\alpha_{min} = 0.75$ case, however, the interface level agreed quite well with the initial data for all three discretizations.

Figure 3.14: Periodic vortex: 400×400, $\mathcal{C} = 0.75$ $\alpha_{min} = 0.05$

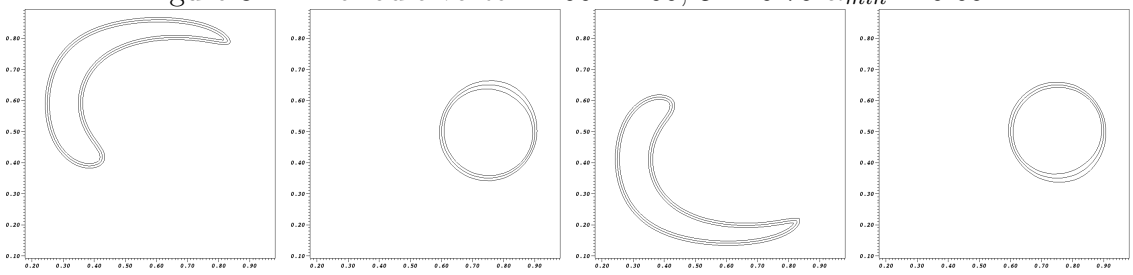

(a) $t = 1$ (b) $t = 2$ (c) $t = 3$ (d) $t = 4$

Figure 3.15: Periodic vortex: 400×400, $\mathcal{C} = 0.75$ $\alpha_{min} = 0.75$

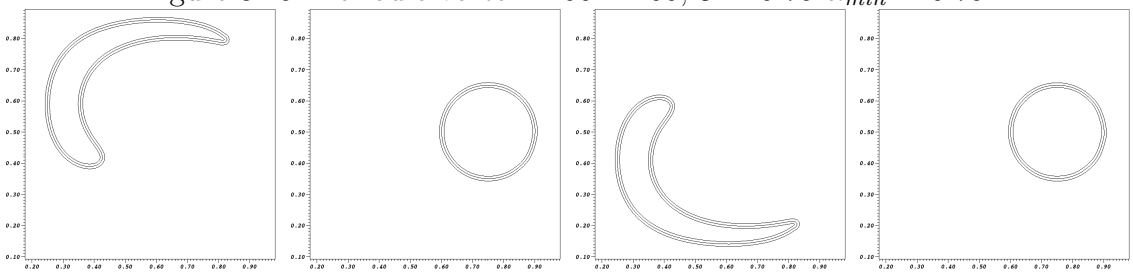

(a) $t = 1$ (b) $t = 2$ (c) $t = 3$ (d) $t = 4$

3.3.5 Non-periodic vortex test

This test appears in [24] and a similar experiment, though with little mention, also arises in [40]; the context of the former is the testing of an extensions of a hybrid particle / level-set method, first introduced by [7], utilizing self-adaptive oriented particles. Our purpose at this time is not a direct comparison with their work but rather to gauge the efficacy of our method in the context of some of the tests suggested therein. Towards that end we consider the non-periodic (in time) vortex given by the vector field

Figure 3.16: Non-periodic vortex at $t = 3$: 200×200, $\mathcal{C} = 0.75$

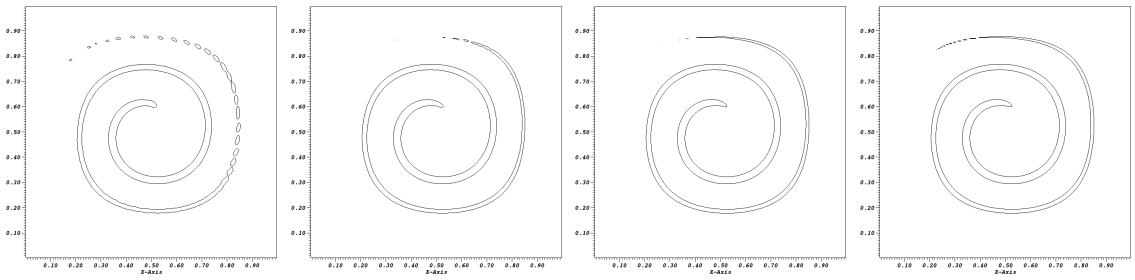

(a) $\alpha_{min} = 0.25$ (b) $\alpha_{min} = 0.05$ (c) $\alpha_{min} = 0.005$ (d) $\alpha_{min} = 0$

Figure 3.17: Non-periodic vortex at $t = 3$: 400×400, $\mathcal{C} = 0.75$

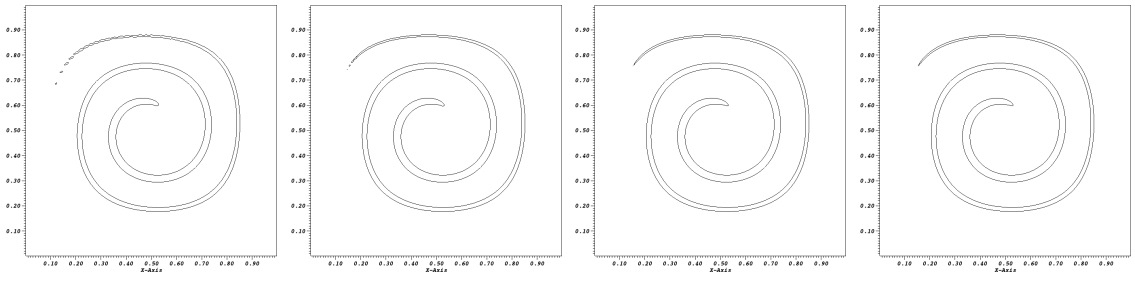

(a) $\alpha_{min} = 0.25$ (b) $\alpha_{min} = 0.05$ (c) $\alpha_{min} = 0.005$ (d) $\alpha_{min} = 0$

$$u(x,t) = -2sin(\pi y)cos(\pi y)sin^2(\pi x)$$

$$v(x,t) = 2sin(\pi x)cos(\pi x)sin^2(\pi y)$$

This vector field continually twists the initial data into a inwardly-spiraling configuration as $t \to \infty$; thus the initial data is thinned continuously until it can no longer be resolved by the grid scale. The purpose here is to observe how well the compressive term can resolve, and maintain the fidelity of, thin regions. [40] notices

some tearing associated to lack of mesh fidelity in his tests whereas [24] notes that the edges of the vortex, in usual level-set approaches, can become 'jagged'. Indeed, our findings corroborate the necessity of mesh fidelity; the usual benchmark discretization of 100×100 mesh points was too low to yield meaningful, reportable results. The end result was also quite sensitive to the parameter α_{min}; high values 'pinched off' thin structures. Figure 3.16 shows the results, for various α_{min} on a 200×200 mesh of $[0,1] \times [0,1]$ whereas figure 3.17 considers a finer discretization of 400×400 grid points. In the context of these test case only the interface level set, $\phi = 0.5$, was tracked as we have no frame of reference, e.g. returning to a starting position, for any other level set configuration. As the interface level set, $\phi = 0.5$, thins it stands to reason that too much compression could cause the same type of 'pinching' phenomena, creating small circular islands, noticed in [40]; towards this end it is expected that the constant compression parameter α_{min} might better preserve the interface level set when it takes on smaller values. This is precisely the effect that is noticed: in figure 3.16 the effect of α_{min} on the interface level set is quite noticeable and is best at $\alpha_{min} = 0$. As expected, high values of α_{min} cause the sequestration of the tail of the interface level set into smaller island-like nodes. In the 400×400 case, figure 3.17, the effect is much less pronounced; the cases $\alpha_{min} = 0.05, 0.005, 0$ are nearly indistinguishable with $\alpha_{min} = 0.25$ exhibiting only a minor pooling phenomena in the tail.

3.3.6 The LeVeque test

[35] proposed a test case for conservative advection algorithms [7]; a sphere of radius $r = 0.15$, initially at $(0.35, 0.35, 0.35)$ is advected on a 100^3 grid point mesh,

via the vector field

$$u(x,y,z,t) = 2sin^2(\pi x)sin(2\pi y)sin(2\pi z)cos\left(\pi\tfrac{t}{T}\right)$$
$$v(x,y,z,t) = -sin(2\pi x)sin^2(\pi y)sin(2\pi z)cos\left(\pi\tfrac{t}{T}\right)$$
$$w(x,y,z,t) = -sin(2\pi x)sin(2\pi y)sin^2(\pi z)cos\left(\pi\tfrac{t}{T}\right)$$

The value $T = 3$ modulates the periodicity of the field in time; other values of T can of course be employed but the chosen value is the canonical one. As noted by [7], and echoed by [24], this test is notoriously difficult for level-set methods alone; towards this end [7] and [24] developed hybrid particle-level-set methods which perform quite well at tracking the interface, $\phi = 0.5$, level set via the use of marker particles. The difficulty in this test lies in the behavior of the advected sphere in the approximate time interval $t \in [1.2, 1.8]$ where the surface of the object becomes so thin that it slips below the resolution of the mesh; as noted in [7] this causes most level set methods to 'lose track' of this portion of the interface after time $t \approx 1.8$ and, as the object is re-assembled by the periodic motion of the vector field, results in a dramatic change in the interface topology. Such behavior breaks the mass conservation of the method as the entire region, which is almost a disc in shape, is lost from the simulation; the object begins as a sphere and ends as two disjoint masses. The one-stage compressive level set proposed was indeed able to overcome this obstacle; however this did involve some experimentation with the compression parameters. The parameters for the entropy-viscosity (c_{max}, c_E), the compressive strength, $\mathcal{C}$, and the minimum compression α_{min} (see equations (3.35) and (3.43)) used were

c_{max}	c_E	$\mathcal{C}$	α_{min}
0.015625	0.1	1.2	0.0

We found this highly unusual because, typically, the parameters c_{max} and c_E, defining the entropy viscosity, need no case-by-case adjustment; they are thought of as artifacts of the domain Ω and the mesh alone. In the context of this problem there is some motivation for this highly unusual approach; [24] utilizes an adaptive technique to increase the density of particles in this very thin region. The term 'thin region' refers to that portion of the object at time $t \approx 1.5$ (half the period) whereby the object embodies a surface incident to a plane; the distribution of the interface level set, $\phi = 0.5$, is sparse atop this plane and hence the region appears to 'tear' here. This 'tearing', we suspect, causes large gradients in this region and, hence, the entropy residual used to construct the entropy viscosity is expected to be large. The substantial value of the entropy residual would, by equation (3.35), result in the use of the first-order term to construct the entropy-viscosity; the entropy-viscosity then determines the amount of compression. In the thin region *too much* compression would result in the breaking of the 'strands' which are, barely, holding the region together; this leads to the disjointing of the object as time increases past $t = 1.5$. The key to maintaining the fidelity of the region, we suspect, lies in the *control* of the compression in thin regions, it must be small, while ensuring large-enough compression to maintain the bulk portions of the level-set as well.

The choice of c_{max} and c_E allows this semi-adaptive behavior to be evinced in the current framework while the otherwise large value of compression strength, $\mathcal{C}$, allows for a larger bulk-compression to be realized. If this is indeed the correct interpretation it hints strongly at an avenue for adaptive techniques to be developed from (3.43) based on the local 'thinness' of an object. As a final mention we note

Figure 3.18: Results of the LeVeque advection test. $100 \times 100 \times 100$

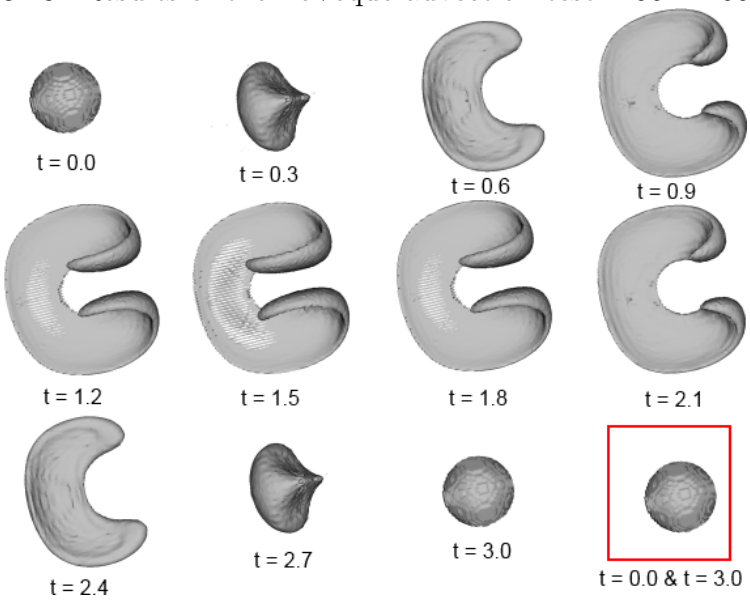

the re-occurrence of a phenomena noted in [24]. The loss of resolution in the 'thin' region causes the presence of small specks of mass to disjoint themselves from the level set. These small aberrations, as mentioned, are noted in the corresponding adaptive tests of [24]; the main difference being that, in the case of the one-stage compression method (3.43), these aberrations are damped to zero by the dissipative entropy-viscosity regularization by the time $t \approx 3$ has been reached. The results are presented in figure 3.18; the last frame in the figure, denoted by the boxed outline, shows the initial data, at time $t = 0$, juxtaposed with the final result at time $t = 3$. The frame at time $t = 1.5$ shows the 'thin region' most prominently; it is demarcated by the 'grating' on the flat portion of the object.

4. INTEGRAL COMMUTATOR THEORY FOR CONSISTENCY ANALYSIS

4.1 The one-dimensional point of view

The objective of this section is to review the current paradigm of consistency error analysis via Taylor expansions for $\mathbb{P}_1$ finite elements and to motivate a novel approach based on an integral commutator. The introduction of these concepts is carried out in one spatial dimension in order to facilitate the analysis.

4.1.1 A P^1 approximation

This subsection briefly outlines a general problem and discusses the approximation problem using P^1 (or Q^1) finite elements in one dimension. This material is by no means new; it is reviewed for completeness. Consider the following one-dimensional transport equation in the domain $\Omega = (a, b)$

$$\partial_t u + \beta \partial_x u = 0, \quad u(x, 0) = u_0(x), \quad (x, t) \in \Omega \times \mathbb{R}_+ \tag{4.1}$$

equipped with periodic boundary conditions. The velocity field, $\beta \in \mathbb{R}$, is assumed constant. The solution to (4.1) is $u_0(x - \beta t)$, where we have identified u_0 and its periodic extension. To frame the Galerkin linear approximation problem, the domain $\Omega = (a, b)$ is partitioned into N intervals $[x_i, x_{i+1}]$ for $i = 0, 1, \ldots, N - 1$. Let the quantity $h_{i+\frac{1}{2}} := |x_{i+1} - x_i|$ denote the diameter of the cell $[x_i, x_{i+1}]$. Let $\{\psi_0, \psi_1, \ldots, \psi_{N-1}\}$ be the family composed of the continuous and piecewise linear Langrange polynomials associated with the nodes $\{x_0, \ldots, x_N\}$ and define $\mathbf{X}_h = \text{span}\,\{\psi_0, \psi_1, \ldots, \psi_{N-1}\}$.

Let $U_0(x) \in \mathbf{X}_h$ denote a reasonable approximation of $u_0(x)$; it could be for instance the Lagrange interpolate or the L^2 projection of u_0. An semi-discrete ap-

proximate solution to (4.1), say $U \in C^1([0,T]; \mathbf{X}_h)$, is constructed by using the Galerkin technique. This approximation satisfies $U(x,0) = U_0(x)$ and

$$b(U,v) := \int_\Omega (\partial_t U + \beta \partial_x U)\, v \, \mathrm{d}x = 0, \quad \forall v \in \mathbf{X}_h,\ \forall t \geq 0. \tag{4.2}$$

Upon using the expansion $U(t,x) = \sum_{j=1}^N U(t,x_j)\, \psi_j(x)$, the above problem can be reformulated as follows:

$$0 = b(U,\psi_i) = \sum_{j=1}^N \left(c_{ij} \partial_t U(t,x_j) + b_{ij} U(t,x_j)\right) \tag{4.3}$$

$$c_{ij} = \int_\Omega \psi_j \psi_i \, \mathrm{d}x, \qquad b_{ij} = \beta \int_\Omega \partial_x \psi_j \psi_i \, \mathrm{d}x. \tag{4.4}$$

The result is a system of ordinary differential equations

$$C\dot{U}(t) = -BU(t), \tag{4.5}$$

which can be solved using suitable methods.

4.1.2 Consistency error analysis

The consistency error of approximation methods is traditionally obtained by inserting the exact solution into the discrete equations defining the approximation. This leads us to the following

Definition 4.1 (Consistency error) *Let u denote the solution to* (4.1)*. The consistency error, at the node x_i, for the Galerkin approximation* (4.2)*, where the coefficients are defined by* (4.4)*, is defined to be*

$$R_i[u](t) = \left(\int_\Omega \psi_i \, \mathrm{d}x\right)^{-1} \left(\sum_{j=1}^N \left(c_{ij} \partial_t u(t,x_j) + b_{ij} u(t,x_j)\right)\right). \tag{4.6}$$

The expression (4.6) is reminiscent of those found in the consistency error analysis of finite difference schemes. The traditional approach to evaluate the truncation error consists of taking the difference of the partial differential equation applied to the solution and the scheme applied to the solution both taken at the fixed grid point x_i. Taylor series about x_i are then utilized to find the consistency error. We define the order of the truncation error for the linear Galerkin approximation in the same spirit as in the finite difference case just discussed.

Definition 4.2 (Order of the consistency error) *The consistency error is of order α at the point x_i if*

$$R_i[u](t) = O\left(h^{\alpha}\right) \tag{4.7}$$

In the next two subsections two one-dimensional example problems, one per section, are discussed which utilize the linear Galerkin approximation just discussed; the consistency error at a node x_i is found for each utilizing the usual Taylor expansion approach. The difference between the two examples is solely in the method utilized to compute the coefficients b_{ij} and c_{ij} of the expressions (4.3) and, consequently, (4.6). In the first case, that of the *consistent mass matrix*, no quadrature is utilized and the coefficients are determined exactly; this yields a particular Taylor expansion showing that the method is free of low-order dispersive consistency error. In the second case a quadrature is utilized to ensure that the linear system (4.5) for the approximate solution is diagonal; this approach is called *mass lumping* and is a common technique in various fields of computational science due to its ease of solution at each time step. It will be shown in the example that the employment of mass lumping introduces a low-order dispersive consistency error. The examples given have been previously discussed in [13]; their treatment incurs extra detail here in order to illustrate the tedious nature of Taylor expansion based analysis.

4.1.3 Analysis of the consistent mass matrix

Consider the model problem (4.1), with solution u, and the one dimensional $\mathbb{P}_1$ Galerkin linear approximation, U, to (4.2). We will assume for simplicity that the mesh $\{[x_i, x_{i+1}]\}_{i=1}^{N-1}$ is uniform with step size h; e.g. $|x_{i+1} - x_i| = h$ for all $i = 1, 2, \ldots, N-1$. Under this assumption the coefficients c_{ij} and b_{ij} in (4.6) satisfy

$$b_{ij} = \begin{cases} \pm\beta\frac{1}{2} & \text{if } j = \pm 1, \\ 0 & \text{otherwise,} \end{cases} \qquad c_{ij} = \begin{cases} \frac{1}{6}h & \text{if } j = \pm 1, \\ \frac{2}{3}h & \text{if } j = i, \\ 0 & \text{otherwise.} \end{cases}$$

Proposition 4.1 *Consider the semi-discrete scheme* (4.2) *with the consistent mass matrix. The dominating term in the consistency error at the grid points* $\{x_i\}_{0\le i\le N}$ *is fourth order and is equal to* $\beta\frac{h^4}{180}\partial_{xxxxx}u(x_i, t)$.

Proof. This is a standard result, but we are going to go through the details of the proof to illustrate the tedious nature of the Taylor expansion based traditional analysis. Consider x_i fixed, giving $x_{i\pm1} = x_i \pm h$, so that the consistency error, (4.6), is

$$R_i[u](t) = \frac{2}{3}\partial_t u(x_i, t) + \frac{1}{6}\partial_t u(x_{i+1}, t) + \frac{1}{6}\partial_t u(x_{i-1}, t) + \beta\frac{1}{2h}\left(u(x_{i+1}, t) - u(x_{i-1}, t)\right)$$

The classical Taylor expansion approach compares the above to the partial differential equation evaluated at x_i; to do so we need to formulate an approximation, using the above, to $\partial_t u(x_i, t) + \beta\partial_x u(x_i, t)$. This is precisely the step in the process which can be a source of difficulty even in one dimension; the main caveat being that human

intervention is required where a purely computational analysis is preferable. By adding and subtracting $\frac{1}{3}\partial_t u(x_i,t)$ to the above equation we can recover the term $\partial_t u(x_i,t)$; gathering terms yields

$$R_i[u](t) = \partial_t u(x_i,t) + \frac{1}{6}\left(\partial_t u(x_{i+1},t) - 2\partial_t u(x_i,t) + \partial_t u(x_{i-1},t)\right) + \frac{\beta}{2h}\left(u(x_{i+1},t) - u(x_{i-1},t)\right).$$

We make use of the Taylor expansions for $\partial_t u(x_{i\pm1},t)$ about x_i given by

$$\partial_t u(x_{i+1},t) = \partial_t u(x_i,t) \pm h\partial_{tx}u(x_i,t) + \frac{h^2}{2}\partial_{txx}u(x_i,t) \pm \frac{h^3}{6}\partial_{txxx}u(x_i,t) + \frac{h^4}{24}\partial_{txxxx}u(x_i,t) + \ldots$$

to reduce the expression $\partial_t u(x_{i+1},t) - 2\partial_t u(x_i,t) + \partial_t u(x_{i-1},t)$ to

$$\partial_t u(x_{i+1},t) - 2\partial_t u(x_i,t) + \partial_t u(x_{i-1},t) = h^2\partial_{txx}u(x_i,t) + \frac{h^4}{12}\partial_{txxxx}u(x_i,t) + O(h^6)$$

Since u solves (4.1) the time derivatives is replaced in the above expansion by using

$$\partial_{txx}u(x_i,t) = \partial_{xx}(\partial_t u(x,t)) = -\beta\partial_{xxx}u(x,t),$$
$$\partial_{txxxx}u(x_i,t) = \partial_{xxxx}(\partial_t u(x,t)) = -\beta\partial_{xxxxx}u(x,t).$$

Substituting back into the expression for the consistency error yields

$$R_i[u](t) = \partial_t u(x_i,t) + -\beta\frac{h^2}{6}\partial_{xxx}u(x_i,t) + -\beta\frac{h^4}{72}\partial_{xxxxx}u(x_i,t) + \beta\frac{1}{2h}\left(u(x_{i+1},t) - u(x_{i-1},t)\right)$$

Taylor expansions about x_i in the term $\beta\frac{1}{2h}\left(u(x_{i+1},t)-u(x_{i-1},t)\right)$ gives

$$\beta\frac{1}{2h}\left(u(x_{i+1},t)-u(x_{i-1},t)\right)=\beta\partial_x u(x_i,t)+\beta\frac{h^2}{6}\partial_{xxx}u(x_i,t)+\beta\frac{h^4}{120}\partial_{xxxxx}u(x_i,t)+O(h^6)$$

Summing these expressions gives the approximation desired

$$\begin{aligned}R_i[u](t)&=\partial_t u(x_i,t)+\beta\partial_x u(x_i,t)-\beta\frac{h^4}{180}\partial_{xxxxx}u(x_i,t)+O(h^5)\\&=-\beta\frac{h^4}{180}\partial_{xxxxx}u(x_i,t)+O(h^5)\end{aligned}$$

Where we used that u solves (4.1) to simplify the expression. □

4.1.4 Analysis of the lumped mass matrix

The traditional rational for lumping the mass matrix in the linear system (4.5) is that the matrix C is diagonal; this eliminates the necessity to invert any matrices when using an explicit method to approximate the time evolution of the system. The process of mass lumping equates to utilizing the quadrature formula $\int_a^b f(x)\,\mathrm{d}x \approx (b-a)\frac{1}{2}(f(a)+f(b))$ to compute the coefficients of (4.3) on each cell $[x_i, x_{i+1}]$. This gives

$$b_{ij}=\begin{cases}\pm\beta\frac{1}{2h} & \text{if } j=\pm1,\\ 0 & \text{otherwise,}\end{cases}\qquad c_{ij}=\begin{cases}1 & \text{if } j=i,\\ 0 & \text{otherwise.}\end{cases}$$

Proposition 4.2 *Consider the semidiscrete scheme given by* (4.2) *in the context of the lumped mass matrix. The dominating term in the consistency error at the grid points* $\{x_i\}_{0\le i\le N}$ *is second-order and is equal to* $\beta\frac{h^2}{6}\partial_{xxx}u(x_i,t)$.

Proof. The consistency error is

$$R_i[u](t) = \partial_t u(x_i, t) + \beta \frac{1}{2h} \left(u(x_{i+1}, t) - u(x_{i-1}, t) \right)$$

The Taylor expansions for the terms $u(x_{i\pm1}, t)$ about x_i are

$$\begin{aligned} u(x_{i+1}, t) = u(x_i, t) \pm h\partial_x u(x_i, t) + \frac{h^2}{2}\partial_{xx} u(x_i, t) \\ \pm \frac{h^3}{6}\partial_{xxx} u(x_i, t) + \frac{h^4}{24}\partial_{xxxx} u(x_i, t) + O(h^5). \end{aligned}$$

Utilizing these expansions in the expression for $R_i[u](t)$ gives

$$R_i[u](t) = \partial_t u(x_i, t) + \beta\partial_x u(x_i, t) + \beta\frac{h^2}{6}\partial_{xxx} u(x_i, t) + O(h^4),$$

which concludes the proof. □

The consistency error is therefore second-order and dispersive; this is in sharp contrast with the fourth-order error from the previous example. The consistency error arising from the use of the quadrature to approximate the coefficients c_{ij}, b_{ij} comes at the cost of loosing super-convergence at the grid points.

4.1.5 An integral commutator to measure consistency error

We want to emphasize again that the Taylor approximation method for analysing the consistency error, while familiar, relies on a tedious, error-prone process; one that is, further, not easily forged into an algorithmic setting. Moreover, as will be shown later, the Taylor approximation approach becomes increasingly intractable as we consider higher dimensional problems; this is due to a non-linear increase in the number of terms to be manipulated as the dimension increases. In this section we introduce a new tool, the integral commutator, for analysis of the consistency error of

the one dimensional model problem (4.1). The integral commutator approach offers a direct route for determining the consistency error.

Definition 4.3 (Integral commutator in one dimension) *Let $g \in C^0(\overline{\Omega})$ and let $\Pi(g(x))$ denote the continuous piecewise-linear Lagrange interpolant of the function g. Define the integral commutator for the $\mathbb{P}_1$ Galerkin linear approximation to the one dimensional problem* (4.1) *by*

$$C_i[g](t) = \Big(\int_\Omega \psi_i \,\mathrm{d}x\Big)^{-1} \Big(\int_\Omega \beta \left[\partial_x \Pi(g) - \Pi(\partial_x g)\right] \psi_i \,\mathrm{d}x\Big) \tag{4.8}$$

The principal motivation for the above definition is the following result, which up to our knowledge, seems to be new:

Proposition 4.3 *Suppose that u is the solution to model problem* (4.1) *then*

$$R_i[u](t) = C_i[u](t)$$

Proof. Using (4.3), (4.6), and the fact that $\Pi(\partial_t u + \beta \partial_x u) = 0$, we get

$$\begin{aligned}
R_i[u](t) \int_\Omega \psi_i \,\mathrm{d}x &= \sum_{j=1}^{N} \left(c_{ij} \partial_t u(t, x_j) + b_{ij} u(t, x_j)\right) \\
&= b(\sum_{j=1}^{N} u(t, x_j)\psi_j, \psi_i) = b(\Pi(u), \psi_i) \\
&= \int_\Omega \left[\partial_t \Pi(u) + \beta \partial_x \Pi(u)\right] \psi_i \,\mathrm{d}x - \int_\Omega \Pi(\partial_t u + \beta \partial_x u)\psi_i \,\mathrm{d}x \\
&= \int_\Omega \left[(\partial_t \Pi(u) - \Pi(\partial_t u)) + \beta(\partial_x \Pi(u) - \Pi(\partial_x u))\right] \psi_i \,\mathrm{d}x
\end{aligned}$$

From $\partial_t \Pi(u(x,t)) = \sum_{j=0}^{N-1} \partial_t \left(u(x_j,t)\psi_j(x)\right) = [\partial_t u](x_j,t)\psi_j(x) = \Pi(\partial_t u)$ it follows that $\partial_t \Pi(u) - \Pi(\partial_t u) = 0$, which in turn implies that

$$R_i[u](t) \int_\Omega \psi_i \, \mathrm{d}x = \int_\Omega \beta \left[\partial_x \Pi(u) - \Pi(\partial_x u)\right] \psi_i \, \mathrm{d}x = C_i[u](t) \int_\Omega \psi_i \, \mathrm{d}x$$

This concludes the proof. □

Proposition 4.3 shows that the integral commutator is an alternate form for the consistency error. At first it is not clear how to analyse the commutator expression as it requires the use of the solution to (4.1) to be wielded in some way other than the a-posteriori use of a Taylor expansion. It turns out that a key to analysis is an a-priori use of Taylor's theorem. Assuming that $tu(t,x)$ is continuously $k+1$ times differentiable, then Taylor's theorem yields $u(x,t) = \mathcal{P}_k^i[u](x,t) + \mathcal{R}_k^i[u](x,t)$, where $\mathcal{P}_k^i[u](x,t)$ is the Taylor polynomial of degree k expressed about the point x_i and $\mathcal{R}_k^i[u](x,t)$ is the corresponding remainder term:

$$\begin{aligned}
\mathcal{P}_k^i[u](x,t) &= u(x_i,t) + \frac{1}{2}\partial_x u(x_i,t)(x-x_i) + \ldots + \frac{1}{k!}\partial_x^{(k)} u(x_i,t)(x-x_i)^k \\
\mathcal{R}_k^i[u](x,t) &= \frac{1}{k!}(x-x_i)^{k+1} \int_0^1 (1-s)^k \partial_x^{k+1} u(s(x-x_i),t) ds
\end{aligned}$$

To simplify the discussion we assume that the point of interest is $x_i = 0$ and therefore drop the superscripts in Taylor terms; the analysis is the same at every point. Writing $u(x,t) = \mathcal{P}_k[u](x,t) + \mathcal{R}_k[u](x,t)$; then

$$C_0(u) = C_0\left(\mathcal{P}_k[u](x,t)\right) + C_0\left(\mathcal{R}_k[u](x,t)\right)$$

by linearity. Assume that $C_0(\mathcal{R}_k[u](x,t)) = O(h^{k+1})$, a proposition which will be proved in Lemma 4.1 for k odd, then it is evident by Proposition 4.3 that the

consistency error at the origin, $R_0[u](x,t)$, can be analysed by considering only $C_0(P_k[u](x,t))$, e.g.

Corollary 4.1 *Under the assumption that the integral commutator applied to the Taylor remainder satisfies* $C_0(\mathcal{R}_k[u](x,t)) = O(h^{k+1})$ *then the consistency error is* $R_0[u](t) = \sum_{m=0}^{k} \frac{1}{m!}\partial_x^{(m)} u(0,t) C_0(x^m) + O(h^{k+1})$.

We now reprove Proposition 4.1 via the integral commutator; the reader should note that, in the proof, tedious or 'tricky' manipulations have been replaced by direct computation via the integral commutator.

Proposition 4.4 (Integral commutator analysis) *The semi-discrete scheme of equation* (4.2) *with the consistent mass matrix has fourth order consistency error at the grid points. That is, the expression* $R_0[u](x,t) = O(h^4)$.

Proof. From Corollary 4.1 and the selection of $k = 3$ it suffices to show that $C_0(1) = C_0(x) = C_0(x^2) = C_0(x^3) = 0$. The cases $C_0(1)$ and $C_0(x)$ are immediately zero. This follows from the fact that $\mathbb{P}_1$ and $\partial_x \mathbb{P}_1 = \mathbb{P}_0$ are both invariant under Π. Now consider $C_0(x^2)$. The Lagrange interpolation preserves even-ness and odd-ness of a function. That is, if g is an even function then so is $\Pi(g)$; this can be checked as it holds nodally, at each x_j, and $\Pi(g)$ is linear. Therefore $\partial_x \Pi(x^2)$ is the derivative of an even function and therefore odd; likewise $\Pi(\partial_x x^2) = \Pi(2x) = 2x$ is odd. Hence, since ψ_0 is even it follows that

$$\int_\Omega \Pi\left(\partial_x x^2\right) \psi_0(x)\, \mathrm{d}x = \int_\Omega \partial_x \Pi\left(x^2\right) \psi_0(\,\mathrm{d}x)\, \mathrm{d}x = 0$$

Thus, the only task remaining is to compute $C_0(x^3)$; to do so we split the integration over the cells $[-h, 0]$ and $[0, h]$.

$$C_0\left(x^3\right) = \frac{\beta}{h}\int_{-h}^{0}\left[\partial_x\Pi\left(x^3\right) - \Pi\left(\partial_x x^3\right)\right]\psi_0\,\mathrm{d}x + \frac{\beta}{h}\int_{0}^{h}\left[\partial_x\Pi\left(x^3\right) - \Pi\left(\partial_x x^3\right)\right]\psi_0\,\mathrm{d}x$$

On both cells, $[-h, 0]$ and $[0, h]$, we have $\Pi(x^3) = h^2 x$; on the cell $[-h, 0]$ we have $3\Pi(x^2) = -3hx$, and on $[0, h]$ we have $3\Pi(x^2) = 3hx$. Therefore:

$$\int_{-h}^{0}\left[\partial_x\Pi\left(x^3\right) - \Pi\left(\partial_x x^3\right)\right]\psi_0\,\mathrm{d}x = \int_{-h}^{0}\left[h^2 + 3hx\right]\psi_0(x) = \int_{-h}^{0}\left[h^2 + 3hx\right]\left(1 + \frac{1}{h}x\right)\mathrm{d}x = 0$$

$$\int_{0}^{h}\left[\partial_x\Pi\left(x^3\right) - \Pi\left(\partial_x x^3\right)\right]\psi_0\,\mathrm{d}x = \int_{0}^{h}\left[h^2 - 3hx\right]\psi_0(x) = \int_{0}^{h}\left[h^2 - 3hx\right]\left(1 - \frac{1}{h}x\right)\mathrm{d}x = 0$$

The result follows readily. □

Remark 4.1 *It is worth recalling that we made the simplifying assumption $\psi_i = \psi_0$ by invoking a linear-shift change of variables. This can be done without loss of generality because the basis $\{\psi_0, \psi_1, \ldots, \psi_{N-1}\}$ is invariant under linear transformation; it can also be noted that, by rescaling, we can consider the mesh size to be $h = 1$. As a result the analysis of the commutator, for $\mathbb{P}^1$ finite elements, need only be carried out for $\psi_i = \psi_0$ on the interval $[-1, 1] = support(\psi_0)$. This theme will be repeated in higher dimensions and is a general simplifying assumption* assuming *that the sup-*

ports of the basis functions $\{\psi_0, \psi_1, \ldots, \psi_{N-1}\}$ *are self-similar; e.g. all supports can be mapped into the support of* ψ_0 *by a linear transformation so that there is only one type of support.*

This concludes the main points of the section; the regularity assumption utilized in Corollary 4.1 is proven for the general n-dimensional case in Lemma 4.1.

4.2 Higher dimensional extensions and anti-dispersion

In this section the one dimensional concepts are extended to arbitrarily high dimensions; in practice dimension two and three are of the most concern.

4.2.1 The integral commutator in arbitrary dimensions

In this section we briefly discuss the requisite definitions for the integral commutator in high dimensions. Multi-index notation is utilized throughout the discussion; by a multi-index we mean an n-tuple $\alpha = (\alpha_1, \alpha_2, ..., \alpha_n)$ and the tuple 1_m is one in the m^{th} position and zero elsewhere; e.g. $(1_m)_j = \delta_j^m$. The length of a multi-index is $|\alpha| = \sum_{i=1}^n \alpha_i$ and a differential operator notation for multi-indices is $D^\alpha := \partial_{x_1}^{\alpha_1}\partial_{x_2}^{\alpha_2}..\partial_{x_n}^{\alpha_n}$. We begin by re-stating the model problem, (4.1), in n dimensional space. Let Ω be the domain $\mathbb{R}^n$ or the n-dimensional torus $\mathbb{T}^n$. We seek the solution to the following transport problem:

$$\partial_t u + \beta \cdot \nabla u = 0, \quad u(\mathbf{x}, 0) = u_0(\mathbf{x}), \quad (\mathbf{x}, t) \in \Omega \times \mathbb{R}_+ \tag{4.1}$$

equipped with periodic boundary conditions. The velocity field, $\beta \in \mathbb{R}^n$, is again assumed constant. The solution to solution to (4.1) is $u_0(\mathbf{x} - \boldsymbol{\beta} t)$ where we abusively denote u_0 the periodic extension of u_0.

To frame the Galerkin linear approximation problem proceed by partitioning the domain Ω into a mesh, $\mathcal{T}_h$, of elements (tetrahedra, hypercubes, etc) of diameter

h and let N denote the number of degrees of freedom. The mesh family $\{\mathcal{T}_h\}_{h>0}$ is assumed to be shape-regular. Let $\{\psi_0, \psi_1, \ldots, \psi_{N-1}\}$ be the family composed of the continuous and piecewise linear Lagrange polynomials associated with the nodes $\{x_0, \ldots, x_N\}$. Let $K \in \mathcal{T}_h$ denote a mesh element (a simplex, a quadrangle or a parallelepiped); the *diameter* of K as well as a global mesh quantity, h, are defined by

$$h_K := \operatorname{diam}(K) := \max_{x_1, x_2 \in K} |x_1 - x_2| \tag{4.2}$$

$$h := \max_{K \in \mathcal{T}_h} h_K. \tag{4.3}$$

Let $\mathbb{P}_k(\mathbb{R}^n)$ and $\mathbb{Q}_k(\mathbb{R}^n)$ denote the polynomials of total degree k and partial degree k, respectively, in n spatial dimensions. In the context of the present work we will focus on piecewise linear approximation. Letting P denote either $\mathbb{P}_1(\mathbb{R}^n)$ or $\mathbb{Q}_1(\mathbb{R}^n)$, we define the finite element approximation space as follows:

$$\mathbf{X}_h = \left\{ v \in C^0(\overline{\Omega}; \mathbb{R}^n) \mid v_{|T_h} \in P, \forall T_h \in \mathcal{T}_h \right\}, \tag{4.4}$$

where $C^0(\overline{\Omega}; \mathbb{R}^n)$ denotes the space of real-valued functions which are continuous over $\overline{\Omega}$. Whenever the symbol $\mathbf{X}_h$ is used in the discourse the interpretation is 'either $P^1(\Omega)$ or $Q^1(\Omega)$'. Again we let $U_0(\mathbf{x})$ denote a reasonable approximation of $u_0(\mathbf{x})$; such as the Lagrange interpolate or L^2 projection of u_0. An approximate solution to (4.1) can then be constructed via an application of the Galerkin technique. A solution $U \in C^1([0, T]; \mathbf{X}_h)$ is sought which satisfies $U(\mathbf{x}, 0) = U_0(\mathbf{x})$ and

$$b(U, v) \; := \; \int_\Omega (\partial_t U + \beta \cdot \nabla U) v \, \mathrm{d}x = 0, \quad \forall v \in \mathbf{X}_h. \tag{4.5}$$

In order to compute the solution U to (4.5) we once more represent $U(t,x)$ in terms of the basis functions $\{\psi_0, \psi_1, \ldots, \psi_{N-1}\}$ as $U(t,x) = \sum_{j=1}^{N} U(t,x_j)\psi_j(x)$. Then

$$0 = b(U,\psi_i) = b\left(\sum_{j=1}^{N} U(t,x_j)\psi_j(x), \psi_i\right) = \sum_{j=1}^{N} \left(c_{ij}\partial_t U(t,x_j) + b_{ij}U(t,x_j)\right) \tag{4.6}$$

$$c_{ij} = \int_\Omega \psi_j\psi_i \,\mathrm{d}x, \quad b_{ij} = \sum_{m=1}^{n} \beta_m \int_\Omega \partial_{x_m}\psi_j\psi_i \,\mathrm{d}x \tag{4.7}$$

Note that the definition of consistency error, equation (4.6), is dimension independent and that the order of the consistency error, equation (4.7), need only be modified by replacing $h_{i+\frac{1}{2}}$ with h; we do not repeat these definitions here. The integral commutator in n dimensions is defined similarly to (4.1) :

Definition 4.1 *(Integral commutator in n dimensions) Let $g \in C^0(\overline{\Omega})$ and $\Pi(g(x))$ denote the $\mathbb{P}_1$ piecewise-linear Lagrange interpolant of the function g; e.g. $\Pi(g(x)) = \sum_{i=1}^{N} g(x_i)\psi_i(x)$. Define the integral commutator for the $\mathbb{P}_1$ Galerkin linear approximation to the one dimensional problem* (4.1) *by*

$$C_i[g] = \left(\int_\Omega \psi_i \,\mathrm{d}x\right)^{-1} \left(\sum_{m=1}^{n} \int_\Omega \beta_m \left[\partial_{x_m}\Pi(g) - \Pi(\partial_{x_m} g)\right]\psi_i \,\mathrm{d}x\right) \tag{4.8}$$

Remark 4.1 *If, in addition, g is a function of time such that $\forall t_0 \in [0,T]$ we have $g(\mathbf{x},t_0) \in C^0(\overline{\Omega})$ the extension of the integral commutator definition is immediate and depends on t.*

Some results are now established for the commutator which will be useful for later analysis; we apply the commutator to a particular family of functions and, in addition, prove an equivalence which will simplify consistency error analysis.

Corollary 4.1 *Let α be a multi-index with $|\alpha| \geq 1$. Denote by ψ_i a nodal basis function of $\mathbf{X}_h$ corresponding to the node $\mathbf{x}_i$. Then $C_i[(\mathbf{x}-\mathbf{x_i})^\alpha]$ is of order less than or equal to $O(h^{|\alpha|-1})$*

Proof. Consider the quantity

$$C_i[(\mathbf{x}-\mathbf{x_i})^\alpha] = \Big(\int_\Omega \psi_i\Big)^{-1} \sum_{m=1}^{n} \int_\Omega \beta_m \left[\partial_{x_m} \Pi\left((\mathbf{x}-\mathbf{x_i})^\alpha\right)\right] - \Big(\int_\Omega \psi_i\Big)^{-1} \sum_{m=1}^{n} \int_\Omega \beta_m \left[\Pi\left(\partial_{x_m}(\mathbf{x}-\mathbf{x_i})^\alpha\right)\right] \psi_i \,\mathrm{d}x.$$

Fix $m \in \{1, 2, ..., n\}$; the proof proceeds by showing that each of the expressions $\int_\Omega \left[\partial_{x_m}\Pi((\mathbf{x}-\mathbf{x_i})^\alpha)\right] \psi_i \,\mathrm{d}x$ and $\int_\Omega \left[\Pi(\partial_{x_m}(\mathbf{x}-\mathbf{x_i})^\alpha))\right] \psi_i \,\mathrm{d}x$ are order less than or equal to $O(h^{|\alpha|-1})$. Accordingly, due to the multiplication by ψ_i in the integrand of these expressions, we need only consider the integral over the support set $S_i = \mathrm{support}(\psi_i)$ and not the entire domain Ω. It suffices to prove that the order estimates hold when integrating over an arbitrary cell $K \subset S_i$, since, the mesh family being shape-regular, the number of cells in S_i is uniformly bounded with respect to h. For the first term is estimated as follows:

$$\begin{aligned}
\Big|\int_K \left[\partial_{x_m}\Pi\left((\mathbf{x}-\mathbf{x_i})^\alpha\right)\right] \psi_i \,\mathrm{d}x\Big| &\leq \|\partial_{x_m}\Pi((\mathbf{x}-\mathbf{x_i})^\alpha\|_{L^\infty(\Omega)} \|\psi_i\|_{L^1(K)} \\
&\leq c\, h_K^{-1} \|\Pi((\mathbf{x}-\mathbf{x_i})^\alpha\|_{L^\infty(K)} \|\psi_i\|_{L^1(K)} \\
&\leq c\, h_K^{-1} \left(\max_{x_j \in V(K)} |\mathbf{x}_j - \mathbf{x}_i|^\alpha\right) \|\psi_i\|_{L^1(K)} \\
&\leq c\, h_k^{-1} h_K^{|\alpha|} \|\psi_i\|_{L^1(K)} \leq c\, h^{|\alpha|-1} \|\psi_i\|_{L^1(K)},
\end{aligned}$$

where $V(K)$ denotes the set of vertices of K. Note that we used the inverse inequality $\|\partial_{x_m}\Pi(f)\|_{L^\infty(K)} \leq c\, h_K^{-1} \|\Pi(f)\|_{L^\infty(K)}$ and the property of the Lagrange interpolation

$\|\Pi(f)\|_{L^\infty(K)} \leq \max\limits_{x_j \in V(K)} |f(x_j)|$. The second quantity is treated similarly:

$$
\begin{aligned}
\left| \int_K \left[\Pi \left(\partial_{x_m} \left(\mathbf{x} - \mathbf{x_i} \right)^\alpha \right) \right] \psi_i \, \mathrm{d}x \right| &\leq \|\psi_i\|_{L^1(K)} \| \Pi \left(\partial_{x_m} \left(\mathbf{x} - \mathbf{x_i} \right)^\alpha \right) \|_{L^\infty(K)} \\
&\leq \alpha_m \| \Pi \left(\left(\mathbf{x} - \mathbf{x_i} \right)^{\alpha - 1_m} \right) \|_{L^\infty(K)} \|\psi_i\|_{L^1(K)} \\
&\leq c \max_{x_j \in V(K)} |\mathbf{x}_j - \mathbf{x}_i|^{\alpha - 1_m} \|\psi_i\|_{L^1(K)} \\
&\leq c \, h_K^{|\alpha|-1} \leq C h^{|\alpha|-1} \|\psi_i\|_{L^1(K)}.
\end{aligned}
$$

This completes the proof since $\sum_{K \subset S_i} \|\psi_i\|_{L^1(K)} = \int_\Omega \psi_i$. □

Remark 4.2 *The proofs of the inverse inequalities and properties properties of the Lagrange interpolant utilized to establish corollary* (4.1) *can be found in [8].*

Corollary 4.2 *Fix a choice of $k \in \mathbb{N}$ and a point $\mathbf{x}_i \in \mathbb{R}^n$. Then $C_i[(\mathbf{x} - \mathbf{x}_i)^\alpha] = 0$ for all α with $|\alpha| \leq k$ if and only if $C_i[\mathbf{x}^\alpha] = 0$ for all α with $|\alpha| \leq k$.*

Proof. ($\leftarrow$): Assume that $C_i[\mathbf{x}^\alpha] = 0$ for all α with $|\alpha| \leq k$. Let a multi-index $\alpha = (\alpha_1, \alpha_2, \ldots, \alpha_n)$ be such that $|\alpha| \leq k$ and consider $C_i[(\mathbf{x} - \mathbf{x}_i)^\alpha]$. Utilizing the binomial theorem to each component of $(\mathbf{x} - \mathbf{x}_i)^\alpha$ and expanding the result yields a sum of terms each having total order less than or equal to k. Applying the linearity of the integral commutator, i.e. $C_i[af + bg] = aC_i[f] + bC_i[g]$, to the expansion of $(\mathbf{x} - \mathbf{x}_i)^\alpha$ and using the hypothesis renders each term in the resulting sum zero. This concludes this direction of the proof.

($\rightarrow$): We proceed by induction on the order of α; we need to show that $C_i[\mathbf{x}^\alpha] = 0$ for all $|\alpha| \leq k$ assuming that whenever $|\alpha| \leq k$ all expressions $C_i[(\mathbf{x} - \mathbf{x}_i)^\alpha] = 0$ holds. For the base case assume that $|\alpha| = 0$. Then $1 = (\mathbf{x} - \mathbf{x}_i)^\alpha = \mathbf{x}^\alpha$ and the result follows by hypothesis. Now suppose that $C_i[\mathbf{x}^{\alpha_0}] = 0$ for all $|\alpha_0| \leq j < k$; we need

to show that $C_i[\mathbf{x}^\alpha] = 0$ for all $|\alpha| = j + 1$. Fix an α with $|\alpha| = j + 1$. Consider $(\mathbf{x} - \mathbf{x}_i)^\alpha$; by hypothesis $C_i[(\mathbf{x} - \mathbf{x}_i)^\alpha] = 0$. The leading term of the expansion of $(\mathbf{x} - \mathbf{x}_i)^\alpha$ is the product of the leading terms of the individual factors $(\mathbf{x}^j - \mathbf{x}_i^j)^{\alpha_j}$. E.g. the leading term is precisely $\mathbf{x}^\alpha$ and $(\mathbf{x} - \mathbf{x}_i)^\alpha = \mathbf{x}^\alpha + p(\mathbf{x})$ where $p(\mathbf{x})$ is a sum of terms of total degree less than or equal to $|\alpha| - 1 = j$. The linearity of the integral commutator and the hypothesis give

$$0 = C_i[(\mathbf{x} - \mathbf{x}_i)^\alpha] = C_i[\mathbf{x}^\alpha] + C_i[p(\mathbf{x})] = C_i[\mathbf{x}^\alpha]$$

since, by linearity of the commutator and the inductive hypothesis, $C_i[p(\mathbf{x})] = 0$. This concludes the proof. □

Remark 4.3 *When performing point-wise consistency error analysis, in the upcoming results, corollary* (4.2) *will allow us to trade a complex expression,* $C_i[(\mathbf{x} - \mathbf{x}_i)^\alpha]$*, for the simpler expression* $C_i[\mathbf{x}^\alpha]$*.*

Just as in the one-dimensional case, as given in proposition (4.3), we have the principal result of equivalence of the integral commutator and consistency error:

Proposition 4.1 *Suppose that* u *is the solution to the model problem* (4.1) *then*

$$R_i[u](t) = C_i[u](t)$$

Proof. The arguments of proposition (4.3) slightly modified

$$
\begin{aligned}
R_i[u](t) \int_\Omega \psi_i \, \mathrm{d}x &= \sum_{j=1}^{N} \left(c_{ij} \partial_t u(x_j, t) + b_{ij} u(x_j, t) \right) \\
&= b \left(\sum_{j=1}^{N} u(x_j, t) \psi_j, \psi_i \right) = b \left(\Pi(u), \psi_i \right) \\
&= \int_\Omega \left[\partial_t \Pi(u) + \beta \cdot \nabla \Pi(u) \right] \psi_i \, \mathrm{d}x - \int_\Omega \Pi \left(\partial_t u + \beta \cdot \nabla u \right) \psi_i \, \mathrm{d}x \\
&= \int_\Omega \left[\left(\partial_t \Pi(u) - \Pi(\partial_t u) \right) + \sum_{m=1}^{n} \beta_m (\partial_{x_m} \Pi(u) - \Pi \left(\partial_{x_m} u \right)) \right] \psi_i \, \mathrm{d}x
\end{aligned}
$$

The rest now follows, just as in proposition (4.3), from the key property of the Lagrange interpolant, namely : $\partial_t \Pi(u) - \Pi(\partial_t u) = 0$.

$$
\begin{aligned}
&\int_\Omega \left[\left(\partial_t \Pi(u) - \Pi(\partial_t u) \right) + \sum_{m=1}^{n} \beta_m (\partial_{x_m} \Pi(u) - \Pi(\partial_{x_m} u)) \right] \psi_i \, \mathrm{d}x = \\
&\sum_{m=1}^{n} \int_\Omega \beta_m \left[\partial_{x_m} \Pi(u) - \Pi(\partial_{x_m} u)) \right] \psi_i \, \mathrm{d}x = C_i[u](t) \int_\Omega \psi_i \, \mathrm{d}x
\end{aligned}
$$

This concludes the proof.□

Just as in the one dimensional case the key to further analysis via the integral commutator is the a-priori expansion of u, the solution to equation (4.4), in terms of of the Taylor series. Assuming again that u is $k+1$ times continuously differentiable in the variables $\mathbf{x} = (x_1, x_2, \ldots, x_n)$ the Taylor polynomial term $\mathcal{P}_k^i[u]$ and remainder $\mathcal{R}_k^i[u]$ are given by

$$\mathcal{P}_k^i[u](\mathbf{x},t) = \sum_{|\alpha|=0}^{k} \frac{1}{\alpha!} D^\alpha u(\mathbf{x}_i,t)(\mathbf{x}-\mathbf{x}_i)^\alpha \tag{4.9}$$

$$\mathcal{R}_k^i[u](x,t) = \sum_{|\alpha|=k+1} \frac{|\alpha|}{\alpha!}(\mathbf{x}-\mathbf{x}_i)^\alpha \int_0^1 (1-s)^{|\alpha|-1} D^\alpha u(\mathbf{x}_i + s(\mathbf{x}-\mathbf{x}_i),t)ds \tag{4.10}$$

Where $\alpha = (\alpha_1, \alpha_2, \ldots, \alpha_n)$ is a multi-index, $|\alpha| := \alpha_1 + \alpha_2 + \ldots + \alpha_n$, $\alpha! := \alpha_1!\alpha_2! \ldots \alpha_n!$ and if $\mathbf{y} = (y_1, y_2, \ldots, y_n)$ then $\mathbf{y}^\alpha := (y_1^{\alpha_1}, y_2^{\alpha_2}, \ldots, y_n^{\alpha_n})$. previously we simplify the discussion by assuming the mesh point of interest is x_0 and drop the superscript in the Taylor terms; we proceed by analysing $C_0[u]$ and $R_0[u]$. Utilizing the expansion about the node x_i, as well as corollary (4.2), the n dimensional result to corollary (4.1) now follows:

Corollary 4.3 *(**Consistency-error analysis for the Integral Commutator**) Under the assumption that the integral commutator applied to the Taylor remainder is of the order $C_i(\mathcal{R}_k^i[u](\mathbf{x},t)) = O(h^{k+1})$ in n dimensions then*

$$R_i[u](t) = \sum_{|\alpha|=0}^{k} \frac{1}{\alpha!} D^\alpha u(\mathbf{x}_i,t) C_i(\mathbf{x}^\alpha) + O(h^{k+1})$$

The hypothesis $C_i(\mathcal{R}_k^i[u](x,t)) = O(h^{k+1})$, for odd k, in n dimensions is proven in lemma (4.1), assuming a particular symmetry, closes the section. Before giving the proof of the lemma we remark that it is not the case, in general, that in n dimensions we have $R_0[u] = O(h^4)$ as we do in one dimension; we will come to see that, in fact, this is true in two dimensions if the mesh is selected with certain symmetry properties. We will analyse to what extent this result does not depend on the velocity, β, or initial date, $u_0(\mathbf{x})$, of the model problem and this will motivate the definition of an *anti-dispersive* approximation setting.

In order to establish lemma (4.1) the concept of a *centro-symmetric set* is needed; we call a convex set, W, *centro-symmetric* about a point $\mathbf{y} \in W$ if whenever $\mathbf{x} \in W$ then the line $l(t) = (1-t)\mathbf{y} + t\mathbf{x}$ is in W for $t \in [-1, 1]$. The point $l(-1)$ is often denoted by $l(-1) = -\mathbf{x}$ or $l(-1) = \mathbf{x}^*$; this point is the 'reflection' of $\mathbf{x}$ through the point $\mathbf{y}$.

Lemma 4.1 *Let $k \in \mathbb{N}$ be odd; then if u is $k+1$ times differentiable in the variables $\mathbf{x} = (x_1, x_2, \ldots, x_n)$ and $S_i = support(\psi_i)$ is centro-symmetric about the point $\mathbf{x}_i$ then $C_i(\mathcal{R}_k^i[u]) = O(h^{k+1})$.*

Proof. By a linear change of coordinates we may assume, without loss of generality, that $\mathbf{x}_i = 0$ and that $\psi_i = \psi_0$; we may then proceed by analysing $C_i(\mathcal{R}_k^0[u])$. By definition

$$
\begin{aligned}
&C_0(\mathcal{R}_k^0[u](t,x)) \\
&\quad = \Big(\int_\Omega \psi_0\Big)^{-1} \left(\sum_{m=1}^{n} \int_\Omega \partial_{x_m} \Pi(\mathcal{R}_k[u](t,\mathbf{x})))\psi_0 d\mathbf{x} - \int_\Omega \Pi(\partial_{x_m}\mathcal{R}_k[u](t,\mathbf{x})))\psi_0 d\mathbf{x}\right)
\end{aligned}
$$

The proof proceeds by analysing the two summed inner terms separately and showing that they are each $O(h^{k+2})$; the result will then follow from summing and the fact that $\int_\Omega \psi_0 \, \mathrm{d}x = O(h)$. In order to facilitate the remainder of the proof define the function $\phi_j(s) = D^\alpha u(t, s x_j)$. The derivative $\phi_j'(s)$ then satisfies

$$
\begin{aligned}
|\phi_j'(s)| &= |\sum_{m=1}^{n} \mathbf{x}_{j,m} D^{\alpha+1_m} u(t, s\mathbf{x}_j)| \\
&\leq \sum_{m=1}^{n} |\mathbf{x}_{j,m}| \max_{|\beta|=|\alpha|+1} |D^\beta u(t, s\mathbf{x}_j)| \\
&\leq Ch \max_{|\beta|=|\alpha|+1} |D^\beta u(t, s\mathbf{x}_j)| \qquad (4.11)
\end{aligned}
$$

First term

Consider the term $\int_\Omega \partial_{x_m}\Pi(\mathcal{R}_k^0[u](t,\mathbf{x})))\psi_0 d\mathbf{x}$ and let $S_0 = \text{support}(\psi_0)$ then

$$\begin{aligned}\int_\Omega \partial_{x_m}\Pi(\mathcal{R}_k^0[u](t,\mathbf{x})))\psi_0 d\mathbf{x} &= \sum_{j=1}^{N} \mathcal{R}_k^0[u](t,x_j)\int_{S_0}\partial_{x_m}\psi_j\psi_0 \\ &= \sum_{j=1}^{N/2}(\mathcal{R}_k^0[u](t,x_j)-\mathcal{R}_k^0[u](t,-x_j))\int_{S_0}\partial_{x_j}\psi_j\psi_0\end{aligned} \tag{4.12}$$

Note that each expression of the form $\partial_{x_m}\psi_j$ is either zero or $O(h^{-1})$; therefore $\int_{S_0}\partial_{x_m}\psi_j\psi_0 = O(C)$ since $\int_{S_0}\psi_0 = O(h)$. Expanding the difference of the terms $(\mathcal{R}_k^0[u](t,x_j)-\mathcal{R}_k^0[u](t,-x_j))$ in the above expression and using the fact that k is odd yields

$$\begin{aligned}&\mathcal{R}_k^0[u](t,x_j)-\mathcal{R}_k^0[u](t,-x_j)\\ &\quad= \sum_{|\alpha|=k+1}\frac{k+1}{\alpha!}\mathbf{x}_j^\alpha\int_0^1(1-s)^k\left[(D^\alpha g)(t,s\mathbf{x}_j)-(D^\alpha g)(t,-s\mathbf{x}_j)\right]ds\\ &\quad= \sum_{|\alpha|=k+1}\frac{k+1}{\alpha!}\mathbf{x}_j^\alpha\int_0^1(1-s)^k\left[\phi(s)-\phi(-s)\right]ds\\ &\quad= \sum_{|\alpha|=k+1}\frac{k+1}{\alpha!}\mathbf{x}_j^\alpha\int_0^1(1-s)^k\int_{-s}^{s}\phi_j'(\xi)d\xi\end{aligned}$$

Taking absolute values and utilizing inequality (4.11) yields

$$\begin{aligned}|R_k^0[u](t,x_j)-\mathcal{R}_k^0[u](t,-x_j)| &\le \sum_{|\alpha|=k+1}\frac{k+1}{\alpha!}|\mathbf{x}_j|^\alpha\int_0^1\int_{-s}^{s}|\phi_j'(\xi)d\xi|\\ &\le \sum_{|\alpha|=k+1}\frac{k+1}{\alpha!}Ch|\mathbf{x}_j|^\alpha\max_{|\beta|=|\alpha|+1}|D^\beta u(t,s\mathbf{x}_j)|\\ &= O(h^{k+2})\end{aligned}$$

Applying this inequality to (4.12) gives

$$\begin{aligned}|\int_\Omega \partial_{x_m}\Pi(\mathcal{R}_k^0[u](t,\mathbf{x})))\psi_0 d\mathbf{x}| &\leq \sum_{j=1}^{N/2} |(\mathcal{R}_k^0[u](t,x_j) - \mathcal{R}_k^0[u](t,-x_j))||\int_{S_0}\partial_{x_j}\psi_j\psi_0 d\mathbf{x}| \\ &\leq \sum_{j=1}^{N/2} O(h^{k+2})\left(|\int_{S_0}\partial_{x_m}\psi_j\psi_0 d\mathbf{x}|\right) = O(h^{k+1})\end{aligned}$$

This is the desired result for the first term.

Second term

For the second term : $\int_\Omega \Pi(\partial_{x_m}\mathcal{R}_k^0[u](t,\mathbf{x}))\psi_0 d\mathbf{x}$. By definition this is

$$\begin{aligned}\int_\Omega \Pi(\partial_{x_m}\mathcal{R}_k^0[u](t,\mathbf{x})))\psi_0 d\mathbf{x} &= \sum_{j=0}^{N}\partial_{x_m}\mathcal{R}_k^0[u](t,\mathbf{x}_j)\int_{S_0}\psi_j\psi_0 d\mathbf{x} \\ &= O(h)\sum_{j=0}^{N}\partial_{x_m}\mathcal{R}_k^0[u](t,\mathbf{x}_j)\end{aligned}$$

Since terms of the form $\int_{S_0}\psi_j\psi_0$ are $O(h)$. To calculate the term $\partial_{x_m}\mathcal{R}_k^0[u](\mathbf{x}_j)$ the integral remainder equation (4.10) is utilized. Consequently

$$\begin{aligned}\partial_{x_m}\mathcal{R}_k^0[u](t,\mathbf{x}) &= \partial_{x_m}\left(\sum_{|\alpha|=k+1}\frac{k+1}{!\alpha}\prod_{l=1}^{n}x_l^{\alpha_l}\int_0^1(1-s)^k D^\alpha g(t,s\mathbf{x})ds\right) \\ &= \sum_{|\alpha|=k+1}\frac{k+1}{\alpha!}\left(A(\alpha;t,\mathbf{x}) + B(\alpha;t,\mathbf{x})\right)\end{aligned}$$

Where, letting $\mathbf{x} = (x_1, x_2, \ldots, x_n)$, the terms $A(\alpha;t,\mathbf{x})$ and $B(\alpha;t,\mathbf{x})$ are

$$A(\alpha;t,\mathbf{x}) = \begin{cases} \alpha_m x_m^{\alpha_m - 1}\prod_{l\neq m}x_l^{\alpha_l}\int_0^1(1-s)^k(D^\alpha g)(t,s\mathbf{x})d\mathbf{s} & \text{if } \alpha_m \neq 0 \\ 0 & \text{if } \alpha_m = 0 \end{cases}$$

$$B(\alpha;t,\mathbf{x}) = \prod_{l=1}^{n}x_l^{\alpha_l}\int_0^1(1-s)^k s(D^{\alpha+\mathbf{1}_m}g)(t,s\mathbf{x})ds$$

and $\mathbf{1}_m$ is the multi-index which is one in the m^{th} position and zero elsewhere. Using

these expressions the expression $\Pi(\partial_{x_m}\mathcal{R}_k[u](t,\mathbf{x}))$ is

$$\begin{aligned}
&\Pi(\partial_{x_m}\mathcal{R}_k^0[u](t,\mathbf{x})) \\
&\quad = \sum_{j=1}^{N}\left[\partial_{x_m}\mathcal{R}_k^0[u](t,\mathbf{x}_j)\right]\psi_j\psi_0 = \sum_{j=1}^{N}\left[A(\alpha;t,\mathbf{x}_j)+B(\alpha;t,\mathbf{x}_j)\right]\psi_j\psi_0 \\
&\quad = \sum_{j=1}^{N/2}\left[A(\alpha;t,\mathbf{x}_j)+A(\alpha;t,-\mathbf{x}_j)+B(\alpha;t,\mathbf{x}_j)+B(\alpha;t,-\mathbf{x}_j)\right]\psi_j\psi_0
\end{aligned}$$

The constituent expressions $A(\alpha;t,\mathbf{x}_j)+A(\alpha;t,-\mathbf{x}_j)$, for $\alpha_j \neq 0$, and $B(\alpha;t,\mathbf{x}_j)+B(\alpha;t,-\mathbf{x}_j)$ can be simplified; note that the first simplification uses the fact that k is odd.

$$\begin{aligned}
&A(\alpha;t,\mathbf{x}_j)+A(\alpha;t,-\mathbf{x}_j) \\
&\quad = \alpha_m(\mathbf{x}_j)_m^{\alpha_m-1}\prod_{l\neq m}^{n}(\mathbf{x}_j)_l^{\alpha_l}\int_0^1(1-s)\left[(D^\alpha g(t,s\mathbf{x}_j)-D^\alpha g(t,-s\mathbf{x}_j)\right]ds \\
&\quad = \alpha_m(\mathbf{x}_j)^{\alpha_m-1}\prod_{l\neq m}(\mathbf{x}_j)_l^{\alpha_l}\int_0^1(1-s)^k\int_0^1\nabla(D^\alpha g)(\xi s\mathbf{x}_j)\cdot 2\mathbf{x}_j d\xi ds
\end{aligned}$$

$$\begin{aligned}
&B(\alpha;t,\mathbf{x}_j)+B(\alpha;t,-\mathbf{x}_j) = \\
&\quad \prod_{l=1}^{n}(\mathbf{x}_j)_l^{\alpha_l}\int_0^1(1-s)^k s\left[(D^{\alpha+\mathbf{1}_m}g)(t,s\mathbf{x}_j)+(D^{\alpha+\mathbf{1}_m}g)(t,-s\mathbf{x}_j)\right]ds
\end{aligned}$$

These equations yield the estimates

$$\begin{aligned}
|A(\alpha;t,\mathbf{x}_j)+A(\alpha;t,-\mathbf{x}_j)| &\leq O(h^k)\left(Ch\sup_{|\alpha|=k+2}||D^\alpha g||_\infty\right) = O(h^{k+1}) \\
|B(\alpha;t,\mathbf{x}_j)+B(\alpha;t,-\mathbf{x}_j)| &\leq O(h^{k+1})\left(2C\sup_{|\alpha|=k+2}||D^\alpha g||_\infty\right) = O(h^{k+1})
\end{aligned}$$

Using these estimates the result is

$$
\begin{aligned}
|\int_{\Omega}\Pi(\partial_{x_m}\mathcal{R}_k[u](t,\mathbf{x})))\psi_0 d\mathbf{x}| &\leq \sum_{j=0}^{N}|\partial_{x_m}\mathcal{R}_k[u](t,\mathbf{x}_j)||\int_{S_0}\psi_j\psi_0 d\mathbf{x}| \\
&\leq O(h)\sum_{j=1}^{N}\left(|\sum_{|\alpha|=k+1}\frac{k+1}{\alpha!}\left(A(\alpha;t,\mathbf{x}_j)+B(\alpha;t,\mathbf{x}_j)\right)|\right) \\
&\leq O(h)\sum_{j=1}^{N/2}\sum_{|\alpha|=k+1}\frac{k+1}{\alpha!}\left(|A(\alpha;t,\mathbf{x}_j)+A(\alpha;t,-\mathbf{x}_j)|\right)+ \\
&O(h)\sum_{j=1}^{N/2}\sum_{|\alpha|=k+1}\left(|B(\alpha;t,\mathbf{x}_j)+B(\alpha;t,-\mathbf{x}_j)|\right) \\
&= O(h)\,O(h^{k+1}) = O(h^{k+2})
\end{aligned}
$$

This concludes the result for term two.

Using the derived results and the fact that

$$
\begin{aligned}
|C_0(\mathcal{R}_k^0[u](t,x))| \leq h\sum_{m=1}^{n}\left(|\int_{\Omega}\partial_{x_m}\Pi(\mathcal{R}_k^0[u](t,\mathbf{x})))\psi_0 d\mathbf{x}|\right)+ \\
h\sum_{m=1}^{n}\left(|\int_{\Omega}\Pi(\partial_{x_m}\mathcal{R}_k^0[u](t,\mathbf{x})))\psi_0 d\mathbf{x}|\right)
\end{aligned}
$$

concludes the proof of the proposition. □

Remark 4.4 *Note that the support of ψ_0 in one dimension is centro-symmetric; this property was used in the one-dimensional proof implicitly when the fundamental theorem of calculus was utilized. Indeed, the centro-symmetry assumption is utilized to employ the fundamental theorem in higher dimensions.*

4.2.2 Anti-dispersive spaces

Before proceeding to computational results in higher dimensions we discuss the last concept of note for integral commutator based analysis of the model problem

(4.1); anti-dispersivity. Intuitively speaking a Galerkin approximation setting is called *anti-dispersive* if for every model problem of the form (4.1) the consistency error satisfies $C_i[u](t) = O(h^4)$ for all $i = 0, 1, \ldots, N-1$. Proposition (4.4) showed that $P^1(\mathbb{R}^1)$ was anti-dispersive if a uniform mesh $\mathcal{T}_h$, of size h, were chosen. In general both the mesh and the underlying approximation space play a role in the consistency error; we refer to the choice of approximation space and underlying mesh as an *approximation setting*. In two dimensions we will show that there exists a uniform mesh $\mathcal{T}_h$ such that the $P^1(\mathbb{R}^2)$ finite element approximation is an anti-dispersive setting. For the purposes of this paper we will only be considering approximation settings where the mesh, $\mathcal{T}_h$ is uniform, of size h, and the finite element spaces are one of

$$P^k(\mathbb{R}^n) = \left\{ v \in C^0_{\#}(\mathbb{R}^n) \mid \forall T_h \in \mathcal{T}_h \;\; v_{|T_h} \in \mathbb{P}_k(\mathbb{R}^n) \right\}$$
$$Q^k(\mathbb{R}^n) = \left\{ v \in C^0_{\#}(\mathbb{R}^n) \mid \forall T_h \in \mathcal{T}_h \;\; v_{|T_h} \in \mathbb{Q}_k(\mathbb{R}^n) \mid \right\}$$

Definition 4.2 *The finite element space $P^k(\mathbb{R}^n)$ or $Q^k(\mathbb{R}^n)$, defined on a uniform mesh $\mathcal{T}_h$, is called an* ***anti-dispersive setting****, for the model problem* (4.1)*, if and only if for all $i = 0, 1, \ldots, N-1$ and $t \in [0, T]$ the point-wise consistency error satisfies*

$$R_i[u](t) = O(h^4)$$

for every model problem of the form (4.1)*.*

Provided some additional structure is assumed a necessary and sufficient condition for an approximation setting of to be anti-dispersive is achieved :

Lemma 4.2 *Consider the finite element space $X_h(\mathbb{R}^n) = P^k(\mathbb{R}^n)$ or $X_h(\mathbb{R}^n) =$*

$Q^k(\mathbb{R}^n)$ defined on a uniform mesh $\mathcal{T}_h$; then if $\mathcal{T}_h$ is such that for each basis function $\{\psi_0, \psi_1, \ldots, \psi_{N-1}\}$ support$(\psi_i(\mathbf{x}))$ is centro-symmetric about the node x_i then the approximation setting $(X_h(\mathbb{R}^n), \mathcal{T}_h)$ is anti-dispersive if and only if for every $i = 0, 1, \ldots, N-1$, every $m = 0, 1, \ldots, n$ and every multi-index α with $|\alpha| \leq 3$ we have

$$\int_\Omega \left[\partial_{x_m} \Pi(\mathbf{x}^\alpha) - \Pi(\partial_{x_m} \mathbf{x}^\alpha)\right] \psi_i(\mathbf{x}) d\mathbf{x} = 0 \tag{4.13}$$

Proof. $(\leftarrow)$: Assume that for every $i = 0, 1, \ldots, N-1$, every $m = 0, 1, \ldots, n$ and every multi-index α with $|\alpha| \leq 3$ equation (4.13) holds. Then, directly from definition (4.1), for every $i = 0, 1, \ldots, N-1$, every $m = 0, 1, \ldots, n$ and every multi-index α with $|\alpha| \leq 3$ we have $C_i[\mathbf{x}^\alpha] = 0$. Therefore, from corollary (4.3) and lemma (4.1), the approximation setting is anti-dispersive.

$(\rightarrow)$: Now assume the approximation setting is anti-dispersive. We need to show that for every $i = 0, 1, \ldots, N-1$, every $m = 0, 1, \ldots, n$ and every multi-index α with $|\alpha| \leq 3$ equation (4.13) holds; fix a particular choice of i and m in this range and let $\mathbf{x}_i = ((x_i)_1, (x_i)_2, \ldots, (x_i)_m)$ be the corresponding i^{th} degree of freedom. By hypothesis, for all model problems of the form (4.1), we have that $R_i[u] = O(h^4)$. Since, by lemma (4.1), $C_i[\mathbf{x}^\alpha] = O(h^{|\alpha|-1})$ corollary (4.3) and lemma (4.1) imply that, for all model problems, $\sum_{|\alpha|=0}^{3} \frac{1}{\alpha!} D^\alpha u(\mathbf{x}_i, t) C_i(\mathbf{x}^\alpha) = 0$ must follow; in particular it must hold for specific model problems of our choosing. Fix a multi-index $\alpha_0 = (\alpha_1, \alpha_2, \ldots, \alpha_n)$ with $|\alpha_0| \leq 3$. Let $t_0 \in [0, T]$ be fixed and take $\beta = \mathbf{1}_m$, being one in the m^{th} position and zero elsewhere, and consider the initial data $u_0(\mathbf{x}) = \prod_{j=1}^{n} \left[((\mathbf{x})_j - (\mathbf{x}_i)_j)\right]^{(\alpha_0)_j}$. The corresponding solution to (4.1) is then

$$u(\mathbf{x}, t) = \left[((\mathbf{x})_m - (\mathbf{x}_i)_m - t)\right]^{(\alpha_0)_m} \prod_{j \neq m}^{n} \left[((\mathbf{x})_j - (\mathbf{x}_i)_j)\right]^{(\alpha_0)_j}$$

Let $\hat{\alpha}$ be a multi-index; we then have $D^{\hat{\alpha}}u(x_i,t) = (\alpha_0!)\delta(\alpha_0,\hat{\alpha})$; here, the quantity $\delta(\alpha_0,\hat{\alpha})$ is defined to be equal to one if $\alpha_0 = \hat{\alpha}$ and zero otherwise. Therefore the identity $\sum_{|\alpha|=0}^{3} \frac{1}{\alpha!} D^{\alpha}u(\mathbf{x}_i,t)C_i(\mathbf{x}^{\alpha}) = 0$, applied to this particular problem, implies that $C_i[\mathbf{x}^{\alpha_0}] = 0$ must follow. Since $\beta = \mathbf{1}_m$ it follows that

$$0 = C_i[\mathbf{x}^{\alpha_0}] = \int_{\Omega} \left[\partial_{x_m}\Pi(\mathbf{x}^{\alpha_0}) - \Pi(\partial_{x_m}\mathbf{x}^{\alpha_0})\right]\psi_i(\mathbf{x})d\mathbf{x}$$

Since α_0 was any multi-index satisfying $|\alpha_0| \leq 3$ the above must hold for all such multi-indices; this is precisely the statement that equation (4.13) must hold for all $|\alpha| \leq 3$. In addition, note that equation (4.13) is independent of the choice of β or initial data $u_0(\mathbf{x})$ for the model problem (4.1). This concludes the proof of the 'only if' statement and, hence, the corollary.□

Lemma 4.3 *Suppose the hypotheses of Lemma 4.2 are satisfied. Then for every* $0 \leq |\alpha| \leq 2$ *equation* (4.13) *holds.*

Proof. We argue case by case and utilize the centro-symmetry hypothesis of the basis function support sets. We may consider the node x_i to be the origin by a linear shift and an application of corollary 4.2. Suppose that $|\alpha| = 0$. Then $\mathbf{x}^{\alpha} = 1$ and $K_j(1) = 0$. If $|\alpha| = 1$ then $\Pi(x^{\alpha}) \in \mathbf{X}_h$ so that, once again, $K_j(\mathbf{x}^{\alpha}) = 0$. Note that if f is even (resp. odd) then $\Pi(f)$ is even (resp. odd) and therefore $K_j(f)$ is odd (resp. even). It follows that if $|\alpha| = 2$ then $K_j(x^{\alpha})$ is odd and since $S_i = \text{support}(\psi_i)$ is centro-symetric about x_i with $\psi_i(\mathbf{x})$ even then $\int_{S_i} K_j(x^{\alpha})\psi_i d\mathbf{x} = 0$ □

Combining these two results together in a final corollary gives

Corollary 4.4 *Suppose the hypotheses of Lemma 4.2 are satisfied. Then the approximation setting* $(\mathbf{X}_h, \mathcal{T}_h)$ *is anti-dispersive if and only if for every* $i = 0, 1, \ldots, N-1$,

every $m = 0, 1, \ldots, n$ *and* $|\alpha| = 3$

$$\int_{\Omega} \left[\partial_{x_m} \Pi(\mathbf{x}^{\alpha}) - \Pi(\partial_{x_m} \mathbf{x}^{\alpha})\right] \psi_i(\mathbf{x}) d\mathbf{x} = 0$$

Proof. Lemmas 4.2 and 4.3.□

4.3 $Q^1(\mathbb{R}^d)$ is anti-dispersive

In this section we show that the approximation setting $Q^1(\mathbb{R}^d)$ on a uniform mesh is anti-dispersive. The one dimensional result generalizes to d dimensions and will be presented beforehand; in fact we will see that the desired one dimensional result was already established in section 4.1.5. For $g \in C^0(\overline{\Omega})$ let $\mathcal{K}_j(f) := \partial_{x_j} \Pi(f) - \Pi(\partial_{x_j} f)$ denote the kernel of equation (4.13) and recall the definition $Q^k(\mathbb{R}^n) = \left\{ v \in C^0_{\#}(\mathbb{R}^n) \mid \forall T_h \in \mathcal{T}_h \;\; v_{|T_h} \in \mathbb{Q}_k(\mathbb{R}^n) \mid \right\}$; furthermore, the space of polynomials of partial degree k over $\mathbb{R}^d$ is $\mathbb{Q}_k(\mathbb{R}^d) = \text{span}\left(\{x_1^{\alpha_1} x_2^{\alpha_2} ... x_d^{\alpha_d} \mid 1 \leq \alpha_1, \alpha_2, ..., \alpha_d \leq k\}\right)$. We can immediately establish the one-dimensional result.

Corollary 4.1 $Q^1(\mathbb{R})$ *is anti-dispersive*

Proof. From corollary 4.4 we need to show that $\int_{\Omega} \mathcal{K}_1(x^{\alpha}) \psi_i(x) \, \mathrm{d}x = 0$ for $\alpha = 0, 1, 2, 3$ and for every $0 \leq i \leq N - 1$ where $N - 1$ is the total number of nodes of a uniform mesh $\mathcal{T}_h$. Since all of the sets support$(\psi_i(x))$ have the same geometry type in one dimension it suffices to show that $\int_{\Omega} \mathcal{K}_1(x^{\alpha}) \psi_0(x) \, \mathrm{d}x = 0$ for $\alpha = 0, 1, 2, 3$. All other values of i will follow from a linear change of variables and corollary 4.2. This result is precisely what is shown in the proof of proposition 4.4 as $Q^1(\mathbb{R}) = P^1(\mathbb{R})$. This proves this claim. □

We now want to approach the d dimensional result. To do so fix a choice of d and define a collection of sign functions corresponding to the d coordinate positions

of $\mathbf{x} = (x_1, x_2, \ldots, x_d) \in \mathbb{R}^d$ as $\sigma_i(\mathbf{x}) := H(x_i) - H(-x_i)$ Where $H : \mathbb{R} \to \mathbb{R}$ denotes the Heaviside function

$$H(x) = \begin{cases} 1 & : x > 0 \\ 0 & : x \leq 0 \end{cases}$$

The proof of the d-dimensional result will be shown to be reducible to proving the conditions of Corollary 4.4 hold for $i = 0$. Towards that end note that the basis function $\psi_0(\mathbf{x})$ is supported on the d-dimensional hypercube support$(\psi_0(\mathbf{x})) = [-1, 1]^d$. If we consider the Lagrange interpolant restricted to the support of ψ_0 we get the following result

Lemma 4.1 *Consider a monomial* $p(x_1, x_2, \ldots, x_d) = \prod_{i=1}^{d} x_{a_i}^{\alpha_i} \in \mathbb{Q}_k(\mathbb{R}^d)$ *and for each* $1 \leq j \leq d$ *define the monomial* $\widehat{p}^j(x_1, x_2, \ldots, x_d) := \prod_{i=1, i\neq j}^{d} x_{a_i}^{\alpha_i}$. *The Lagrange interpolant* $\Pi : C^0(\mathbb{R}^d) \to \mathbb{Q}_1([-1, 1]^d)$ *and the integral kernel* $\mathcal{K}_j : C^1(\mathbb{R}^d) \to C^0(\mathbb{R}^d)$ *applied to* $p(\mathbf{x})$ *satisfy the following relations*

$$\Pi(p) = \Pi\left(x_{a_1}^{\alpha_1} x_{a_2}^{\alpha_2} \ldots x_{a_d}^{\alpha_d}\right) = \prod_{i=1}^{d} \Pi\left(x_i^{\alpha_i}\right) = \prod_{i=1}^{d} \left(\sigma_i(x_i)^{\alpha_i+1} x_i\right)^{H(\alpha_i)} \tag{4.1}$$

$$\mathcal{K}_j(p) = \mathcal{K}_j\left(x_{a_1}^{\alpha_1} x_{a_2}^{\alpha_2} \ldots x_{a_d}^{\alpha_d}\right) = \mathcal{K}_j\left(x_j^{\alpha_j}\right) \Pi\left(\widehat{p}^j\right) \tag{4.2}$$

Proof. Note first that $H(\alpha_i)$ is the Heaviside function applied to the exponent $\alpha_i \geq 0$ and has the effect of setting $(\sigma_i(x_i)^{\alpha_i+1} x_i)^{H(\alpha_i)} = 1$ if $\alpha_i = 0$. The Heaviside function is utilized in this manner for overall compactness of notation. To establish equation (4.1) define $S(\mathbf{x}) = \prod_{i=1}^{d} (\sigma_i(x_i)^{\alpha_i+1} x_i)^{H(\alpha_i)}$; then $S(\mathbf{x}) \in \mathbb{Q}_1(\mathbb{R}^d)$ and coincides with $\Pi(x_{a_1}^{\alpha_1} x_{a_2}^{\alpha_2} \ldots x_{a_d}^{\alpha_d}) \in \mathbb{Q}^1(\mathbb{R}^d)$ at the vertices of $[-1, 1]^d$. The two functions are therefore equal. Now fix $1 \leq j \leq d$ and $\alpha_j \in \mathbb{Z}^+$; set $\alpha_i = \delta_{ij}\alpha_j$. Then $\Pi(x_j^{\alpha_j}) = (\sigma_i(x_i)^{\alpha_i+1} x_i)^{H(\alpha_i)}$ as a special case. To establish equation (4.2) we utilize equation

(4.1) both in the identity $\Pi(x_j^{\alpha_j}) = (\sigma_j(x_j)^{\alpha_j+1}x_j)^{H(\alpha_j)}$ and to factor the Lagrange interpolation of a monomial as the product of the interpolations of its constituent terms

$$\begin{aligned}
\mathcal{K}_j(x_{a_1}^{\alpha_1}x_{a_2}^{\alpha_2}\dots x_{a_k}^{\alpha_k}) &= \partial_{x_j}\Pi(x_{a_1}^{\alpha_1}x_{a_2}^{\alpha_2}\dots x_{a_k}^{\alpha_k}) - \Pi(\partial_{x_j}x_{a_1}^{\alpha_1}x_{a_2}^{\alpha_2}\dots x_{a_k}^{\alpha_k}) \\
&= \partial_{x_j}\left(\prod_{i=1}^{k}\Pi(x_{a_i}^{\alpha_i})\right) - \left(\alpha_j\Pi(x_j^{\alpha_j-1})\prod_{i\neq j}^{k}\Pi(x_{a_i}^{\alpha_i})\right) \\
&= \left(\partial_{x_j}\Pi(x_{a_j}^{\alpha_j})\prod_{i\neq j}\Pi(x_{a_i}^{\alpha_i})\right) - \left(\alpha_j\Pi(x_{a_j}^{\alpha_j-1})\prod_{i\neq j}\Pi(x_{a_i}^{\alpha_i})\right) \\
&= \left(\partial_{x_j}\Pi(x_{a_j}^{\alpha_j}) - \Pi(\partial_{x_j}x_{a_j}^{\alpha_j})\right)\prod_{i\neq j}\Pi(x_{a_i}^{\alpha_i}) = \mathcal{K}_j(x_j^{\alpha_j})\Pi(\widehat{p}^j)
\end{aligned}$$

This concludes the proof of the identities. □

We are now ready to establish the d-dimensional result

Proposition 4.1 *$Q^1(\mathbb{R}^d)$ is anti-dispersive*

Proof. A uniform grid for $Q^k(\mathbb{R}^d)$ consists of d dimensional hypercubes of equal side length; therefore, a unique such grid exists which contains the origin and x-y plane. If we consider $Q^1(\mathbb{R}^d)$ then the degrees of freedom lie on the hypercube vertices; as a consequence the support of each basis function $\psi_i(\mathbf{x})$ of $Q^1(\mathbb{R}^d)$ will have the same type of support geometry. Therefore applying a linear change of coordinates and Corollary 4.2 it suffices, by Corollary 4.4, to show for $1 \leq m \leq d$ and all multi-indices $|\alpha| \leq 3$ that $\int_\Omega \mathcal{K}_m(\mathbf{x}^\alpha)\psi_0 d\mathbf{x} = 0$. The proof of the d-dimensional result will be shown to be reducible to proving the conditions of Corollary 4.4 hold for $i = 0$. Towards that end note that the basis function $\psi_0(\mathbf{x})$ is supported on the d-dimensional hypercube $\text{support}(\psi_0(\mathbf{x})) = [-1, 1]^d$. If we consider the Lagrange interpolant restricted to the support of ψ_0 we get the following result The basis

function $\psi_0(\mathbf{x})$ can be expressed in terms of the sign functions as $\psi_0(\mathbf{x}) = \prod_{i=1}^{d}(1 - \sigma_i(x_i)x_i)$. Let $\alpha = (\alpha_1, \alpha_2, \ldots, \alpha_d)$ be a multi-index with $|\alpha| \leq 3$ and fix $1 \leq j \leq d$. Then in particular $0 \leq \alpha_j \leq 3$ and an application of equation (4.1) and Fubini's theorem gives

$$\begin{aligned}\int_\Omega \mathcal{K}_j(\mathbf{x}^\alpha)\psi_0 d\mathbf{x} &= \int_{[-1,1]^d} \mathcal{K}_j(x_{a_1}^{\alpha_1} x_{a_2}^{\alpha_2} \ldots x_{a_k}^{\alpha_k}) \prod_{i=1}^{d}(1 - \sigma_i(x_i)x_i) d\mathbf{x} \\ &= \left(\int_{[-1,1]} \mathcal{K}_j(x_j^{\alpha_j})(1 - \sigma_j(x_j)x_j)\,\mathrm{d}x_j\right) \int_{[-1,1]^{d-1}} \Pi(\widehat{p}^j) \prod_{i\neq j}(1 - \sigma_i(x_i)x_i) d\mathbf{x}\end{aligned}$$

The integral $\int_{[-1,1]} \mathcal{K}_j(x_j^{\alpha_j})(1-\sigma_j(x_j)x_j)\,\mathrm{d}x_j = \int_\Omega \mathcal{K}_j(x_j^{\alpha_j})\psi_0(x_j)\,\mathrm{d}x_j = 0$ as Corollary (4.1) requires all expressions of this form where $0 \leq \alpha_j \leq 3$ are zero. This concludes the proof. □

4.4 $P^1(\mathbb{R}^2)$ antidispersivity

Recall the finite element approximation space space $P^k(\mathbb{R}^d)$ is defined by

$$P^k(\mathbb{R}^n) = \left\{v \in C^0_\#(\mathbb{R}^n) \mid \forall T_h \in \mathcal{T}_h \;\; v_{|T_h} \in \mathbb{P}_k(\mathbb{R}^n)\right\}$$

In section 4.1 consistency error was analyzed in one dimension for the consistent P^1 mass matrix. In the one dimensional setting there is a unique uniform mesh, $\mathcal{T}_h$, of size h which contains the origin given by intervals of the form $[x_i, x_{i+1}]$ where $x_{i+1} - x_i = h$ for every i; furthermore every basis function $\psi_i(x)$ of $P^1(\mathbb{R}^1)$ has the same type of support geometry in the one-dimensional setting. It follows then that Proposition 4.4 is a proof that the approximation setting $(P^1(\mathbb{R}^1), \mathcal{T}_h)$ is antidispersive. In the case of P^1 finite elements in higher dimensions than one there are several uniform meshes that have the property that the shape functions have centrosymmetric support; this was not the case with Q^1 finite elements. In the following

sections we present an anti-dispersive approximation setting for $P^1(\mathbb{R}^2)$ and provide some computed results for $P^1(\mathbb{R}^3)$.

In two dimensions we consider the mesh generated by tiling the following plane with the triangles, having edge length h; this tiling, along with its shaded and annotated typical nodal support, is shown in figure 4.1. The degrees of freedom, as well as the mesh nodes, coincide with the vertices of the triangles. The support set of a typical nodal basis function is observably centro-symmetric about the center mesh node and every node has the same geometry type for its associated basis function support set. Therefore, as in previous sections, it suffices to show that Corollary 4.4 is satisfied for $i = 0$; all other values of i will follow by linear translation and an application of Corollary 4.2. We continue to utilize the notation $K_j(f) = \partial_{x_j}\Pi(f) - \Pi(\partial_{x_j} f)$ where $\Pi : C^0(\mathbb{R}^2) \to P^1(\mathbb{R}^2)$ is the Lagrange interpolant.

Figure 4.1: Tiling for a uniform $P^1(\mathbb{R}^2)$ finite element mesh

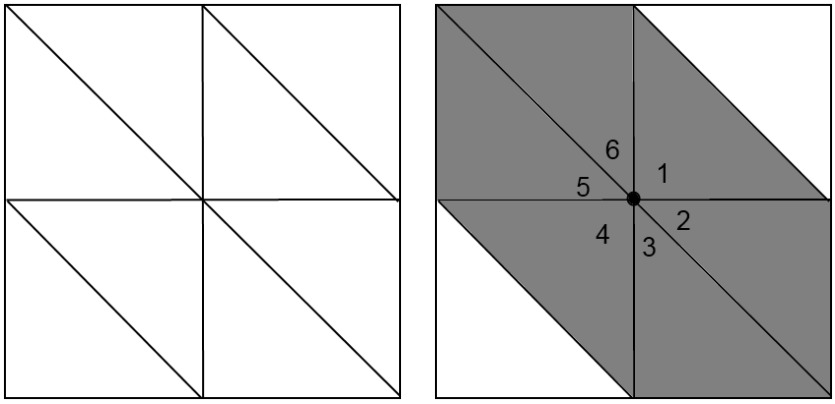

(a) Basic tile

(b) Shaded, annotated nodal support

Proposition 4.1 *Let $\mathcal{T}_h$ be the mesh generated by tiling figure 4.1. Then the ap-*

proximation setting $(P^1(\mathbb{R}^2), \mathcal{T}_h)$ *is anti-dispersive.*

Proof. As discussed it suffices to show that Corollary 4.4 holds for $i = 0$. Let $S_0 = \text{support}(\psi_0(\mathbf{x}))$ and consider $\int_{S_0} K_j(\mathbf{x}^\alpha)\psi_0 d\mathbf{x}$ for $j = 1, 2$ and $|\alpha| = 3$. Since $\mathbf{x}^\alpha$ is odd $K_j(\mathbf{x}^\alpha)$ is even. Let $T_1, T_2, \ldots, T_6$ be the triangles, numbered as in figure 4.1, comprising the set S_0; since ψ_0 is even on S_0 we have

$$\int_{S_0} K_j(\mathbf{x}^\alpha)\psi_0 d\mathbf{x} = 2\int_{T_1 \cup T_2 \cup T_3} K_j(\mathbf{x}^\alpha)\psi_0 d\mathbf{x}$$

$\mathbf{x}^\alpha$	∂_x	T_1	T_2	T_3	∂_y	T_1	T_2	T_3
x^3		$1/24$	$-1/12$	$1/24$		0	0	0
y^3		0	0	0		$1/24$	$1/24$	$-1/12$
x^2y		0	$1/12$	$-1/12$		$-1/24$	$1/12$	$-1/24$
xy^2		$-1/24$	$-1/24$	$1/12$		0	$-1/12$	$1/12$

Table 4.1: Values of $\int_{T_i} K_j(\mathbf{x}^\alpha)\psi_0(\mathbf{x})d\mathbf{x}$ on the individual triangular elements of $\text{support}(\psi_0)$

Considering each possibility for $\mathbf{x}^\alpha$ where $|\alpha| = 3$ on each triangle the computed values for the expression $\int_{T_s} K_j(\mathbf{x}^\alpha)\psi_0(\mathbf{x})d\mathbf{x}$ where $1 \leq s \leq 3$ and $j = 1, 2$ are given in Table 4.1. It follows that for each $j = 1, 2$ we have $\int_{T_1 \cup T_2 \cup T_3} K_j(\mathbf{x}^\alpha)\psi_0 d\mathbf{x} = \sum_{s=1}^{3} \int_{T_s} K_j(\mathbf{x}^\alpha)\psi_0 d\mathbf{x} = 0$ so that the anti-dispersivity condition of Corollary 4.4 is satisfied. This completes the proof. □

5. SUMMARY AND CONCLUSION

As indicated in sections 1.1 and 1.3 the inherent difficulties of the incompressible Navier-Stokes equations at high Reynolds number are significant; despite these difficulties they remain the foundation of pragmatic engineering undertakings. Therefore, while progress towards a comprehensive theoretical understanding is a vein of current research, the engineering and scientific communities benefit greatly from the application of new mathematical ideas and techniques towards computational aspects of the issue. The accomplishments of the current work is mainly two-fold: first, from a mathematical point of view, the efficacy of entropy-viscosity for usage in modern models has been demonstrated; the notion of localized viscosity has transitioned from its inception as an a-posteriori error correction technique into a more central role. From a scientific computing and engineering vantage point the entropy-viscosity has been demonstrated as a useful tool in reducing the overwhelming complexity requirements typically associated with simulating incompressible flow at high Reynolds numbers; both in the absence and presence of a diffusionless tracer or immiscible fluid.

In chapter 2 a large eddy simulation (LES) model was proposed based on an entropy-viscosity; the results show that, at a minimum, such a model can evince a a sixty-four fold reduction in computational complexity while refraining from overdamping turbulent effects. In chapter 3 a one-stage advection-compression method is broached which combines several previous approaches into a monolithic framework; the artificial compressor (ACF) is based on an entropy-viscosity. In chapter 4 an integral commutator approach to consistency error was developed; such an approach gives rise to the theory of anti-dispersive approximation spaces and a suc-

cinct, computable form of the consistency error. The implications of the integral commutator theory extend beyond the simple wrest from the cumbersome Taylor approach; rather, as discussed, it can be utilized to verify schemes are free of low-order dispersion error via a set of simple computations, construct correction schemes for use with mass lumping techniques and has potential for use as a general theoretical framework for error analysis. Indeed, the theory was applied at the end of chapter 4 to prove previously unapproachable results regarding Q^1 finite elements in arbitrary dimension.

REFERENCES

[1] J. Andrews and K. Morton. A posteriori error estimation based on discrepancies in an entropy variable. *Int. J. Comput. Fluid Dyn.*, 10(3):183–198, 1998.

[2] U. Ascher. *Numerical methods for evolutionary differential equations*. SIAM, Philadelphia, PA, 2008.

[3] A. Baggaley, C. Barenghi, A. Shukurov, and Y. Sergeev. Coherent vortex structures in quantum turbulence. *EPL (Europhysics Letters)*, 98(2):26002, 2012.

[4] I. Berselli and W. Layton. *Mathematics of large eddy simulation of turbulent flows*. Springer-Verlag, New York, 2010.

[5] S. Chen, B. Dhruva, S. Kurien, K. Sreenivasan, and M. Taylor. Anomalous scaling of low-order structure functions of turbulent velocity. *J. Fluid Mech.*, 533:183–192, 2005.

[6] S. Douady, Y. Couder, and M. Brachet. Direct observation of the intermittency of intense vorticity filaments in turbulence. *Phys. Rev. Lett.*, 67:983–986, Aug 1991.

[7] D. Enright, R. Fedkiw, J. Ferziger, and I. Mitchell. A hybrid particle level set method for improved interface capturing. *J. Comput. Phys.*, 183(1):83–116, 2002.

[8] A. Ern and J.-L. Guermond. *Theory and practice of finite elements*, volume 159 of *Applied Mathematical Sciences*. Springer-Verlag, New York, 2004.

[9] L. Evans. *Partial differential equations*. American Mathematical Society, Providence, RI, 1998.

[10] M. Germano, U. Piomelli, P. Moin, and W. Cabot. A dynamic subgrid-scale eddy viscosity model. *Physics of Fluids A*, 3(7):1760, 1991.

[11] J. Glimm, O. McBryan, R. Meinkoff, and D. Sharp. Front tracking applied to rayleigh-taylor instability. *SIAM J. Sci. Stat. Comput.*, 7:230 – 251, 1986.

[12] J.-L. Guermond, P. Minev, and A. Salgado. Convergence analysis of a class of massively parallel direction splitting algorithms for the Navier-Stokes equations in simple domains. *Math. Comp.*, 81(280):1951–1977, 2012.

[13] J.-L. Guermond and R. Pasquetti. A correction technique for the dispersive effects of mass lumping for transport problems. *Comput. Methods Appl. Mech. Engrg.*, 253:186–198, 2013.

[14] J.-L. Guermond, R. Pasquetti, and B. Popov. Entropy viscosity method for nonlinear conservation laws. *J. Comput. Phys.*, 230(11):4248–4267, 2011.

[15] J.-L. Guermond, R. Pasquetti, and B. Popov. From suitable weak solutions to entropy viscosity. *J. Sci. Comput.*, 49(1):35–50, 2011.

[16] F. Harlow and J. Welch. Numerical calculation of time-dependent viscous incompressible flow of fluid with free surface. *The Physics of Fluids*, 8(12), 1965.

[17] A. Harten. The artificial compression method for computation of shocks and contact discontinuities. I. Single conservation laws. *Comm. Pure Appl. Math.*, 30(5):611–638, 1977.

[18] A. Harten. On the symmetric form of systems of conservation laws with entropy. *J. Comput. Phys.*, 49:151 – 164, 1982.

[19] A. Harten, J. Hyman, and P. Lax. On finite-difference approximations and entropy conditions for shocks. *Communications on pure and applied mathematics*, 29:297 – 322, 1976.

[20] J. Holman. *Heat Transfer*. McGraw-Hill, Boston, MA, 10 edition, 2010.

[21] E. Hopf. Über die anfangswertaufgabe für die hydrodynamischen grundgleichungen. *Math. Nachr.*, 4:213 – 231, 1951.

[22] T. Hughes, L. Franca, and M. Mallet. A new finite element formulation for computational fluid dynamics: I.symmetric forms of the compressible euler and navier-stokes equations and the second law of thermodynamics. *Computer methods in applied mechanics and engineering*, 54:223 – 234, 1985.

[23] T. Hughes, M. Mallet, and A. Mizukami. A new finite element formulation for computational fluid dynamics: II. beyond SUPG. *Computer methods in applied mechanics and engineering*, 54:352 – 355, 1986.

[24] S. Ianniello and A. Di Mascio. A self-adaptive oriented particles Level-Set method for tracking interfaces. *J. Comput. Phys.*, 229(4):1353–1380, 2010.

[25] G. Jennings. Discrete shocks. *Communications on pure and applied mathematics*, 27:25 – 37, 1974.

[26] A. Johnson, C. Szepessy and P. Hansbo. On the convergence of shock-capturing streamline diffusion finite element methods for hyperbolic conservation laws. *Mathematics of Computation*, 54(189):107 – 129, 1990.

[27] R. Kerr. Higher-order derivative correlations and the alignment of small scale structures in isotropic numerical turbulence. *J. Fluid. Mech.*, 259:241–264, 1994.

[28] S. Kurien, M. Taylor, and T. Matsumoto. Isotropic third-order statistic in turbulence with helicity: the 2/15-law. *J. Fluid Mech.*, 515:87–97, 2004.

[29] O. Ladyzhenskaya. Solution "in the large" to the boundary-value problem for the navier-stokes equations in two space variables. *Soviet Physics. Dokl.*, 123:1128 – 1131, 1958.

[30] O. Ladyzhenskaya. Solution "in the large" of the nonstationary boundary value problem for the navier-stokes system with two space variables. *Comm. Pure Appl. Math.*, 12:427 – 433, 1959.

[31] P. Lax and B. Wendroff. Systems of conservation laws. *Communications on pure and applied mathematics*, 13:217 – 237, 1960.

[32] J. Leray. Etude de diverses equations integrales non lineaires et de quelques problemes que pose l'hydrodynamique. *J. Math. Pures Appl.*, 12:1 – 82, 1933.

[33] J. Leray. Essai sur le mouvement d'un liquide visqueux emplissant l'espace. *Acta Math*, 63:193 – 248, 1934.

[34] J. Leray. Essai sur les mouvements plans d'un liquide visqueux qui limitent des parois. *J. Math. Pures Appl.*, 13:341 – 418, 1934.

[35] R. Leveque. High-resolution conservative algorithms for advection in incompressible flow. *SIAM J. Numer. Anal.*, 33(2):627–665, 1996.

[36] J.-L. Lions and G. Prodi. Un theoreme d'existence et unicite dans les equations de navier-stokes en dimension 2. *Acad. Sci. Paris*, 248:3519 – 3521, 1959.

[37] H. Moffatt, S. Kida, and K. Ohkitani. Stretched vortices - the sinews of turbulence; large-reynolds-number asymptotics. *J. Fluid. Mech.*, 259:241–264, 1994.

[38] W. Mulder and S. Osher. Computing interface motion in compressible gas dynamics. *Journal of computational physics*, 100:209–228, 1990.

[39] O. Oleinik. Discontinuous solutions of nonlinear differential equations. *Uspekhi Ma Nauk (Amer. Math Soc. Transl. Ser. 2, 26, pp 95-172)*, 12:3 – 73, 1957.

[40] E. Olsson, G. Kreiss, and S. Zahedi. A conservative level set method for two phase flow. II. *J. Comput. Phys.*, 225(1):785–807, 2007.

[41] S. Osher and J. Sethian. Fronts propagating with curvature-dependent speed: algorithms based on hamilton-jacobi formulations. *J. Comput. Phys.*, 79:12 – 49, 1988.

[42] M. Overholt and S. Pope. A deterministic forcing scheme for direct numerical simulations of turbulence. *Comput. Fluids*, 27(1):11–28, 1998.

[43] D. Peng, B. Merriman, S. Osher, H. Zhao, and M. Kang. A PDE-based fast local level set method. *J. Comput. Phys.*, 155(2):410–438, 1999.

[44] S. Pope. *Turbulent flows*. Cambridge University Press, Cambridge, 2000.

[45] G. Puppo. Numerical entropy production for central schemes. *SIAM J. Sci. Comput.*, 25(4):1382–1415 (electronic), 2003/04.

[46] R. Scardovelli and S. Zaleski. Direct numerical simulation of free-surface and interfacial flow. *Annu. Rev. Fluid Mech*, 31:567 – 603, 1999.

[47] V. Scheffer. Hausdorff measure and the Navier-Stokes equations. *Comm. Math. Phys.*, 55(2):97–112, 1977.

[48] F. Schmitt. About boussinesq's turbulent viscosity hypothesis: historical remarks and a direct evaluation of its validity. *Comptes Rendus Mécanique*, 335:9–10, 1977.

[49] G. Seregin and V. Sverak. Navier-stokes equations with lower bounds on the pressure. *Arch. Ration. Mech. Anal.*, 163:65 – 86, 2002.

[50] J. Smagorinsky. General circulation experiments with the primitive equations. *Monthly weather review*, 91(3):99–164, 1963.

[51] K. Sreenivasan and R. Antonia. The phenomenology of small-scale turbulence. In *Annual review of fluid mechanics, Vol. 29*, volume 29 of *Annu. Rev. Fluid Mech.*, pages 435–472. Annual Reviews, Palo Alto, CA, 1997.

[52] M. Sussman. *A level set approach for computing solutions to incompressible two-phase flow*. ProQuest LLC, Ann Arbor, MI, 1994. Thesis (Ph.D.)–University of California, Los Angeles.

[53] A. Szepessy. Convergence of a shock-capturing streamline diffusion finite element method for a scalar conservation law in two space dimensions. *Mathematics of Computation*, 53(188):527 – 545, 1989.

[54] M. Taylor, S. Kurien, and G. Eyink. Recovering isotropic statistics in turbulence simulations: the Kolmogorov 4/5th law. *Phys. Rev. E (3)*, 68(2):026310, 8, 2003.

[55] R. Temam. *Navier-Stokes Equations: Theory and Numerical Analysis*. AMS Chelsea publishing, Providence, RI, 1984.

[56] G. Tryggvason. Computations of three-dimensional rayleigh-taylor instability. *Phys. Fluids A*, 2:656 – 659, 1990.

[57] L. Ville, L. Silva, and T. Coupez. Convected level set method for the numerical simulation of fluid buckling. *International Journal for Numerical Methods in Fluids*, 66(3):324–344, 2011.